Formulation development, characterization & stability studies

4. FORMULATION DEVELOPMENT, CHARACTERIZATION & STABILITY STUDIES

4.1 INTRODUCTION

PACLITAXEL a diterpenoid derived from the needles and bark of the Pacific yew tree is having potent antineoplastic activity against a wide range of cancers. But the potential drawback is that it is a P-gp substrate (Wani et al., 1971; Spencer & Foulds, 1994). Pgp prevents intracellular accumulation of many anticancer agents (that are its substrates) and hence causes a reduction in their cytotoxic activity mainly by preventing active uptake and increasing cellular efflux of positively charged amphipathic drugs in an ATP-dependent manner (Endicott & Ling, 1989; Ambudkar et al., 1992; Schinkel 1999).

The rationale behind association of drugs with colloidal carriers like nanoparticles or liposomes for reversal of MDR is the fact that P-gp probably recognizes the drug to be effluxed out of the tumoral cell only when it is present in the plasma membrane and not in case when it is located in the cytoplasm or lysosomes after its endocytosis. NPs of biodegradable polymers can provide a way of sustained, controlled and targeted drug delivery to improve the therapeutic effects and reduce the side effects of the formulated drugs. Poly(D,L-lactide-co-glycolide) (PLGA), poly (n-butyl cyanoacrylate) (PBCA), poly (iso-hexyl cyanoacrylate) etc are widely used as polymeric carriers for preparation of NPs.

Poly(lactide) (PLA) and poly(D,L-lactide-co-glycolide) (PLGA) are FDA-approved biodegradable polymers, which are used most often in the literature of drug delivery (Desai et al., 1997; Fonseca et al 2002; Konan et al., 2002). It has been proved by Kabanov and colleagues that Pluronics (P-85, F-68, L-61) reduce the respiration rate of both MDR and drug sensitive cells which results in hypersensitivity to chemotherapeutic agents. Because cells often achieve their drug resistance via the efflux of drugs through energy-dependent transporters, the reduction in respiration impairs this mechanism. Another possibility is that cytoplasmic vesicles of MDR cells, in which chemotherapeutic agents such as anthracycline accumulate, are more readily permeabilized by Pluronics than the vesicles of drug-sensitive cells. This means that the anti-cancer drug is released more readily from the vesicles to its target, the nucleus (Owens 2001).

Surface modification of PLGA NPs has been attempted by conjugating either their surface with different ligands or coating with different surfactants. Ligands which have been reported are folic acid (Stella et al., 2000), transferrin (Sahoo et al., 2004), lectins (Sharma et al., 2004) etc. These ligands bind specifically to the receptors on the plasma membrane of the target tissue which leads to the internalization of plasma membrane receptors along with the delivery system i.e. NPs. Transferrin (Tf) is a structurally related class of metal-binding glycoproteins of approximately 80 kDa in size whose primary function is the binding and transportation of non-heme iron through the blood to cells through transferrin receptors (TfR). Since TfR are overexpressed in malignant tissues compared to normal tissue, Tf is being extensively investigated as a ligand for drug targeting. Further TfR are overexpressed in certain body tissue such as liver, epidermis, intestinal epithelium and vascular endothelium of the brain capillary. Another motivation for using Tf as a ligand is its potential to overcome drug resistance due to membrane associated drug resistant proteins such as P-gp (Sahoo and Labhasetwar, 2005; Qian et al., 2002).

The poly(alkylcyanoacrylate) (PACA) NPs have recently gained increasing interest in targeting and drug delivery, because of the ease of synthesis, biodegradability, ability to alter biodistribution of drugs and lower toxicity [19-21]. PACA NPs have also showed good encapsulation properties and ability to cross the blood–brain barrier which makes PACA NPs ideal for cancer therapy, especially for brain tumours (Woods, 1996; Kreuter 1996). The PACA NPs are reported as a novel tool to deal with resistant cancer because of its unique drug delivery mechanism. Drug loaded in PACA NPs forms ions pairs with degraded polymer products at the physiological pH and thus protects the drug from getting efflexed out from intracellular domain by resistance mechanism of the P-glycoprotein, i.e. MDR-1 type (Hu, 1996; Colin de Verdie`re 1997). Poly alkyl(butyl cyanoacrylate) nanoparticles are generally prepared from butyl cyano acrylate monomers by emulsion anionic polymerisation in an acidic aqueous solution of a colloidal stabilizer such as dextran 70, polysorbates, and poloxamers. The polymerization is initiated by the hydroxyl ions of water, and elongation of the polymer chains occurs by an anionic polymerization mechanism. It has to be understood that the anionic polymerization of such a reactive monomer can be controlled in an aqueous medium.

Inclusion of drug can be made during the polymerization process or by adsorption on the preformed nanoparticles. The length of the alkyl pendant governs degradation rates (Müller et al. 1990, 1992) and toxicity (Lherm et al. 1992; Kante et al. 1982) of poly(alkyl cyanoacrylate) nanoparticles, which decrease in the order methyl> ethyl> butyl/isobutyl> hexyl/isohexyl.

In recent years, increasing attention has also been addressed to solid lipid nanoparticles (SLNs), due to their biodegradability and ability to entrap a variety of biologically active compounds, in the area of modified drug delivery technology to overcome drawbacks in conventional dosage forms (Muller et al., 1995; Muller et al., 2000; Mehnert and Mader 2001). SLN are particles made from solid lipids (i.e. lipids solid at room temperature and also at body temperature) and stabilized by surfactant. Most of solid lipids have an approved status, such as the GRAS (Generally regarded as safe) status, due to their low toxicity. By definition, the lipids can be highly purified triglycerides, complex glyceride mixtures or even waxes (Muller et al., 1996). The solid matrix of the SLN can protect the incorporated actives against chemical degradation and provide highest flexibilities in the modulation of the drug release profiles. Moreover, body-drug distribution can be successfully modified when it is incorporated within a carrier, such as a colloidal system, and these properties can be successfully exploited to address specifically a drug to its target site at cell or tissue level. In particular, SLNs have been investigated as possible carriers for modified intravenous drug delivery and targeting (Heitai et al., 1998; Yang et al., 1999; Cavalli et al 2000) or as oral drug carriers to overcome administration problem of drugs that are unstable in the gastrointestinal tract or are inadequately absorbed (Yang et al., 1999). A clear advantage of SLN is that the lipid matrix is made by physiological lipids and this fact strongly decreases acute and chronic toxicity effects. The use of solid lipids instead of liquid oils is a very attractive to achieve controlled drug release because drug mobility in a solid lipid should be considerably lower compared with a liquid oil.

Drug explusion from SLN occurs if the lipid matrix consists of especially similar molecules (i.e. tristearin or tripalmitin) as a perfect crystal with few imperfections is formed. Since incorporated drugs are located between fatty acid chains, between the lipid layers and

also in crystal imperfections, a highly ordered crystal lattice cannot accommodate large amounts of drug (Mehnert et al., 1997). Therefore, the use of more complex lipids (mono-, di-, triglycerides of different chain lengths) is more sensible for higher drug loading. The transition to highly ordered lipid particles is also the reason for drug expulsion. Directly after production, lipids crystallize partially in higher energy modifications (α, β') with more imperfections in the crystal lattice (Freitas et al., 1999, Hagemanne 1988; Hernqvist 1988, Radtke and Muller, 2001). The preservation of the α-modification during storage and transformation after administration (e.g. by temperature changes) could lead to a triggered and controlled release and has recently been investigated for topical formulations (Jenning et al., 2000). If however a polymorphic transition to β form takes place during storage, the drug will be expelled from the lipid matrix and it can then neither be protected from degradation nor released in a controlled way. Moreover, recently it has been reported that PTX entrapped in novel cetyl alcohol/polysorbate-80 based NPs could overcome multidrug resistance in-vitro in a human colon adenocarcinoma cell line (HCT-15) (Koziara et al., 2004). Also Koziara and co-workers (2006) have shown enhancement of PTX activity in PTX loaded SLN in comparison to free drug. It was attributed to the ability of the PTX loaded SLN to overcome multidrug resistance via enhanced delivery as well as anti-angiogenic effect.

In addition to the art of formulation, optimization by factorial design is an efficient method of indicating the relative significance of a number of variables and their interactions. The response surface method, first reported by Box and Wilson, 1951, has been applied to dosage form design for various kinds of drugs by several other researchers (Li et al., 2005; Gibaly and Ghaffar, 2005; Bhavsar et al., 2006). Factorial design is a very efficient tool to obtain an appropriate mathematical model with minimum experiments for optimization of formulation design. A specific purpose of the experiments and a quantitative target function of the system are required to be accurately defined before experiments are designed. Most important variables affecting the system function are selected and systemic experiments are performed to the specified factorial design. The number of independent variables selected decides the number of experiments that are to be performed. The response/s (Y) is/are measured for each experiment and either a simple linear, interactive, or quadratic model is

generated by carrying out multiple regression analysis and F-statistics to identify statistically significant terms. Responses obtained from the reduced equation (neglecting non-significant terms) are used for drawing response surface plots to visualize the impact of changing variables. The optimum point can be identified from the plot and replicate trials may be run to verify the prediction of optimum response (Gohel and Amin, 1998).

4.2 MATERIALS

PLGA 502H, (lactide/glycolide ratio 50:50, inherent viscosity 0.22dl/g) was obtained as a gift sample from Boehringer Ingelheim, Germany. Paclitaxel (PTX) was obtained as a gift sample from Sun Pharma Advanced Research Centre, Vadodara, India. Polyvinyl alcohol (PVA, Mol wt. 30000-70000 KDa; hydrolyzed 87-89%) was purchased from Sigma Chemicals, India. Transferrin Holo Human was purchased from Merck Specialities, India. Coumarin-6 was obtained from Neelikon dyes, Mumbai, India. Polyglycerol polyglycidyl ether (SR4GL®) was obtained as gift sample from Sakamoto Yakuhin Kogyo Co., Ltd., Japan. Zinc tetrafluoroborote hydrate was purchased from Acros Organics, Belgium. n-butyl cyanoacrylate was obtained as a gift sample from Tong Shen enterprise Ltd., Taiwan. Dynasan®118 (tri glyceride derivative of 18 carbon fatty acid stearic acid and glycerol) (GTS), was obtained from Sasol GmbH, Germany. Precirol®ATO 5 and Compritol®888 was obtained from Colorcon, India. Pluronic®P85 (poloxamer 185) and Pluronic®F68 (poloxamer 188) was obtained from BASF, Mumbai, India. Dextran 70 was provided as gift sample by Claris life sciences, India. HPLC grade acetonitrile, ethanol, methanol, isopropyl alcohol, chloroform and acetone were purchased from S. D. Fine Chemicals, India. All other reagents used were of analytical grade. Distilled water used was filtered through 0.22µm filter by Millipore, India.

4.3 METHODS

4.3.1 PTX LOADED PLGA NPS

4.3.1.1 Preparation and optimization of PTX loaded PLGA NPs

PTX loaded PLGA NPs were prepared by solvent diffusion (nanoprecipitation) technique as described by Fessi et al., 1989. Based on preliminary experiments critical formulation

parameters i.e. polymer concentration, stabilizer concentration and volume of organic phase were identified. Further optimization of PTX loaded PLGA NPs was done by 3^3 factorial design (27 batches were prepared) followed by multiple regression analysis. Briefly, 5mg PTX and PLGA (100, 150 and 200 mg corresponding to 1: 20, 1: 30 and 1: 40 drug: polymer ratio) was dissolved in acetone: ethanol (4:1) mixture (2.5, 5 and 7.5mL corresponding to Organic: aqueous phase volume ratio of 0.25, 0.5 and 0.75). The organic phase containing drug and polymer was slowly poured at 0.5mL/min into 10ml of aqueous phase containing PVA (0.5, 1 and 1.5%w/v) as stabilizer on a magnetic stirrer (Remi Equipments, Mumbai). With the diffusion of solvent in to the aqueous phase, the polymer precipitates while encapsulation of PTX occurs leading to formation PTX loaded PLGA NPs. The resulting nanoparticle dispersion was further stirred to evaporate the organic phase under vacuum. NPs were recovered by centrifugation for 30 min at 20,000 rpm (Sigma 3K30, Germany) washed with distilled water to remove excess PVA, and then lyophilized for 24 hrs (Heto Drywinner, Denmark).

4.3.1.1.1 3^3 factorial design

It is important to understand the complexity of pharmaceutical formulations by using established statistical tools such as factorial designs. Studies based on factorial designs allow all the factors to be varied simultaneously, thus enabling evaluation of the effects of each variable at each level and showing interrelationship among them.

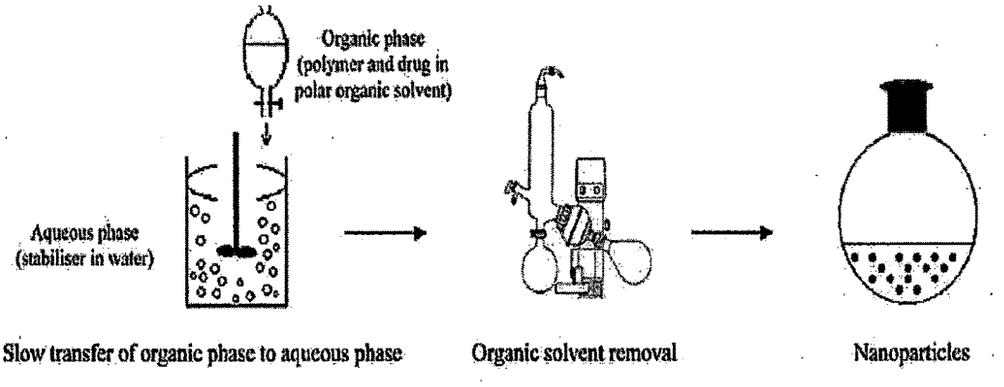

Figure 4. 1: Schematic presentation of formation of nanoparticles by nanoprecipitation technique.

Factorial designs are of choice when simultaneous determination of the effects of several factors and their interactions on predetermined parameters is required. A prior knowledge and understanding of the process and the process variables under investigation are necessary for achieving a more realistic model for optimizing the formulations. Based on the results obtained in preliminary experiments, polymer concentration, stabilizer concentration and organic: aqueous phase volume ratio were found to be the major independent variables in determining the two dependent variables particle size (nm) and entrapment efficiency (%). Hence these variables were selected to find the optimized condition for smaller particle size and a higher EE using 3^3 factorial design and Contour plots. The coded or the transformed values are calculated according to the equation.

$$\text{Transformed value} = \frac{Xi - Average\ of\ high\ and\ low\ levels}{\frac{1}{2} difference\ between\ high\ and\ low\ levels} \qquad \text{Eq. 1}$$

The coded values for the dependent variables are tabulated in Table 4.1 and the experimental design and the response is tabulated in Table 4.2. The results obtained were subjected to multiple regression analysis and a polynomial equation was derived based on the results.

Table 4. 1: Coded values of the dependent variables

Coded values	Independent variables		
	Polymer conc. (mg) (X_1)	PVA conc. (%w/v) (X_2)	Organic: aqueous phase volume ratio (X_3)
-1	100	0.5	0.25
0	150	1	0.50
1	200	1.5	0.75

Twenty-seven batches of different combinations were prepared by taking values of selected independent variables (X_1, X_2 and X_3) at different levels (-1, 0, +1) as shown in Table 4.2. The prepared batches were evaluated for entrapment efficiency and particles size (dependent variables). The results are recorded in Table 4.2. Mathematical

modeling of the preparation of PTX loaded PLGA NPs by nanoprecipitation technique was carried out to obtain a second order polynomial equation Eq. 2.

$$Y = b_0 + b_1X_1 + b_2X_2 + b_3X_3 + b_{11}X_{11} + b_{22}X_{22} + b_{33}X_{33} + b_{12}X_1X_2 + b_{23}X_2X_3 + b_{13}X_1X_3 + b_{123}X_1X_2X_3 \quad \text{Eq. 2}$$

Where b_0 is the arithmetic mean response of 27 runs and b_1, b_2 and b_3 is the estimated coefficients for the factors X_1, X_2 and X_3, respectively. The main effects represent the average result of changing one factor at a time from its low to high value. The interactions show the change in particle size when two or more factors are varied simultaneously. The following equations (full model) were derived by the best-fit method to describe the relationship of the particle size (Y) and entrapment efficiency (Y) with the concentration of polymer (X_1), PVA concentration (X_2) and the volume of organic phase (X_3) (Eq. 3 & 4).

$$Y_{PS} = 164.6 + 5.37X_1 + 8.19X_2 - 17.77X_3 - 0.08X_{11} + 0.18X_{22} + 4.88X_{33} + 0.22X_1X_2 - 0.68X_2X_3 + 1X_1X_3 + 0.37X_1X_2X_3 \quad \text{Eq. 3}$$

$$Y_{EE} = 73.13 + 3.84X_1 + 3.12X_2 - 8.27X_3 - 0.22X_{11} - 2.44X_{22} - 6.93X_{33} + 0.04X_1X_2 - 0.05X_2X_3 + 0.23X_1X_3 - 0.57X_1X_2X_3 \quad \text{Eq. 4}$$

Neglecting non-significant ($p > 0.05$) terms from the full model establishes a reduced model (Eq. 5 & 6) which facilitates the optimization technique by plotting contour plots keeping one major contributing independent formulation variable constant and varying other two independent formulation variables, to establish the relationship between independent and dependent formulation variables.

$$Y_{PS} = 164.66 + 5.37X1 + 8.19X2 - 17.77X3 + 4.88X33 \quad \text{Eq. 5}$$

$$Y_{EE} = 72.98 + 3.84X1 + 3.12X2 - 8.27X3 - 2.44X22 - 6.93X33 \quad \text{Eq. 6}$$

4.3.1.1.2 Multiple Regression Analysis

Transformed values of the independent variables; Polymer concentration (X_1), stabilizer concentration (X_2), and Organic: aqueous phase volume ratio (X_3) and its products as in Eq. 1 along with the EE and PS values (dependent variable) were subjected to multiple regression to determine the coefficients (b_0, b_i, b_{ij}, b_{ijk}) and the p-values of each term of the equation. A 2^{nd} order polynomial equation was derived by substituting the values of b_0, b_i, b_{ij}, b_{ijk} in Eq. 2. This equation represents a full model (Eq. 3 & 4). Neglecting non-significant ($p>0.05$) terms from equation 3 & 4, a reduced polynomial equation is obtained (Eq. 5 & 6). Results of ANOVA of full model and reduced model (Table 4.4 and 4.5) was carried out and then F-statistic was applied to check whether the non-significant terms can be omitted or not from the full model. The computed t value and P-value are described in Table 4.3. The coefficient value of variable, X_2 in reduced model for PS (Eq. 5) and variable X_1 in reduced model for EE (Eq. 6) was found to be highest and expected to be major contributing in the preparation of PTX loaded PLGA NPs prepared by nanoprecipitation technique. Hence, it was fixed at -1, 0, and 1 level varying other two independent variables for establishing contour plots.

Table 4. 2: Experimental design for PTX loaded PLGA NPs (n=3)

X_1	X_2	X_3	X_{11}	X_{22}	X_{33}	X_1X_2	X_1X_3	X_2X_3	$X_1X_2X_3$	PS ± SD	EE ± SD
-1	-1	-1	1	1	1	1	1	1	-1	173.0 ± 0.91	64.70 ± 1.29
0	-1	-1	0	1	1	0	0	1	0	180.6 ± 0.29	69.82 ± 0.67
1	-1	-1	1	1	1	-1	-1	1	1	187.0 ± 1.50	71.30 ± 0.98
-1	0	-1	1	0	1	0	1	0	0	182.3 ± 1.78	69.98 ± 2.09
0	0	-1	0	0	1	0	0	0	0	184.0 ± 0.86	77.43 ± 0.45
1	0	-1	1	0	1	0	-1	0	0	192.0 ± 2.40	78.65 ± 1.23
-1	1	-1	1	1	1	-1	1	-1	1	189.0 ± 0.50	70.40 ± 0.87
0	1	-1	0	1	1	0	0	-1	0	197.0 ± 1.08	72.80 ± 0.39
1	1	-1	1	1	1	1	-1	-1	-1	201.0 ± 3.70	79.21 ± 1.52
-1	-1	0	1	1	0	1	0	0	0	152.0 ± 2.81	63.70 ± 0.95
0	-1	0	0	1	0	0	0	0	0	156.4 ± 0.99	66.20 ± 1.28
1	-1	0	1	1	0	-1	0	0	0	160.0 ± 1.52	69.81 ± 2.41
-1	0	0	1	0	0	0	0	0	0	159.7 ± 0.78	68.78 ± 1.64
0	0	0	0	0	0	0	0	0	0	169.3 ± 1.20	76.31 ± 0.32
1	0	0	1	0	0	0	0	0	0	173.5 ± 4.50	77.45 ± 1.18
-1	1	0	1	1	0	-1	0	0	0	164.2 ± 1.12	69.38 ± 0.59
0	1	0	0	1	0	0	0	0	0	171.0 ± 2.03	74.32 ± 1.64
1	1	0	1	1	0	1	0	0	0	175.9 ± 2.10	76.27 ± 0.39
-1	-1	1	1	1	1	1	-1	-1	1	139.0 ± 0.98	49.53 ± 0.75
0	-1	1	0	1	1	0	0	-1	0	143.1 ± 0.56	51.57 ± 3.01
1	-1	1	1	1	1	-1	1	-1	-1	147.0 ± 1.30	58.49 ± 0.43
-1	0	1	1	0	1	0	-1	0	0	145.5 ± 2.32	52.47 ± 1.62
0	0	1	0	0	1	0	0	0	0	147.9 ± 0.74	53.87 ± 2.07
1	0	1	1	0	1	0	1	0	0	156.0 ± 2.21	60.34 ± 0.58
-1	1	1	1	1	1	-1	-1	1	-1	158.0 ± 3.09	56.42 ± 2.10
0	1	1	0	1	1	0	0	1	0	162.5 ± 0.43	59.64 ± 0.79
1	1	1	1	1	1	1	1	1	1	167.0 ± 1.50	62.98 ± 0.81

Table 4. 3: Computed t values and P-values for PS and E.E.

	PS		EE%	
Factor	**Computed t-value**	**P-value**	**Computed t-value**	**P-value**
Intercept	126.3851	1.98E-25	71.78739	1.66E-21
X_1	8.91094	1.33E-07	8.14446	4.39E-07
X_2	13.59218	3.32E-10	6.631951	5.77E-06
X_3	-29.4789	2.26E-15	-17.5493	7.11E-12
X_{11}	-0.0798	0.937382	-0.27612	0.78599
X_{22}	0.17557	0.862834	-2.9938	0.00859
X_{33}	4.676547	0.000253	-8.49036	2.54E-07
X_1X_2	0.304724	0.764504	0.08512	0.933222
X_1X_3	-0.92546	0.368477	-0.09955	0.921941
X_2X_3	1.354328	0.194451	0.412615	0.685365
$X_1X_2X_3$	0.414677	0.683885	-0.81456	0.42728

Table 4. 4: ANOVA of full and reduced models for Particle size

		Df	SS	MS	F	R^2	Adjusted R^2
Regression	FM	10	7576.16	757.61	115.80	0.9931	0.9931
	RM	4	7556.59	1889.14	334.47	0.9838	0.9838
Residual (error)	FM	16	104.67 (E1)	6.54			
	RM	22	124.25 (E2)	5.64			

E1 and E2 indicated Sum of squares of error of full and reduced model respectively; F, Fischer ratio; FM, full model; MS, Mean squares; RM, reduced model; and SS, Sum of squares.

Number of parameters omitted = 6;

†SSE2 – SSE1 = 124.2567-104.6775 = 19.57917

MS of error (full model) = 6.54

§F calculated = (19.57/6)/6.54= 0.4987

F tabulated = 2.741

Since $F_{cal} < F_{tab}$, the omitted parameters are non significant and the hypothesis is accepted.

Table 4. 5: ANOVA of full and reduced models for Entrapment efficiency

		Df	SS	MS	F	R^2	Adjusted R^2
Regression	FM	10	2002.934	200.29	50.027	0.9690	0.9690
	RM	5	1999.222	399.84	123.89	0.9672	0.9672
Residual (error)	FM	16	64.0592 (E1)	4.0037			
	RM	21	67.7713 (E2)	3.2272			

Number of parameters omitted = 5;
†SSE2 – SSE1 = 67.7713 -64.0592 = 3.712081
MS of error (full model) = 4.003
§F calculated = (3.71/5)/4.003= 0.185432
F tabulated = 2.852
Since $F_{cal} < F_{tab}$, the omitted parameters are non significant and the hypothesis is accepted.

4.3.1.1.3 Construction of contour plots

2D contour plots were established using reduced polynomial equation. Values of X_1 and X_3 were computed at prefixed values of particle size for different levels of X_2 and values of X_2 and X_3 were computed at prefixed values of EE for different levels of X_1.

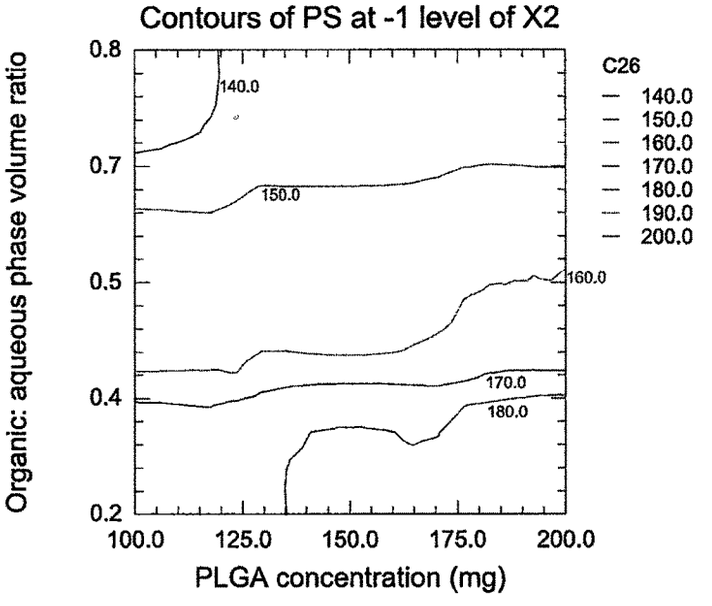

a)

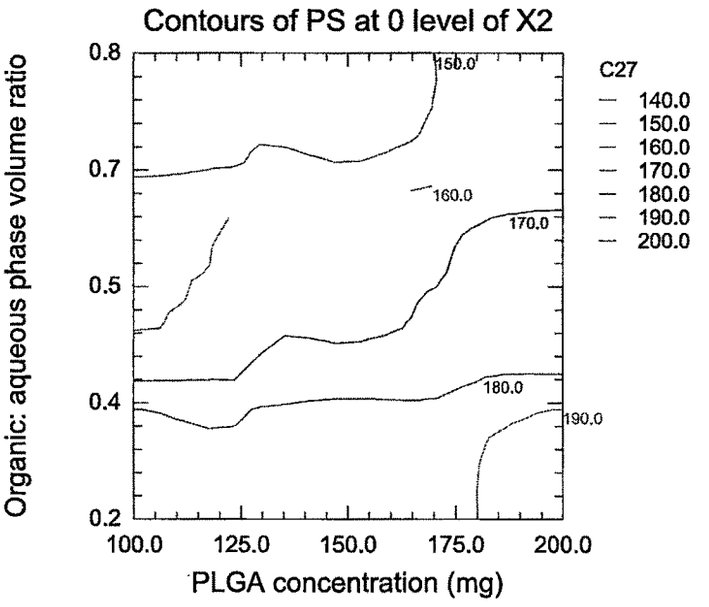

b)

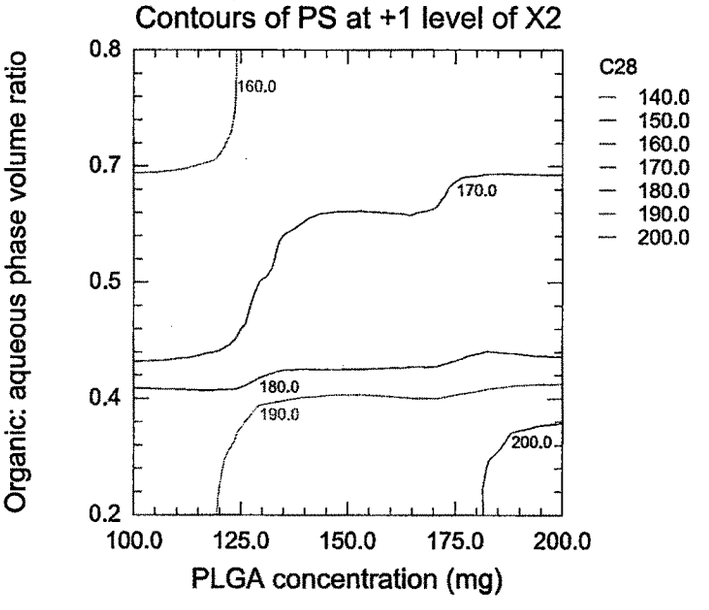

c)

Figure 4. 2: Contour plots of effect of PLGA concentration and Organic to aqueous phase volume ratio on PS a) -1 level of X_2 b) 0 level of X_2 c) +1 level of X_2

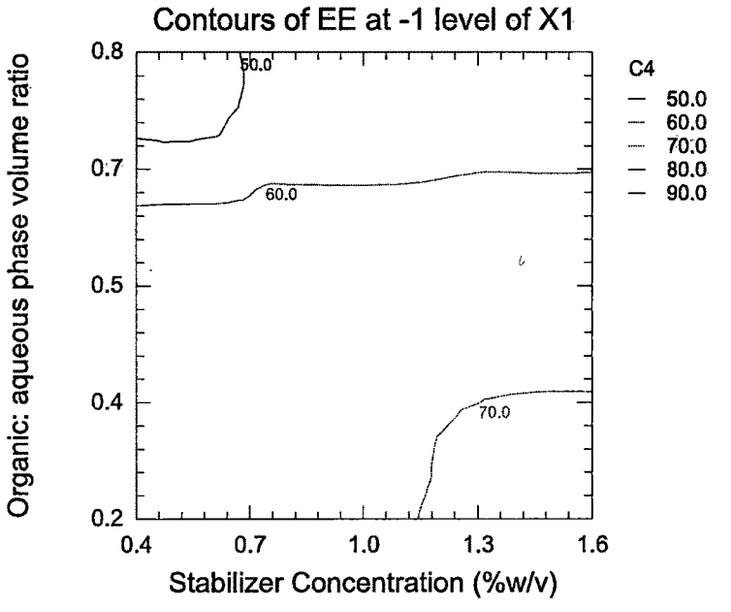
Contours of EE at -1 level of X1
Organic: aqueous phase volume ratio
0.8
0.7
0.5
0.4
0.2
0.4
0.7
1.0
1.3
1.6
Stabilizer Concentration (%w/v)
60.0
60.0
70.0
C4
50.0
60.0
70.0
80.0
90.0

a)

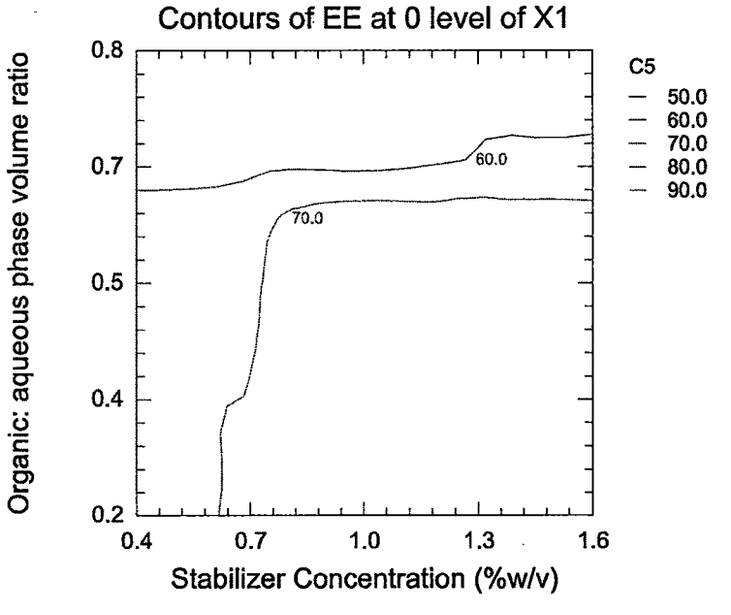
Contours of EE at 0 level of X1
Organic: aqueous phase volume ratio
0.8
0.7
0.5
0.4
0.2
0.4
0.7
1.0
1.3
1.6
Stabilizer Concentration (%w/v)
60.0
70.0
C5
50.0
60.0
70.0
80.0
90.0

b)

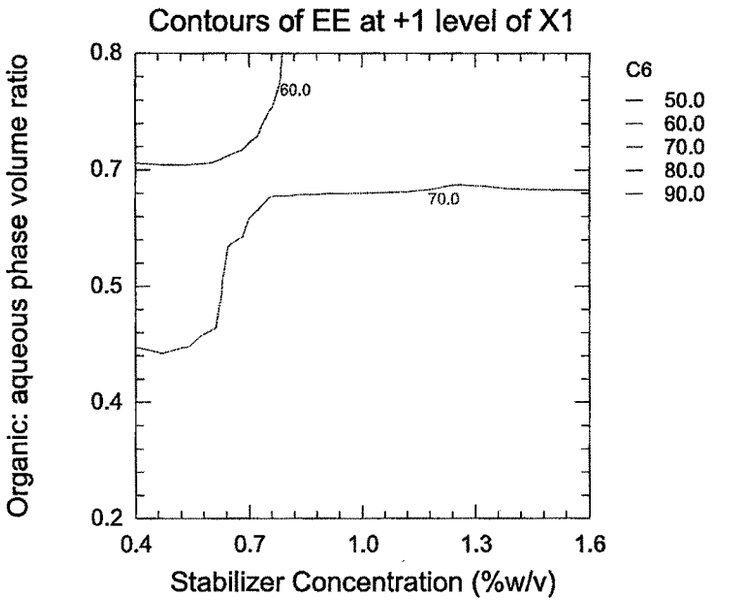

c)

Figure 4. 3: Contour plot of effect of PVA concentration and Organic to aqueous phase volume ratio on EE(a) -1 level of X_2 (b) 0 level of X_2 (c) +1 level of X_2

4.3.1.1.4 Validation of established relationships

A check point analysis was performed to confirm the utility of established contour plots and reduced polynomial equation in the preparation of PTX-PLGA NPs by nanoprecipitation technique. Values of two independent variables were taken from three check points each on contour plots plotted at fixed levels i.e. -1, 0 and 1 of third variable and the values of PDE and PS were generated by NCSS software (Table 4.6). PTX PLGA NPs were prepared experimentally by taking the amounts of the independent variables on the same check points. Each batch was prepared in triplicate and mean values were determined (Table 4.14). Difference of theoretically computed values of entrapment efficiency and particle size and the mean values of experimentally obtained entrapment efficiency and particle size was compared using student 't'test method.

Table 4. 6: Validation of established relationships

Independent variables			Predicted PS (nm)
X_1	X_2	X_3	
135.29	0.5	0.27	179.93
164.70	1.0	0.44	170.17
117.64	1.5	0.76	158.47
Independent variables			**Predicted EE (%)**
X_1	X_2	X_3	
100	0.75	0.34	67.62
150	1.38	0.64	59.83
200	1.24	0.41	77.12

4.3.1.2 Surface modification by coating with Pluronic®P85

The optimized batch of PTX loaded PLGA NPs was surface modified by coating with Pluronic®P85 for possible inhibition of P-gp efflux of PTX. Coating was performed as decribed by Muller and Wallis (1993). Briefly, coating was performed by mixing equal volumes of particle suspension (0.2%) and aqueous solution of Pluronic® P85 (1%) and incubation overnight. After incubation each batch of nanospheres was cleaned of excess surfactant by ultracentrifugation at 20,000 rpm for 30 min. Collect the pellet and redisperse in distilled water.

4.3.1.3 Surface modification by conjugation with Transferrin (Tf)

Conjugation of Tf to the NP surface was carried out by a two step process as described by Sahoo and Labhasetwar, 2005 that involves the activation of NP with an epoxy compound followed by the conjugation of Tf to the activated NP. In the first step, to the lyophilized NPs (5mg/ml) dispersed in borate buffer pH 5.0 (50mM), was added zinc tetrafluoroborate hydrate (0, 3, 6, 10mg) as a catalyst and a solution of SR-4GL (epoxy compound that acts as a linker) (5, 10, 15 mg) in 2mL borate buffer. The reaction mixture was stirred on a magnetic stirrer at 37°C for 30mins. The NPs were centrifuged at 20,000 rpm for 30mins at 4°C and were washed thrice with borate buffer to remove unreacted SR-4GL. In the second step, to the dispersion of the epoxy-activated NPs was added a solution of Tf in borate buffer (5, 10, 15 mg/ml) and the reaction mixture was

stirred for on magnetic stirrer at 37°C for 2hrs. The NPs were centrifuged at 20,000 rpm for 30mins at 4°C, to remove the unreacted transferrin. The NPs were washed twice with borate buffer and were lyophilized for 24hrs.

The amount of the transferrin conjugated to the NP surface was estimated using the BCA protein estimation (Genei, Bangalore). The amount of the transferrin in the supernatant and the washings was subtracted from the amount of the transferrin added for conjugation to get the amount of conjugated transferrin. The amount of Tf associated per mg of NPs was calculated after finding the amount of transferrin conjugated. The % conjugation efficiency was calculated as follows:

$$\%CE = \frac{Amount\ of\ Tf\ conjugated}{Amount\ of\ Tf\ added\ for\ conjugation} * 100 \qquad \text{Eq. 7}$$

4.3.1.3.1 Optimization of the conjugation parameters

The different factors that were found to affect the conjugation of transferrin on NPs surface are concentration of linker and concentration of transferrin added during conjugation process. These different parameters were varied as presented in Table 4.7.

Table 4. 7: Design of experiments for conjugation of Tf to PLGA NPs

Sr. No.	Amount of epoxy linker SR4GL (mg)	Amount of transferrin (mg)
1	5	10
2	10	10
3	15	10
4	10	2.5
5	10	5
6	10	10
7	10	15

4.3.1.4 Preparation of coumarin-6 loaded PLGA NPs, Pluronic®P85 coated and Tf conjugated PLGA NPs

For cell uptake studies NPs were labeled with a lipophilic fluorescent dye coumarin-6, using the same procedure as describe above except that 500µg of the dye was added to organic phase prior to addition into the aqueous phase. The dye acts as a fluorescent probe for NPs and offers a sensitive method to quantitatively determine their intracellular uptake (Panyam et al., 2003). The dye remains associated with the NPs even after their incubation in PBS (Desai et al., 1997).

4.3.1.5 Estimation of residual PVA

The amount of PVA associated with nanoparticles was determined by a colorimetric method based on the formation of a colored complex between two adjacent hydroxyl groups of PVA and an iodine molecule (Joshi et al, 1979). Briefly, 2 mg of lyophilized nanoparticle sample was treated with 2 ml of 0.5 M NaOH for 15 min at 60 °C. Each sample was neutralized with 900 µl of 1 N HCl and the volume was adjusted to 5 ml with distilled water. To each sample, 3 ml of a 0.65 M solution of boric acid, 0.5 ml of a solution of I_2/KI (0.05 M/0.15 M), and 1.5 ml of distilled water were added. Finally, the absorbance of the samples was measured at 690 nm after 15 min incubation.

4.3.1.6 Entrapment efficiency and in-vitro drug release

The drug entrapped was determined by extracting and quantifying the encapsulated PTX. 5mg NPs were dissolved in 5ml acetonitrile and the resulting solution was suitably diluted and measured by UV-Visible spectrophotometer (UV-1601, Shimadzu, Japan) at 230nm. The entrapment efficiency (%) was calculated as a ratio of the total entrapped paclitaxel to the total amount of paclitaxel used.

$$\%EE = \frac{Amount\ of\ drug\ in\ NP}{Amount\ of drug\ added\ in\ formulation} * 100 \qquad \text{Eq. 8}$$

The in-vitro drug release of PTX loaded NPs was carried out in 20% ethanolic phosphate-buffer saline (PBS) pH 7.4 at 37°C (Chen et al., 2001). NPs equivalent to 1mg drug were suspended in 10 ml of PBS in a screw capped tubes, which were placed in a horizontal

shaker bath maintained at 37°C and shaken at 60min^{-1}. At specific time following incubation samples were taken out and centrifuged at 20,000 rpm for 30min. The supernatent was collected and absorbance measured at 230nm on a UV-Visible spectrophotometer.

For coumarin-6 loaded PLGA NPs the estimation of coumarin-6 was done by spectrofluorimetry at excitation and emission wavelength of 435nm and 490nm respectively.

4.3.1.7 Particle size and zeta potential

A 2.0 mg sample of NPs was dispersed in distilled water and subjected to particle size and zeta potential analysis on Zetasizer (Malvern Zetasizer 3000 HAS, Malvern Instruments, Worcestershire, UK) based on the principle of photon correlation spectroscopy.

4.3.1.8 Effect of different cryoprotectants added during freeze drying on stability of NPs

The major limitation of colloidal carriers is their instability i.e. they tend to agglomerate during storage particularly in liquid formulations that be caused due to a greater surface area of the system and the resulting thermodynamic instability that favors aggregation of colloidal particles. Hence do freeze drying of the liquid NPs formulations as it is one of the well established methods of preservation of unstable molecules over a long period of time. To the suspension of the optimized batch from the above studies, different cryoprotectants like lactose, mannitol and trehalose were added in different concentrations before freeze-drying. The effect of these cryoprotectants at different cryoprotectant to nanoparticle ratios (1:1, 2:1 and 3:1) on the redispersibility of the freeze-dried formulations and the size of the nanoparticles before and after freeze-drying was investigated and recorded in Table 4.18.

4.3.1.9 Differential Scanning calorimetry (DSC)

The thermogram characters of PTX loaded PLGA NPs were analyzed by Differential scanning calorimeter (DSC822E, Shimadzu, Japan) using Mettler Toledo star SW 8.01

software. An empty aluminium pan was used as the reference for all measurements. Each sample (4-6mg) was sealed separately in a standard aluminium pan, the samples were purged in DSC with pure dry nitrogen. The temperature ramp speed was set at 10° C/min and nitrogen at 5ml/min, and the heat flow was recorded from 25° C to 300° C, under nitrogen atmosphere.

4.3.1.10 NMR spectroscopy

The proton NMR spectrum of Tf-conjugated NPs was recorded to confirm the conjugation of transferrin to hydroxyl groups on surface of NPs. The NPs were dissolved in DMSO (Merck, Germany) and transferred to a 5 mm NMR tube. NMR tube containing sample was placed in 5 mm broad band probe head and pulse programming was performed using Brucker 300MHz (Switzerland) and the NMR spectra was recorded.

4.3.1.11Transmission electron microscopy

Nanoparticles were dispersed in de-ionized water at a concentration of 1mg/ml. To measure the morphology and size distribution of nanoparticles, a drop of sample was placed onto a 300-mesh copper grid coated with carbon. Approximately 2 min after deposition, the grid was tapped with filter paper to remove surface water and air-dried. Negative staining was performed using a droplet of 0.5% phosphotungstic acid. TEM was performed using Morgagni 268, Philips (Netherlands) transmission electron microscope at 60 kV and 30X.

4.3.2 PTX LOADED POLY(N-BUTYL CYANOACRYLATE) NPS

4.3.2.1 Preparation of PTX loaded poly(n-butylcyano acrylate) (PBCA) NPs

PTX loaded PBCA NPs were prepared by **emulsion polymerization** and **dispersion polymerization** techniques previously described by Huang et al., 2007. Briefly, Paclitaxel was dissolved in monomer with aid of mild heating. NPs were prepared by using an acidic polymerization medium (0.01M HCl, pH 2.5) containing poloxamer 188 as a stabilizer for emulsion polymerization and dextran 70 for dispersion polymerization. To the prepared aqueous acidic polymerization medium, monomer was added dropwise under constant magnetic stirring at 700rpm (Remi equipment Pvt. Ltd., India). The

polymerization was allowed to continue for 4 hours. The NP suspension was neutralized with 0.1N sodium hydroxide solution and stirred for additional 30 minutes to ensure completion of polymerization. Formed drug loaded NPs were separated by ultracentrifugation at 20,000 rpm for 45 min at 4°C (Sigma 3K30, Germany) and pellet redispersed in water and lyophilized (Heto Drywinner, Denmark). The paclitaxel loaded nanoparticles were characterized for drug entrapment efficiency (%), particle size (nm) and zeta potential (mV) and were evaluated for in-vitro drug release. Different formulation and process variables that were found to affect PS and entrapment efficiency are monomer concentration, surfactant/stabilizer concentration, type of surfactant /stabilizer, PTX concentration, speed of stirring, pH of polymerization medium and temperature.

4.3.2.2 Coumarin-6 loaded PBCA NPs

For cell uptake studies NPs were labeled with a lipophilic fluorescent dye coumarin-6, using the same procedure as described for drug loaded NPs except that 500µg of the dye was added instead of drug. The dye acts as a fluorescent probe for NPs and offers a sensitive method to determine intracellular uptake (Panyam et al., 2003). The dye remains associated with the NPs even after their incubation in PBS buffer (Desai et al., 1997).

4.3.2.3 Turbidimetric studies to monitor particle formation

The turbidity measurements of particle formation of PBCA NPs is based on the particle size and the corresponding turbidity of the dispersion. As the formation of nanoparticles is related to increase particle size with corresponding increase in turbidity of the suspension, this method would give a qualitative idea of the particle formation process. For particle formation study polymerization of the PBCA monomer was carried out by EP and DP technique at 25°C and the %Transmittance of the dispersion was monitored continuously in a UV-Visible spectrophotometer (UV 1700, Shimadzu, Japan) at 546nm.

4.3.2.4 Entrapment efficiency and In-vitro drug release

Lyophilized NPs (5mg) were dissolved in 5ml acetonitrile. PTX content was determined by 1st derivative spectroscopy at 248.4 nm on UV Visible Spectrophotometer (UV-1601,

Shimadzu, Japan). The entrapment efficiency (%) was calculated as a ratio of the total entrapped paclitaxel to the total amount of paclitaxel used.

Nanoparticles equivalent to 1mg of drug were dispersed in 10 ml of phosphate buffer (PBS, pH 7.4 containing 20% ethanol) in a capped centrifuge tube and placed in a shaking incubator at 37°C. At predetermined time points, the sample was centrifuged and the supernatant was analyzed at 230nm on a UV-Visible spectrophotometer (UV-1601, Shimadzu, Japan).

4.3.2.5 Particle size and zeta potential analysis:

Lyophilized PBCA-NPs (2mg) were suspended in 10mL of deionized water and mixed for 5 min on a vortex mixer. The particle size and zeta potential were determined by photon correlation spectroscopy using Zetasizer (Malvern Zetasizer 3000 HAS, UK)

4.3.2.6 Effect of different cryoprotectants added during freeze drying on stability of NPs

To the suspension of the optimized batch from the above studies, different cryoprotectants like glucose, mannitol and trehalose were added in different concentrations before freeze-drying. The effect of these cryoprotectants at different ratios of cryoprotectant to nanoparticles (1:1, 2:1 and 3:1) on the redispersibility of the freeze-dried formulations and the size of the nanoparticles before and after freeze-drying was investigated and recorded in Table 4.26.

4.3.2.7 FTIR studies

IR spectra of the monomer and the polymer were recorded on Shimadzu Fourier transform infrared spectrophotometer (Shimadzu, Japan).

4.3.2.8 Differential scanning calorimetry (DSC) studies

The thermogram characters of PTX loaded PBCA NPs were analyzed by Differential scanning calorimeter (Mettler Toledo star SW 8.01). An empty aluminium pan was used as the reference for all measurements. Each sample (4-6mg) was sealed separately in a standard aluminium pan, the samples were purged in DSC with pure dry nitrogen at

5ml/min. The temperature ramp speed was set at 10° C/min and the heat flow was recorded from 25° C to 300° C, under nitrogen atmosphere.

4.3.2.9 Molecular weight determination

Gel permeation chromatography was carried out to determine the molecular weights of the formed polymers. The molecular weights of BCA polymer was determined by gel permeation chromatography (GPC) equipped with a Waters 510 pump, 50, 10-3 and 10-4 °A Phenogel columns serially set (Phenomenex, USA) and a Waters 410 differential refractometer. The mobile phase was tetrahydrofuran (THF) at a flow rate of 1.0 ml/min. Purified polymer was dissolved in THF to the concentration of 2% (w/v) and 50 µl of it was injected to the system.

4.3.2.10 NMR spectroscopy

The proton NMR spectrum of PBCA NPs was recorded to confirm complete conversion of monomer into polymer. The NPs were dissolved in DMSO (Merck, Germany) and transferred to a 5 mm NMR tube. NMR tube containing sample was placed in 5 mm broad band probe head and pulse programming was performed using Brucker 300MHz (Switzerland) and the NMR spectra was recorded.

4.3.2.11 Transmission electron microscopy

Sample preparation was done as described for PLGA NPs and images were taken on Morgagni 268, Philips (Netherlands) transmission electron microscope.

4.3.3 PTX LOADED DYNASAN®118 (GLYCERYL TRISTEARATE) (GTS) SLN

4.3.3.1 Partitioning of PTX between lipids and distilled water

5 mg of PTX was dispersed in a mixture of melted lipid (1 g) and 1 ml of hot distilled water and shaken in a hot water bath (maintained at 10°C above the melting point of the lipid under investigation) using mechanical shaker for 30 min (Venkateswarulu et al., 2004). The aqueous phase was separated from the lipid by centrifugation of the above mixture at 25,000 rpm for 20 min in a high speed centrifuge (Sigma, 3K30, Germany). The clear supernatant obtained after centrifugation was diluted suitably with $CHCl_3$:

MeOH (1:1) and PTX content was determined spectrophotometrically at 230nm against solvent blank. The partition coefficient of PTX in lipid / distilled water was calculated as following

$$\text{Partition coefficient} = \frac{Amount\ of\ PTX\ added - Amount\ of\ PTX\ in\ Dist.Water}{Amount\ of\ PTX\ in\ Dist.Water} \quad \text{Eq. 9}$$

Different lipids tested were stearic acid, Compritol®888 ATO (Mixture of mono, di and tri glycerides of behenic acid), Dynasan®118 (Tristearin D18), Precirol®ATO5 (Glyceryl distearate).

4.3.3.2 Preparation of PTX loaded Glyceryl tristearate (GTX) SLN

Based on preliminary experiments critical formulation parameters i.e. Drug: lipid ratio, Concentration of lecithin (lipid composition) and surfactant concentration were identified as the major factors contributing to the PS and EE% of the SLN. Further optimization of PTX loaded GTS SLN was done by 3^3 factorial design (27 batches were prepared) followed by multiple regression analysis. PTX loaded GTS (Dynasan®118) solid lipid nanoparticles were prepared by solvent diffusion method as reported by Yuan et al., 2008 as per the experimental design in Table 4.9. Briefly, appropriate quantities of drug, lipid and lecithin were dissolved in 5ml isopropyl alcohol (IPA) at 75°C in a water bath. The dissolved lipid, and drug mixture was added to 40 ml of Pluronic®F68 solution previously heated at same temperature while stirring at 500rpm on a magnetic stirrer. Keep it in heated condition for 10min and then rapidly cool the dispersion in an ice-bath (2-3°C) for the SLN to solidify. The SLN in dispersion was aggregated by adding 0.1 mL of 10 mg/mL protamine sulfate solution, and the dispersion was centrifuged at 8000 rpm (Remi cooling centrifuge, Mumbai, India) to obtain the pellet. 0.1 ml of the supernatant was diluted suitably with CHCl3: MeOH (1:1) and the free drug content was determined in a UV-visible spectrophotometer (Shimadzu, Japan) at 230 nm against suitable solvent blank. The pellet obtained was washed with distilled water and lyophilized.

4.3.3.2.1 3^3 factorial design

Based on the results obtained in preliminary experiments, drug: lipid ratio, concentration of lecithin i.e. lipid composition and surfactant concentration were found

to be the major independent variables in determining the two dependent variables particle size (nm) and entrapment efficiency (%). Hence these variables were selected to find the optimized condition for smaller particle size and a higher EE using 3^3 factorial design and Contour plots. The coded or the transformed values are calculated according to the equation Eq.1. The coded values for the dependent variables are tabulated in Table 4.8 and the experimental design and the response is tabulated in Table 4.9. The results obtained were subjected to multiple regression analysis and a polynomial equation was derived based on the results.

Table 4. 8: Coded values of the dependent variables

Coded values	Dependent variables		
	Drug: lipid ratio	Concentration of lecithin (%w/w of total lipid)	Surfactant concentration (%w/v)
-1	1:10	10	0.5
0	1:15	20	1.0
1	1:20	30	1.5

Twenty seven batches of different combinations were prepared by taking values of selected variables; X_1, X_2 and X_3 at different levels as shown in Table 4.8. The prepared batches were evaluated for entrapment efficiency and particle size; dependent variables. The results are recorded in Table 4.9. Mathematical modeling of the preparation of PTX loaded GTS SLN by solvent diffusion technique was carried out to obtain a second order polynomial equation Eq.2.

Where b_0 is the arithmetic mean response of twenty seven runs and b_1, b_2 and b_3 are estimated coefficients for the factors X_1, X_2 and X_3 respectively. The main effects represent the average result of changing one factor at a time from its low to high value. The interactions show the change in particle size when two or more factors are varied simultaneously. The following equations (full model) were derived by the best-fit method to describe the relationship of the particle size (Y) and entrapment efficiency (Y) with the Drug: lipid ratio (X_1), Concentration of lecithin (X_2) and the concentration of surfactant (X_3) (Eq. 10 & 11).

$$Y_{PS} = 224.86 + 4.9X_1 - 6.77X_2 - 9.92X_3 - 0.35X_{11} + 0.71X_{22} - 1.55X_{33} - 0.09X_1X_2 + 2.74X_2X_3 + 1.51X_1X_3 - 0.037X_1X_2X \quad \text{Eq. 10}$$

$$Y_{EE} = 81.27 + 2.66X_1 + 2.45X_2 + 1.04X_3 + 0.22X_{11} - 0.07X_{22} - 1.96X_{33} + 0.22X_1X_2 - 0.425X_2X_3 + 0.41X_1X_3 - 0.35X_1X_2X_3 \quad \text{Eq. 11}$$

Neglecting nonsignificant ($p > 0.05$) terms from the full model establishes a reduced model (Eq. 12 & 13) which facilitates the optimization technique by plotting contour plots keeping one major contributing independent formulation variable constant and varying other two independent formulation variables, to establish the relationship between independent and dependent formulation variables.

$$Y_{PS} = 224.06 + 4.9X_1 - 6.77X_2 - 9.92X_3 + 2.74X_2X_3 \quad \text{Eq. 12}$$

$$Y_{EE} = 81.36 + 2.66X_1 + 2.45X_2 + 1.04X_3 - 1.96X_{33} \quad \text{Eq. 13}$$

4.3.3.2.2 Multiple Regression Analysis

Transformed values of independent variables; drug: lipid ratio (X_1), concentration of lecithin (X_2) and surfactant concentration (X_3) and its products as in equation 2 along with the entrapment efficiency and particle size values (dependent variable) were subjected to multiple regression to determine the coefficients (b_0, b_i, b_{ij}, b_{ijk}) and the p-values of each term of the equation. A second order polynomial equation was derived by substituting the values of b_0, b_i, b_{ij}, b_{ijk} in equation 2. This equation represents a full model (Eq. 10 & 11). The terms of full model having p-values non-significant ($p>0.05$) have negligible contribution in determining the response variable and are thus neglected. Neglecting non-contributing terms of equation 10 & 11 gave a reduced polynomial equation 12 & 13. Results of ANOVA of full model and reduced model (Table 4.11 and 4.12) was carried out and then F-statistic was applied to check whether the non-significant terms can be omitted or not from the full model. The computed t value and p-value are described in Table 4.10. The coefficient value of variable, drug: lipid ratio (X_1) in reduced model for particle size and EE was found to be highest and expected to be major contributing in the preparation of PTX loaded GTS SLN prepared by solvent diffusion technique. Hence, it was fixed at -1, 0, and 1 level varying other two independent variables for establishing contour plots.

Table 4. 9: Experimental design for PTX loaded GTS SLN (n=3)

X_1	X_2	X_3	X_{11}	X_{22}	X_{33}	X_1X_2	X_1X_3	X_2X_3	$X_1X_2X_3$	PS ± SD	EE ± SD
-1	-1	-1	1	1	1	1	1	1	-1	238.4 ± 4.3	73.13 ± 1.24
0	-1	-1	0	1	1	0	0	1	0	241.5 ± 2.8	74.86 ± 1.87
1	-1	-1	1	1	1	-1	-1	1	1	249.2 ± 6.4	77.18 ± 0.79
-1	0	-1	1	0	1	0	1	0	0	231.8 ± 6.1	76.73 ± 1.16
0	0	-1	0	0	1	0	0	0	0	237.1 ± 5.6	79.32 ± 2.01
1	0	-1	1	0	1	0	-1	0	0	225.7 ± 7.2	82.17 ± 0.68
-1	1	-1	1	1	1	-1	1	-1	1	219.0 ± 3.7	78.24 ± 0.92
0	1	-1	0	1	1	0	0	-1	0	226.7 ± 5.3	80.16 ± 1.07
1	1	-1	1	1	1	1	-1	-1	-1	231.8 ± 4.2	83.46 ± 1.85
-1	-1	0	1	1	0	1	0	0	0	228.0 ± 4.5	76.32 ± 2.34
0	-1	0	0	1	0	0	0	0	0	231.4 ± 6.3	78.16 ± 1.46
1	-1	0	1	1	0	-1	0	0	0	242.3 ± 2.8	81.74 ± 2.13
-1	0	0	1	0	0	0	0	0	0	219.5 ± 3.5	78.34 ± 0.96
0	0	0	0	0	0	0	0	0	0	224.0 ± 8.2	82.52 ± 1.37
1	0	0	1	0	0	0	0	0	0	230.7 ± 5.7	83.19 ± 1.62
-1	1	0	1	1	0	-1	0	0	0	211.8 ± 7.3	82.10 ± 0.87
0	1	0	0	1	0	0	0	0	0	216.9 ± 2.9	84.68 ± 1.15
1	1	0	1	1	0	1	0	0	0	221.3 ± 8.5	85.27 ± 1.39
-1	-1	1	1	1	1	1	-1	-1	1	210.3 ± 5.9	75.86 ± 0.74
0	-1	1	0	1	1	0	0	-1	0	216.5 ± 3.4	77.89 ± 1.14
1	-1	1	1	1	1	-1	1	-1	-1	222.1 ± 4.6	83.09 ± 1.53
-1	0	1	1	0	1	0	-1	0	0	209.6 ± 7.2	76.34 ± 1.86
0	0	1	0	0	1	0	0	0	0	213.9 ± 4.9	79.12 ± 2.51
1	0	1	1	0	1	0	1	0	0	220.0 ± 2.6	83.25 ± 1.75
-1	1	1	1	1	1	-1	-1	1	-1	203.0 ± 4.3	80.19 ± 2.37
0	1	1	0	1	1	0	0	1	0	210.7 ± 1.9	82.46 ± 3.49
1	1	1	1	1	1	1	1	1	1	216.5 ± 3.7	85.78 ± 0.97

Table 4. 10: Computed t values and P-values for PS and E.E.

	PS		EE%	
Factor	**Computed t-value**	**P-value**	**Computed t-value**	**P-value**
Intercept	115.4795	8.36E-25	155.9656	6.85E-27
X_1	5.436087	5.49E-05	11.02756	6.93E-09
X_2	-7.5193	1.23E-06	10.15927	2.2E-08
X_3	-11.0078	7.11E-09	4.313831	0.000535
X_{11}	-0.22774	0.822734	0.537213	0.598513
X_{22}	0.455478	0.654886	-0.18483	0.855683
X_{33}	-0.99636	0.333907	-4.70859	0.000237
X_1X_2	-0.08303	0.934854	-0.76726	0.454104
X_1X_3	1.373836	0.188436	1.416037	0.175937
X_2X_3	2.483473	0.024474	-1.4386	0.169537
$X_1X_2X_3$	-0.02774	0.978216	-0.97078	0.346103

Table 4. 11: ANOVA of full and reduced models for Particle size

		Df	SS	MS	F	R^2	Adjusted R^2
Regression	FM	10	3167.40	316.74	21.6576	0.9312	0.8882
	RM	4	3121.37	780.34	61.3074	0.9176	0.9027
Residual (error)	FM	16	233.99 (E1)	14.624			
	RM	22	280.02 (E2)	12.72			

E1 and E2 indicated Sum of squares of error of full and reduced model respectively; F, Fischer ratio; FM, full model; MS, Mean squares; RM, reduced model; and SS, Sum of squares.

Number of parameters omitted = 6;

†SSE2 – SSE1 =280.02-233.99 = 46.026

MS of error (full model) = 14.624

§F calculated = (46.026/6)/14.624= 0.524

F tabulated = 2.741

Since $F_{cal} < F_{tab}$, the omitted parameters are non significant and the hypothesis is accepted.

Table 4. 12 ANOVA of full and reduced models for Entrapment efficiency

		Df	SS	MS	F	R^2	Adjusted R^2
Regression	FM	10	284.37	28.43	27.1526	0.9443	0.9095
	RM	4	278.16	69.54	66.6156		
Residual (error)	FM	16	16.757 (E1)	1.047			
	RM	22	22.966 (E2)	1.043			

Number of parameters omitted = 6;
†SSE2 – SSE1 = 22.966 – 16.757 = 6.209
MS of error (full model) = 1.047
§F calculated = (6.209/6)/1.047= 0.9881
F tabulated = 2.741
Since $F_{cal} < F_{tab}$, the omitted parameters are non significant and the hypothesis is accepted.

4.3.3.2.3 Construction of contour plots

2D contour plots were established using reduced polynomial equation. Values of X_2 and X_3 were computed at prefixed values of particle size and entrapment efficiency for different levels of X_1.

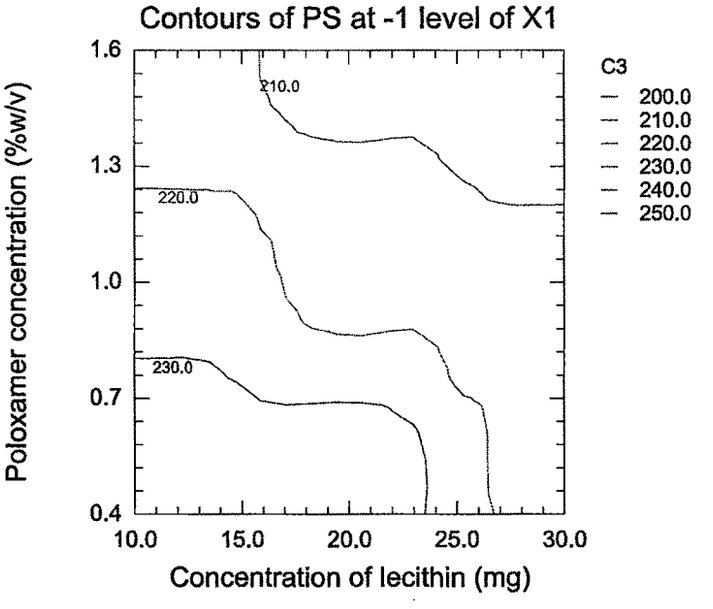

a)

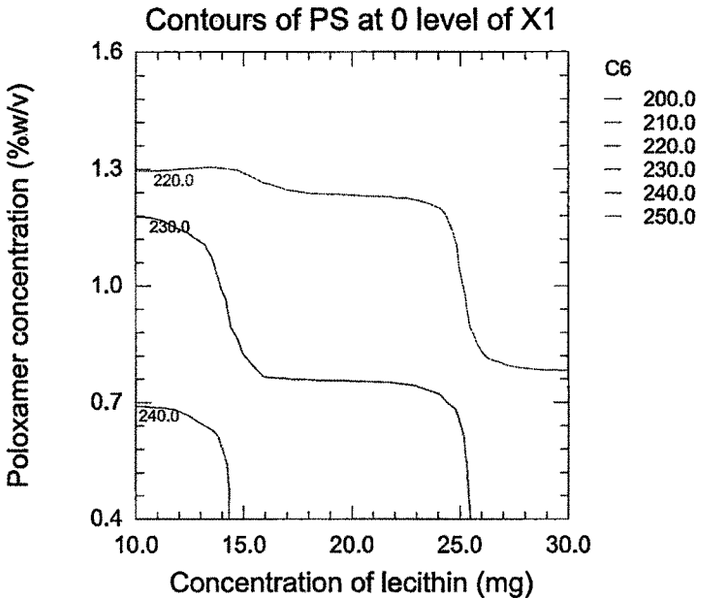

b)

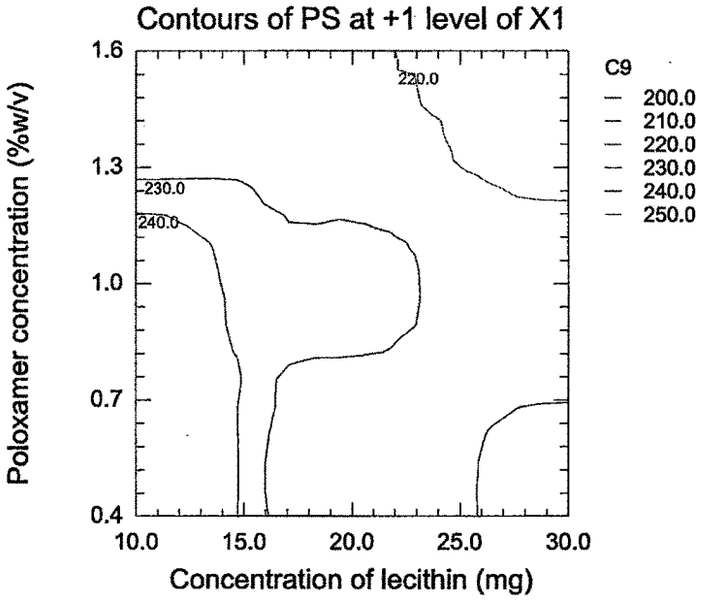

c)

Figure 4. 4: Contour plots of effect of concentration of lecithin and poloxamer on PS (a) -1 level of X_2 (b) 0 level of X_2 (c) +1 level of X_2

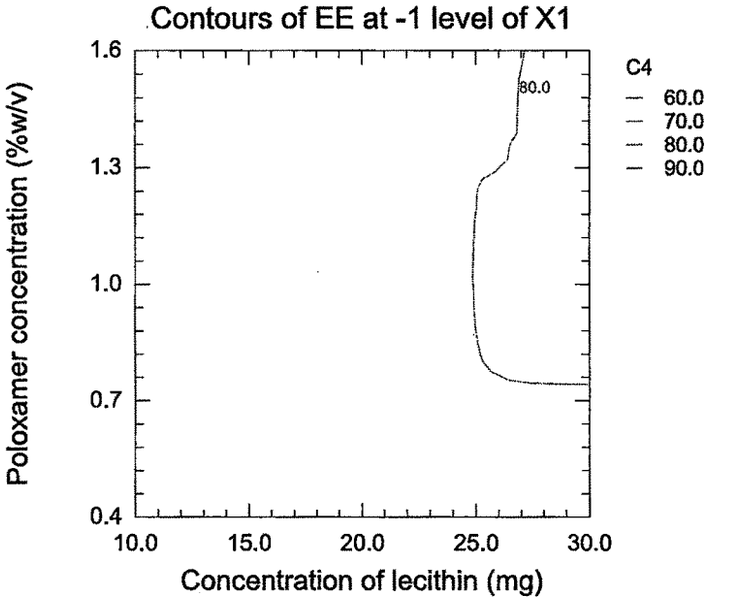
Contours of EE at -1 level of X1
Poloxamer concentration (%w/v)
1.6
1.3
1.0
0.7
0.4
10.0
15.0
20.0
25.0
30.0
Concentration of lecithin (mg)
80.0
C4
60.0
70.0
80.0
90.0

a)

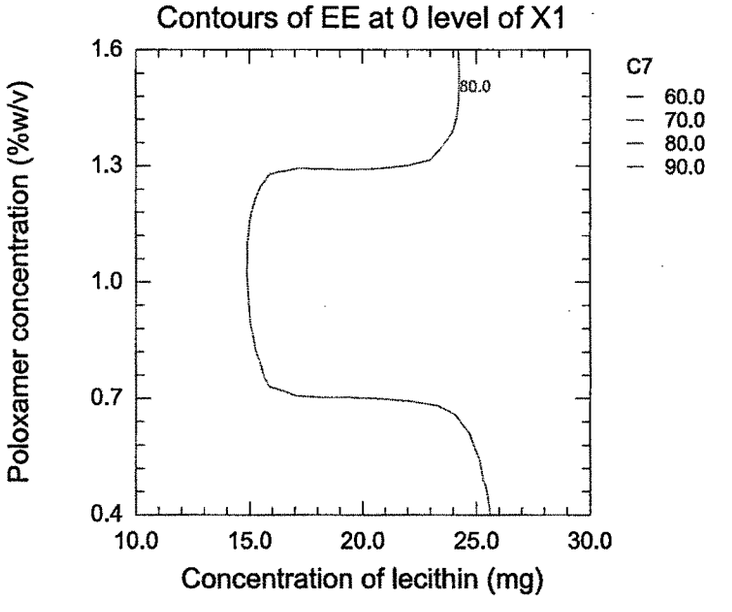
Contours of EE at 0 level of X1
Poloxamer concentration (%w/v)
1.6
1.3
1.0
0.7
0.4
10.0
15.0
20.0
25.0
30.0
Concentration of lecithin (mg)
80.0
C7
60.0
70.0
80.0
90.0

b)

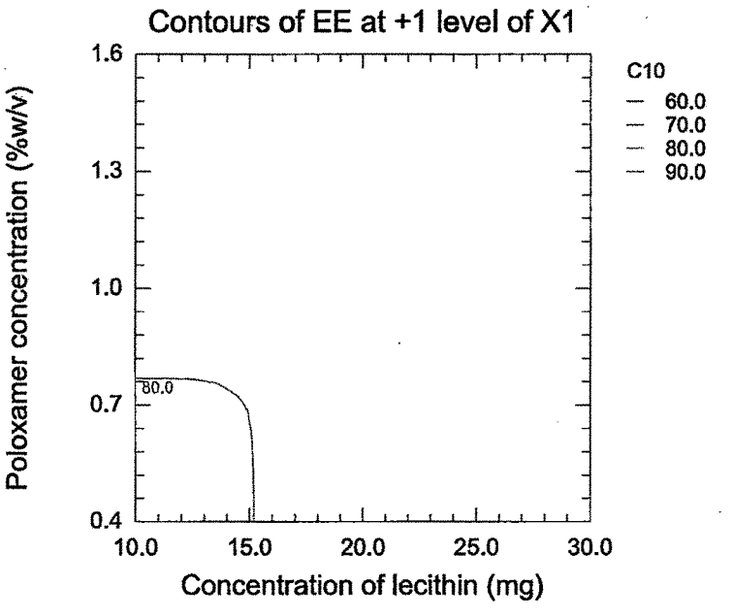

c)

Figure 4. 5: Contour plots of effect of concentration of lecithin and poloxamer on PS (a) -1 level of X_2 (b) 0 level of X_2 (c) +1 level of X_2

4.3.3.2.4 Validation of established relationships

A check point analysis was performed to confirm the utility of established contour plots and reduced polynomial equation in the preparation of PTX-GTS SLN. Values of independent variables (X_1 and X_2) were taken from three check points each on contour plots plotted at fixed levels i.e. -1, 0 and 1 of X_3 and the values of PDE and PS were generated by NCSS software (Table 4.13). PTX GTS SLN were prepared experimentally by taking the amounts of the independent variables (X_1 and X_2) on the same check points. Each batch was prepared in triplicate and mean values were determined Table 4.28. Difference of theoretically computed values of entrapment efficiency and particle size and the mean values of experimentally obtained entrapment efficiency and particle size was compared using student 't'test method.

Table 4. 13: Validation of established relationships

Independent variables			Predicted PS (nm)	Predicted EE (%)
X_1	X_2	X_3		
1:10	15.88	0.75	225.9	77.33
1:15	22.94	1.38	214.2	79.45
1:20	26.47	1.45	216.9	85.55

4.3.3.3 Preparation of coumarin-6 loaded GTS SLN

For cell uptake studies NPs were labeled with a lipophilic fluorescent dye coumarin-6, using the same procedure as described for drug loaded NPs except that 500μg of the dye was added instead of drug.

4.3.3.4 Entrapment efficiency and in-vitro drug release

The SLN dispersion was aggregated by adding 0.1 mL of 10 mg/mL protamine sulfate solution, and the dispersion was centrifuged at 8000 rpm (Remi cooling centrifuge, Mumbai, India) to obtain the pellet. 0.1 ml of the supernatant was diluted suitably with CHCl3: MeOH (1:1) and the free drug content was determined in a UV-visible spectrophotometer (Shimadzu, Japan) at 230 nm against suitable solvent blank. The pellet obtained was washed with distilled water and lyophilized. Accurately weighed lyophilized powder was dissolved in a mixture of methanol-chloroform (1:1); and suitably diluted with the same solvent mixture and analyzed in a UV-visible spectrophotometer at 230 nm against suitable solvent blank. The % entrapment efficiency was calculated as a ratio of the total entrapped paclitaxel to the total amount of paclitaxel used. For coumarin-6 loaded GTS SLN the estimation of coumarin-6 was done by spectrofluorimetry at excitation and emission wavelength of 435nm and 490nm respectively.

The in-vitro drug release of PTX loaded GTS SLN was carried out in 20% ethanolic phosphate-buffer saline (PBS) pH 7.4 at 37°C (Chen et al., 2001). NPs equivalent to 1mg drug were suspended in 10 ml of PBS in a screw capped tubes, which were placed in a horizontal shaker bath maintained at 37°C and shaken at $60min^{-1}$. At specific time following incubation samples were taken out and centrifuged at 20,000 rpm for 30min.

The supernatant was collected and absorbance measured at 230nm on a UV-Visible spectrophotometer.

4.3.3.5 Particle size and zeta potential

A 2.0 mg sample of NPs was dispersed in distilled water and subjected to particle size and zeta potential analysis on Zetasizer (Malvern Zetasizer 3000 HAS, UK) based on the principle of photon correlation spectroscopy.

4.3.3.6 Effect of different cryoprotectants added during freeze drying on stability of NPs

To the suspension of the optimized batch from the above studies, different cryoprotectants like glucose, mannitol and trehalose were added in different concentrations before freeze-drying. The effect of these cryoprotectants at different ratios of cryoprotectant to nanoparticles (1:1, 2:1 and 3:1) on the redispersibility of the freeze-dried formulations and the size of the nanoparticles before and after freeze-drying was investigated and recorded in Table 4.29.

4.3.3.7 Differential Scanning calorimetry (DSC)

The thermogram characters of PTX loaded GTS SLN were analyzed by Differential scanning calorimeter (Mettler Toledo star SW 8.01). An empty aluminium pan was used as the reference for all measurements. Each sample (4-6mg) was sealed separately in a standard aluminium pan, the samples were purged in DSC with pure dry nitrogen. The temperature ramp speed was set at 10° C/min and nitrogen at 5ml/min, and the heat flow was recorded from 25° C to 300° C, under nitrogen atmosphere.

4.3.3.8 X ray diffraction studies

Powder X-ray diffraction patterns were obtained using an X-ray diffractometer (Philips PW 1710) with Cu Kα radiation generated at 30 mA and 40 kV. X-ray diffraction patterns of plain PTX, bulk GTS, PTX loaded GTS SLN are shown in Figure 4.27.

4.3.3.9 Transmission electron microscopy

Nanoparticles were dispersed in de-ionized water at a concentration of 1mg/ml. To

measure the morphology and size distribution of nanoparticles, a drop of sample was placed onto a 300-mesh copper grid coated with carbon. Approximately 2 min after deposition, the grid was tapped with filter paper to remove surface water and air-dried. Negative staining was performed using a droplet of 0.5% phosphotungstic acid. Transmisssion electron microscopy was performed using Morgagni 268, Philips (Netherlands) transmission electron microscope at 60kV and 20X.

4.3.3.10 Determination of in vitro steric stability by electrolyte induced flocculation test

The electrolyte induced flocculation test was performed for SLN dispersions stabilized with 1.0% poloxamer 188. The effect of poloxamer 188 on the ability of the SLN to resist electrolyte induced flocculation was investigated by this test. Sodium sulphate solutions ranging from 0 M to 1.5 M were prepared in 16.7 %w/v sucrose solution (Subramanian et al., 2003). An appropriate volume of SLN dispersion was made up to 5 ml using the sodium sulphate solutions of varying concentrations (0 M,0.3 M,0.6 M,0.9 M,1.2 M and 1.5 M) to obtain a final concentration of 1mg/ml lipid. The absorbance of the resulting dispersions was measured within 5 min at 400 nm using a UV–Visible spectrophotometer (Shimadzu, Japan) against respective blank.

4.3.4 STABILITY STUDIES

Stability is defined as the capacity of a drug substance or drug product to remain within established specifications to maintain its identity, strength, quality, and purity throughout the retest or expiration dating periods (Draft guidance, Stability Testing of Drug Substances and Drug Products, FDA, 1998). Stability testing provides evidence that the quality of a drug substance or drug product under the influence of various environmental factors changes with time (ICH Draft guidance, Stability Testing of New Drug Substances and Products, Q1A (R2), 2003). Nanoparticles have been extensively used to deliver a wide range of drugs as they can protect the drug from metabolizing enzymes, Long-term stability of PBCA nanoparticle suspensions sustain the release, be administered orally or injected locally, and target specific tissues by incorporating surface ligand moieties. During preparation, particulate delivery systems are lyophilized and, although compactly arranged, can be readily resuspended in aqueous media after

being stored at 4°C. However, storage temperature is important in maintaining the integrity of these delivery systems.

In general, "significant change" for a drug product is defined as:

1. A 5% change in assay from its initial value;
2. Any degradation product's exceeding its acceptance criterion;
3. Failure to meet the acceptance criteria for appearance, physical attributes, and functionality test (e.g., particles size, drug content and zeta potential)
4. Failure to meet the acceptance criteria for in-vitro drug release.

4.3.4.1 Stability testing protocol

The stability studies were performed for the lyophilized nanoparticles. The samples were kept in transparent glass vials and stored at 5°C ± 3°C (in refrigerator) and at 25°C ± 2°C/60 ± 5%RH. At different time points the samples were withdrawn and were subjected to particle size, zeta potential and drug content studies. At the end of six months drug release study was also performed for different NPs formulations. During sampling, the vials were visually examined for the evidence of caking and discoloration.

4.4 Results and Discussion

4.4.1 PTX LOADED PLGA NPS

4.4.1.1 Preparation and optimization of PTX loaded PLGA NPs

Nanoprecipitation technique involves a spontaneous gradient-driven diffussion of amphiphilic organic solvents into the continous aqueous phase. This process may apparently appear simple, but it may involve complex interfacial hydrodynamic phenomenon. Here the addition of acetonic-oily solution of polymer and drug resulted in spontaneous emulsification of the oily solution in the form of nanodroplets. This occurs as a result of some kind of interface instability arising from rapid diffusion of the acetone across the interface and marked decrease in the interfacial tension. The origin of the mechanism of nanosphere formation could be explained in terms of interfacial turbulence between two unequilibrated liquid phases, involving flow, diffusion and surface processes (Marangoni effect). Davis and Rideal, 1962 suggested that the interfacial turbulence is caused by localized lowering of the interfacial tension where the

oil phase undergoes rapid and erratic pulsations each of which is quickly damped out by a viscous drag. The molecular mechanism of interfacial turbulence could be explained by the continuous formation of eddies of solvent (e.g. acetone) at the interface. Such eddies originate either during drop formation or in thermal inequality in the system. Thus, once the process has started, movements associated with previous kicks change the pressure inside the solvent by increasing the surface pressure inside the solvent or decreasing the interfacial tension. Thus, if the solvent droplets formed contain polymer, these will tend to aggregate and form nanoparticles because of continuous diffusion of solvents and because of the presence of a non-solvent medium (Guerrero et al., 1998). Among various factors, solute transfer out of the phase of higher viscosity, concentration gradients near the interface and interfacial tension sensitive to solute concentration are the most important factors. The presence of surfactant may markedly complicate the situation since they act to suppress interfacial flow and the rapid diffusion of acetone to the aqueous phase. The main advantage of surfactants in process is the instantaneous and reproducible formation of nanometric, monodispersed nanospheres exhibiting a high drug loading capacity (Fessi et al., 1989; Derakhshandeh et al., 2007).

As the organic phase along with acetone, ethanol was selected to study the effect of a non-solvent (PLGA is insoluble in ethanol) water miscible organic solvent on NP properties. Ethanol in the organic phase will reduce the solubility of PLGA in organic solvent which in turn will initiate early precipitation of the polymer upon contact with the aqueous phase and formation of a polymeric wall at a shorter distance from the primary nanodroplet centre, associated with a decrease in the size of NPs (Chorny et al., 2002). This technique is inferior to other formulation procedures in terms of achievable drug loading probably due to high affinity of the drug for the organic solvents used during nanosphere preparation that causes diffusion of the drug away from the polymer matrix and hence more amount of polymer is required to get desired drug loading (Layre et al., 2005; Musumeci et al., 2006).The zeta potential value is an important particle characteristic as it can influence both particle stability as well as particle mucoadhesion. More pronounced zeta potential values, being positive or negative, tend to stabilize particle suspensions. The electrostatic repulsion between particles with the same

electrical charge prevents the aggregation of the spheres (Feng and Huang, 2001).

Effect of polymer concentration on PS and EE

The effect of the concentration of the PLGA tested is negative or positive. A positive effect would imply that increasing the concentration causes the emulsion to have larger droplets, hence leading to larger particles. A negative effect means that increasing the concentration causes the emulsion to be more stable, hence leading to smaller particles. The stabilizing properties of the polymers can be explained by their viscosity, their ability to lower surface tension or their three dimensional structure at the interface (Couvreur et al., 1997). PLGA concentration had a positive effect on particle size i.e. a dramatic increase in particle size ($p < 0.05$) was observed that can be attributed to increase in viscosity of the organic phase which led to a reduction in net shear stress and promoting the formation of droplets with larger size. Also the increased viscosity of the organic phase would hinder rapid dispersion of PLGA solution into the aqueous phase resulting in larger droplets. These large droplets would form larger NPs as the solvent evaporates (Govender et al., 2000; Chorny et al., 2002). In addition, as the polymer concentration increases the amount of PVA (stabilizer) that is available is insufficient to cover the surface of droplets completely resulting in coalescence of droplets during solvent evaporation and hence aggregation of NPs occurs with a resulting increase in the hydrodyanamic diameter of the NPs. Increase in PLGA concentration also increased the entrapment efficiency of PTX probably due to the increased viscosity of the solution resulting in increase in drug's diffusional resistance into the aqueous phase and thus enhance the entrapment efficiency of PTX in NPs (Song et al., 2008a). Additionally, the increase of particle size may be relevant to the increase of drugs entrapment efficiencies (Budhian et al., 2007). The increase of nanoparticles size with the increasing PLGA concentration can increase the length of diffusional pathways of drugs from the organic phase to the aqueous phase, thereby reducing the drug loss through diffusion and increasing the drugs entrapment efficiencies (Song et al., 2008b). As the polymer concentration increases there is an increase in the zeta potential towards the negative side because of the improperly shielded functional groups on the surface.

Effect of PVA concentration on PS and EE

With increase in PVA concentration the particle size of PLGA NPs was found to increase which may be attributed to the increased viscosity of the external phase that caused a decrease in net shear stress resulting in increased particle size (Budhian et al., 2007). The miscibility of acetone with aq. PVA solution results in partitioning of PVA into the polymeric part of the organic phase. More molecules of PVA can be physically incorporated onto the NPs surface (Boury et al., 1995; Rodriguez et al., 2004). Hence a large number of hydroxyl groups extending into the medium could be hydrated forming a hydrated layer at the surface of NPs surface to hinder nanoparticle aggregation. Increase in PVA concentration had a positive effect on entrapment efficiency. With increase in PVA concentration, more molecules of PVA would be adsorbed onto the surface of nanoparticles (PVA effectively covers the surface of NPs) hence resulting in a decrease in porosity of the NPs and hence an increase in entrapment efficiency (Rizkalla et al., 2006). As the amount of surfactant increases there is a decrease in zeta potential. PLGA NPs prepared without any surfactant has a negative zeta potential of -45.2mV which tends to decrease as the amount of surfactant increases because the surfactant effectively shields the functional groups on the NPs surface that inturn shifts the shear plane outwards, resulting in a reduction of the zeta potential (Ballard et al., 1984).

Effect of Organic: aqueous phase volume ratio on PS and EE

Organic: aqueous phase volume ratio was found to have a profound effect on particle size and entrapment efficiency. As the ratio was increased the particle size decrease as well as the entrapment decreased. This can be attributed to faster solvent evaporation and faster polymer precipitation at lower ratios which leads to formation of more porous NPs. The more porous structure provides more mobility to the polymer chains and allows water to plasticize the polymer chains. This leads to an increase in particle size at lower ratios (Hyvonen et al., 2005). As the ratio increases the entrapment decreases because the evaporation rate of solvent is less and the drug diffuses into the aqueous phase and also the viscosity of the organic phase is less at higher ratios. Hence the droplet size formed before precipitation is smaller resulting lower entrapment efficiency (Chorny et al., 2002, Song et al., 2008).

4.4.1.1.1 Optimization and multiple regression analysis

27 batches of PTX loaded PLGA NPs were prepared by nanoprecipitation technique by using 3^3 factorial design varying three independent variables i.e. Polymer concentration, stabilizer concentration and organic: aqueous phase volume ratio. The NPs were characterized for particle size and entrapment efficiency and recorded in Table 4.2. The results were subjected to multiple regression analysis using Microsoft Excel 2007 to obtain a full model equation (Eq. 3 & 4).

The main effects of X_1, X_2 and X_3 represent the average result of changing one variable at a time from its low to high value. The interactions (X_1X_2, X_1X_3, X_2X_3 and $X_1X_2X_3$) show how the response changes when two or more variables were simultaneously changed. The significance of each coefficient of the equation of full model was determined by student't' test and p-value, which are listed in Table 4.3. The larger the magnitude of the t value and the smaller the p value, the more significant is the corresponding coefficient (Adinarayana et al, 2002; Akhnazarova et al, 1982). This implies that the quadratic main effects of the independent variables in the present study are very significant for PS and EE. The second order main effects of only organic to aqueous phase volume ratio is very significant for PS but for EE the second order main effects of stabilizer concentration and organic to aqueous phase volume ratio are found to be significant as is evident from their p-values. The interaction between X_1X_2, X_1X_3, X_2X_3 and $X_1X_2X_3$ are found to be non-significant from their p-values.

F statistic was applied to the results of analysis of variance (ANOVA) of full model and reduced model to check whether the non-significant terms can be omitted or not from the full model. For both the case $F_{cal} < F_{tab}$ (0.498 < 2.741 at α=0.05, V1= 6and V2= 16 for PS and 0.185 < 2.852 at α=0.05, V1= 5 and V2= 16 for EE) which indicates that the neglected terms do not significantly affect the PS and EE and therefore the hypothesis is accepted. The goodness of fit of the model was checked by the determination coefficient (R^2). In this case, the values of the determination coefficients (R^2 = 0.9863 for full model and 0.9838 for reduced model of PS and R^2 = 0.9690 for full model and 0.9672 for reduced model of EE) indicated that over 90 % of the total variations are explained by the model. The values of adjusted determination coefficients (adj R^2 = 0.9778 for full

model and 0.9808 for reduced model of PS and adj R^2 = 0.9496 for full model and 0.9594 for reduced model of EE) are also very high which indicates a high significance of the model. A higher values of correlation coefficients (R = 0.9931 for full model and 0.9918 for reduced model for PS and R = 0.9843 for full model and 0.9834 for reduced model of EE) signifies an excellent correlation between the independent variables (Box et al, 1978). All the above considerations indicate an excellent adequacy of the regression model (Adinarayana et al, 2002; Akhnazarova et al, 1982; Box et al, 1978; Cochran et al, 1992; Yee et al, 1993).

4.4.1.1.2 Validation of established relationships

At fixed levels of -1, 0 and 1 of independent variable X2, three check points were selected each on three plotted contours for PS and at fixed levels of X1 three check points were selected from the contours for EE. The computed particle size (nm) and entrapment efficiency (%) values from the contours at -1, 0 and 1 level are tabulated (Table 4.6). PTX-PLGA NPs at these three checkpoints were prepared experimentally using the same procedure keeping the other process variables as constants with the amounts of independent variables at the selected check points. The experiment was repeated three times and the experimentally obtained mean PS (nm) and EE (%) values were shown in Table 4.14. Both experimentally obtained and theoretically computed PDE values were compared using student 't' test and the difference was found to be non significant ($p>0.05$). This proves the role of a derived reduced polynomial equation and contour plots in the preparation of PTX PLGA NPs of predetermined PS and EE (%).

Table 4. 14: Experimental and predicted values of Particle size and entrapment efficiency (n=3)

Independent variables			Predicted PS (nm)	Experimental PS (nm) ± SD
X_1	X_2	X_3		
135.29	0.5	0.27	179.93	180.0 ± 1.09*
164.70	1.0	0.44	170.17	169.5 ± 0.07*
117.64	1.5	0.76	158.47	157.8 ± 0.42*
Independent variables			**Predicted EE (%)**	**Experimental EE (%) ± SD**
X_1	X_2	X_3		
100	0.75	0.34	67.62	68.02 ± 0.08*
150	1.38	0.64	59.83	60.65 ± 1.36*
200	1.24	0.41	77.12	76.98 ± 0.85*

*The difference between predicted and experimental response is non-significant (p>0.05)

4.4.1.2 Surface modification by coating with Pluronic®P85

The use of pluronic® block copolymers to treat drug resistant cancers is a rapidly developing area of drug delivery for cancer chemotherapy. Studies by Alakhov et al., 1996 have demonstrated the Pluronic® block copolymers sensitize resistant cancer cell line (that express P-glycoprotein) resulting in increase in cytotoxic activity of the drug by 2-3 orders of magnitude. The use of Pluronics® has also been reported for resistant tumors in-vivo. Hence, in an attempt to increase the cytotoxicity of PTX towards resistant tumors coating of NPs with Pluronic®P85 was done. It was observed that after coating the mean PS of the NPs increase by ~10nm due to the coating layer thickness.

4.4.1.3 Surface modification by conjugation with Transferrin

PTX a potent anticancer agent has serious side effects which limit its clinical usefulness. In order to avoid the toxic effects, different approaches to target the drug specifically to tumor tissue have been investigated. These include formulating the drug into colloidal carrier systems like NPs, liposomes, micelles etc., and then conjugation with tumor specific ligands. Targeting via Tf receptors is an important approach as Tf receptors are over-expressed 2- to 10- folds in most cancer cells. In the present study Tf was chemically coupled to the hydroxyl groups of the surface PVA (estimated to be 5.89 ±

1.34%) associated with the NP surface through a multifunctional epoxy compound, SR4GL. It is a hexa epoxy; atleast one of its epoxy groups may have been conjugated to the hydroxyl group of the PVA associated with NPs, and the other epoxy groups to the amine group of Tf (Figure 4.6). It has been reported that PVA forms an interconnected network at the NP interface and remains bound to the particle surface despite repeated washing, and thus can be used for surface modification of NPs (Sahoo et al., 2002). The effect of different variables affecting conjugation of Tf onto NPs surface and particles size after conjugation is shown in Table 4.15. From the results the optimized concentration of catalyst was found to be 6mg as below 6 mg the amount of Tf conjugation is less and above 6 mg not much increase in Tf conjugation is found but a significant increase in particle size has been observed. The linker was optimized at a concentration of 10 mg as more concentration of linker increases the particle size significantly. The amount of Tf added was 10mg as good conjugation was obtained but with increased amount of Tf the conjugation has to be compromised with the particle size. 1H NMR spectroscopy to determine the chemical composition of Tf conjugated NPs demonstrated a peak at 2.2 ppm, confirming that the amino group of Tf has conjugated to epoxy groups (Figure 4.7). The amount of Tf conjugated to NPs was 32.8 ± 0.873 µg/mg of NPs with a conjugation efficiency of 6.56 ± 1.23% with respect to the amount of Tf added during conjugation.

Table 4. 15: Variables affecting Tf conjugation and PS during conjugation

Sr. No.	Amount of linker	Amount of transferrin	Conjugation efficiency (%)	Surface transferrin (µg of Tf/mg NPs)	PS (nm)
1	5	10	4.81	24.08	173
2	10	10	6.56	32.8	182
3	15	10	7.52	37.64	211
4	10	2.5	12.3	15.37	170
5	10	5	12.64	31.6	178
6	10	10	6.56	32.8	182
7	10	15	4.98	37.35	202

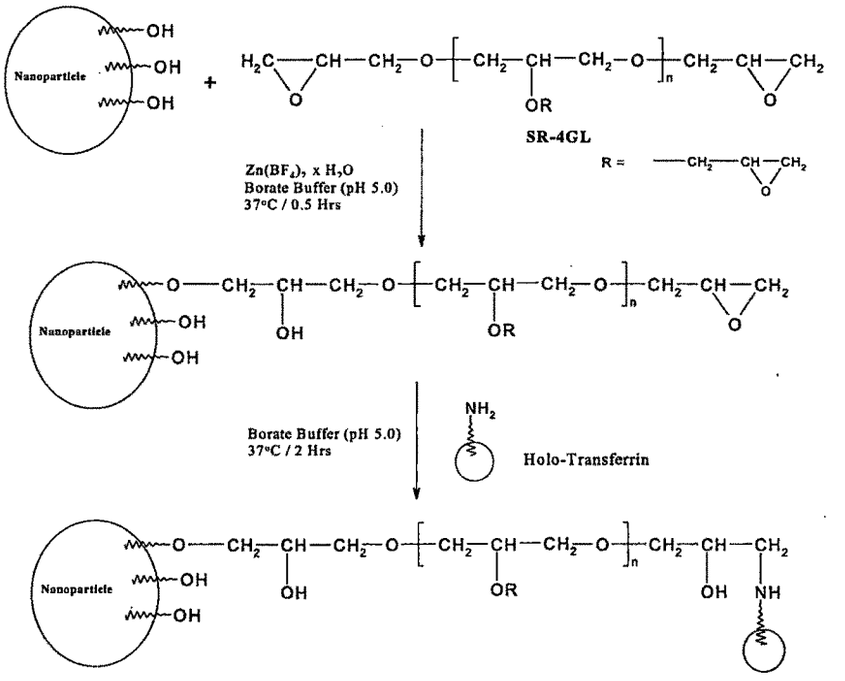

Figure 4. 6: Schematic diagram of conjugation of Tf on PLGA NP surface

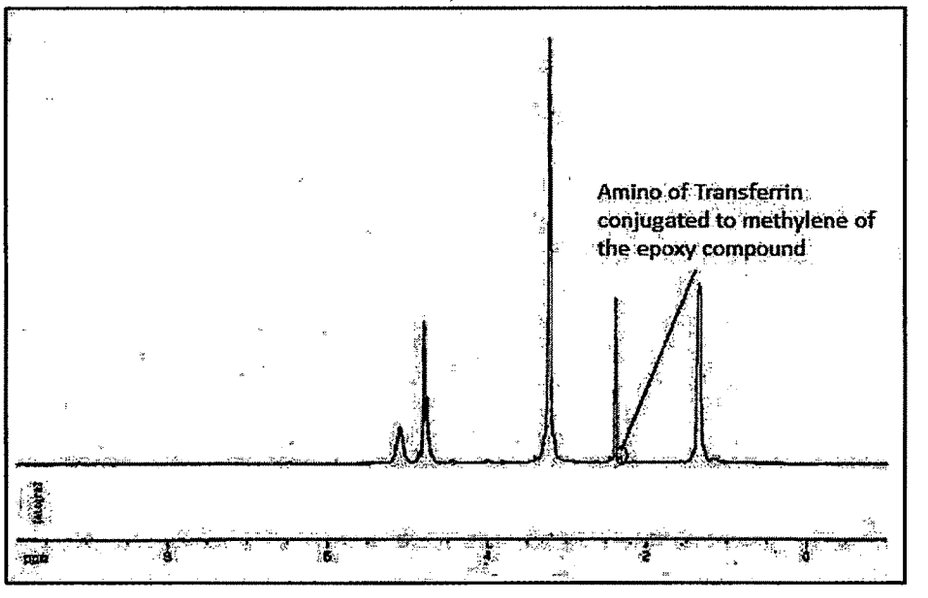

Figure 4. 7: NMR spectra of Tf conjugated to PLGA NPs

4.4.1.4 Estimation of residual PVA

One of the important parameters to be estimated in this case is the residual PVA content as it has been reported that NPs with high amounts of surface PVA may have lower cellular uptake despite their lower particle size. It has been demonstrated that a

fraction of PVA used in formulation of NPs was shown to remain associated with NPs despite repeated washings (Surface associated PVA) and forms NP interface. It is the hydroxyl groups of this surface PVA that are used for epoxy activation followed by conjugation with transferrin (Sahoo et al., 2002). The residual PVA on PTX loaded PLGA NPs was estimated to be 5.89 ± 1.34%.

4.4.1.5 Characterization of PTX loaded NPs

The optimized batches of PTX loaded PLGA NPs (concentration of lipid 150mg, 1% w/v PVA and 0.5 as the ratio of organic to aqueous phase), Pluronic®P85 coated PLGA NPs and transferrin conjugated PTX loaded PLGA NPs (10mg SR4GL and 10mg Tf) were characterized for particle size, entrapment efficiency and zeta potential. NPs demonstrated a mean hydrodynamic diameter of 169.3 ± 4.16nm with a polydispersity index of 0.014 suggesting a uniform particle size distribution. Conjugation reaction slightly increased the mean PS of NPs to 182.8 ± 3.78. The EE (%) was found to be 76.31 ± 0.88 % in case of unconjugated NPs and pluronic®P85 coated NPs exhibited a slight decrease in EE where as Tf conjugated NPs had an EE of 69.47 ± 1.76 attributed to the loss of surface drug fractions during incubation and conjugation purpose. The zeta potential of Tf conjugated nanoparticles was slightly more negative than unconjugated ones that can be attributed to charge contributed by Tf. By coating the NPs surface with nonionic surfactant Pluronic®P85 the charge decreases.

Table 4. 16: Characterization of PTX loaded PLGA, Pluronic®P85 coated PLGA NPs and Tf-PLGA NPs

(n=3)	Unconjugated NPs	NPs Coated with Pluronic®P85	Tf-conjugated PLGA NPs
Particle size (nm)	169.3 ± 4.16	180 ± 5.32	182.8 ± 3.78
Entrapment efficiency (%)	76.31 ± 0.88	75.87 ± 0.95	69.47 ± 1.76
Zeta potential (mV)	-8.4 ± 1.61	-3.45 ± 0.58	-11.72 ± 2.27
µg of Tf/mg of NPs	-	-	32.8 ± 0.873

4.4.1.6 Coumarin-6 loaded PLGA NPs

Particles labelled with fluorescent dyes are frequently used to study cellular uptake quantitatively using a microplate reader and qualitatively by flourescence/confocal microscopy. Coumarin-6 is a lipophilic flourescent dye that is encapsulted in NPs for intracellular uptake studies. The major advantage of it is its high fluorescence even at low dye loading in NPs. It has been reported that only 0.6 % of the incorporated dye could leach from the NPs over 48 hrs. Hence it can be assumed that the dye does not leach from the NPs during the experimental time frame and therefore the fluorescence seen in the cells is caused by NPs and not by the free dye. The PS and EE for coumarin-6 loaded NPs are tabulated in Table 4.17.

Table 4. 17: Characterization of coumarin-6 loaded PLGA NPs

(n=3)	Unconjugated NPs	NPs coated with Pluronic® (P85)	Tf-conjugated PLGA NPs
Particle size (nm)	175 ± 3.46	185.4 ± 2.38	189.3 ± 1.21
Entrapment efficiency (%)	98.36 ± 4.71	90.75 ± 1.24	87.42 ± 2.39
Zeta potential (mV)	-8.03 ± 2.09	-5.43 ± 0.43	-12.36 ± 1.78
µg of Tf/mg of NPs)	-	-	30.22 ± 0.85

4.4.1.7 Effect of different cryoprotectants added during freeze drying on stability of NPs

Freeze-drying has been the most utilized drying method of nanoparticle suspensions. It is a promising way to increase chemical and physical stability of NPs over extended period of time. Transformation of the NPs suspension into a solid form will prevent Ostwlad ripening and avoid hydrolysis reaction. It is expected that solid state of lyophilizates would have a better chemical and physical stability than aqueous dispersions. Two important transformations occur during the process. The 1st is from aqueous dispersion to powder which involves freezing of the sample and evaporation of water under vacuum. Freezing of the sample might cause instability due to the freezing out effects which results in changes of osmolarity and pH. The second transformation is

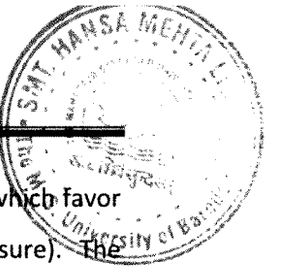

resolubilization of the powder. Here atleast in initial stages, situations arise which favor particle aggregation (low water and high particle content, high osmotic pressure). The protective effect of the surfactant can be compromised by lyophilization. After freeze drying, easy and rapid reconstitution and non-Significant changes particle size of the product are important features. In order to decrease NPs aggregation and to obtain a dry product addition of cryoprotectors will be necessary. For nanoparticles carbohydrates have been perceived to be suitable cryoprotectants since they are chemically innocuous and can be easily vitrified during freezing. There are considerable differences in the cryoprotective abilities of different carbohydrates. Cryoprotectants decrease the osmotic activity of water and crystallization and favor the glassy state of the frozen samples. They are space holders which prevent the contact between the discrete NPs. Furthermore, they interact with the polar head groups of the surfactants and serve as a kind of "pseudo hydration shell" (Mahnert and Mader, 2001). It could be expected that particle size would increase after lyophilization, because nanoparticles tend to aggregate during this process. If the aggregated particles do not separate during redispersion, then larger particle sizes will be measured. Cryoprotectant when present at the nanoparticle surface, protects the particles from aggregation and make sure the redispersion requires a minimum of energy, being attributed to the formation of a steric barrier between the particles during lyophilization or to a stabilization of the particle dispersion due to electrostatic repulsions (Quintanar-Guerrero et al., 1998; Vandervoort and Ludwig 2002). Typical cryoprotectors are sorbitol, mannitol, lactose, glucose, trehalose. Carbohydrates like mannitol and lactose can separate from frozen solution in the form of crystalline phases (Franks, 1998) whereas glucose and trehalose form amorphous masses at very temperatures (Saez et al., 2000). The optimized batch of nanoparticles was lyophilized using different concentrations of glucose, mannitol and trehalose. The redispersibility of the freeze-dried formulations, particle size and zeta potential of the nanoparticles before and after freeze-drying was measured and recorded in Table 4.18. Significant increase in PS was measured in the absence of cryoprotectant. Glucose was not effective cryoprotectant at any concentration. Reconstitution of NPs to which glucose was added was more difficult compared to other formulations because of the sticky nature of of the freeze dried cake, while NPs with other cryoprotectant showed a fluffy porous cake after freeze drying.

Table 4. 18: Effect of different cryoprotectants on the particle size and redispersion

Cryoprotectant (CP)	NPs: CP	Particle size (nm)		Sf/Si	Redispersibility
		Before (Si)	After (Sf)		
None	-	173	897.3	5.18	Aggregates and difficult to redisperse
Glucose	1:1	173	-	-	Solid mass, no redispersion
	1:2	173	544.95	3.15	Difficult
	1:3	173	494.78	2.86	Difficult
Mannitol	1:1	154	405.02	2.63	Flakes/Aggregates
	1:2	154	334.18	2.17	Difficult
	1:3	154	224.84	1.46	Easy
Trehalose	1:1	169	342.76	2.04	Easy
	1:2	169	182.59	1.08	Easy
	1:3	169	180.83	1.07	Easy

Sameti et al., 2003 have reported that after freeze drying, condensed and salt-like residues were obtained for glucose while residues appeared voluminous and snow like for trehalose and mannitol. Mannitol gave a good redispersiblity at NPs: CP ratio of 1:3 but the particle size was very high. Mannitol is known to show polymorphism and has a strong tendency to crystallize (Yu et al., 1998). Trehalose at 2 times w.r.t to the total solid content was found to be optimum to be added during freeze drying for preserving the particle size of the NPs. The cryoprotective effect was attributed to the ability of the sugar additive to form a glassy amorphous matrix around the particles, preventing the particles from sticking together during removal of water (Konan et al., 2002). Hence trehalose was found to be the best as a cryoprotectant to preserve the initial properties of NPs suspension after freeze drying.

4.4.1.8 In-vitro drug release

Different groups round the globe have described the drug release mechanism from PLGA based matrices. PLGA degrades by hydrolysis of its ester linkages in the presence of water. In general the mechanism by which active agent is released from a delivery vehicle is a combination of diffusion of the active agent from the polymer matrices, bulk erosion of the polymer, swelling and degradation of the polymer. The degradation of PLGA is slow, therefore the release of PTX from NPs may depend on drug diffusion and PLGA surface and bulk erosion or swelling (Mu and Feng 2003). The curves of release of PTX from PLGA NPs depict a bi-phasic drug release (Figure 4.8). PTX release from NPs involved an initial rapid release phase followed by a lag phase of relatively slow release. A high initial burst was observed which can be attributed to the immediate dissolution and release of PTX adhered on the surface and located near the surface of the NPs (Magenheim et al., 1993). It is evident from the curves that about 30% of the drug is released within 24 hrs in case of unconjugated NPs whereas, no initial burst is observed in case of Pluronic®P85 coated and Tf-conjugated PTX PLGA NPs due to absence of drug on the surface of conjugated NPs. The initial burst for unconjugated nanoparticles could be due to the diffusion release of drugs distributed at or just beneath the surface of the NPs. Then release is mainly due to the diffusion of drug molecules through the polymeric matrix of the NPs afterwards, the matrix material would require time to erode in the aqueous environment, and then the release mechanisms of surface release and polymer erosion might be the main causes of the release behavior (Esmaeili et al., 2008). 82% of the drug is released within 21 days in case of Pluronic®P85 coated PTX PLGA NPs. About 83% of the drug is released in 18 days in unconjugated NPs whereas in Tf conjugated NPs the drug release after 21 days was found to 80%.

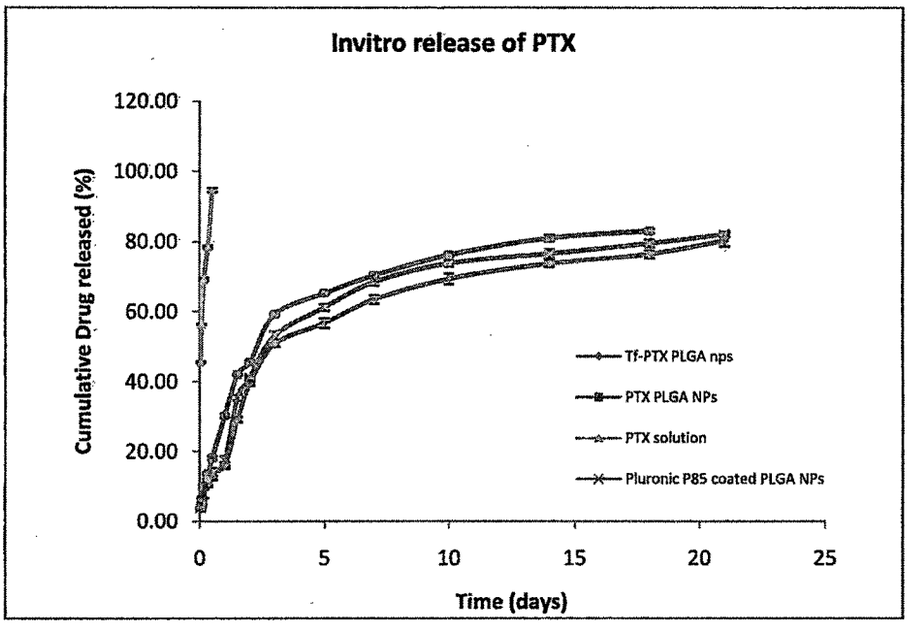

Figure 4. 8: In-vitro release of PTX in pH 7.4 PBS containing 20% ethanol

4.4.1.9 DSC studies

DSC thermograms demonstrated that only pure Tx had an endothermic peak of melting at 215-217°C whereas control or drug-loaded NPs had no such peak in the range 150-250 °C (Figure 4.9). The results thus indicate that Tx encapsulated in NPs is in the amorphous or disordered-crystalline phase of a molecular dispersion or in the solid-state solubilized form in the polymer matrix of NPs after fabrication (Mu and Feng, 2002, Esmaeili et al., 2008).

4.4.1.10 Transmission electron microscopy

TEM images of Conjugated and unconjugated nanoparticles reveal the spherical shape and smooth surface of the NPs. It confirms the particle size in the nanometric range. The spherical nature of the NPs was not altered after conjugation. In case of conjugated NPs a corona appears around the NPs surface which may be due to the Tf molecules attached on the surface. There is a difference in PS measured by TEM and PCS. PCS technique measures the hydrodynamic diameter and hydration of the surface associated PVA probably contributes toward the hydrodynamic diameter of NPs (Sahoo et al., 2005).

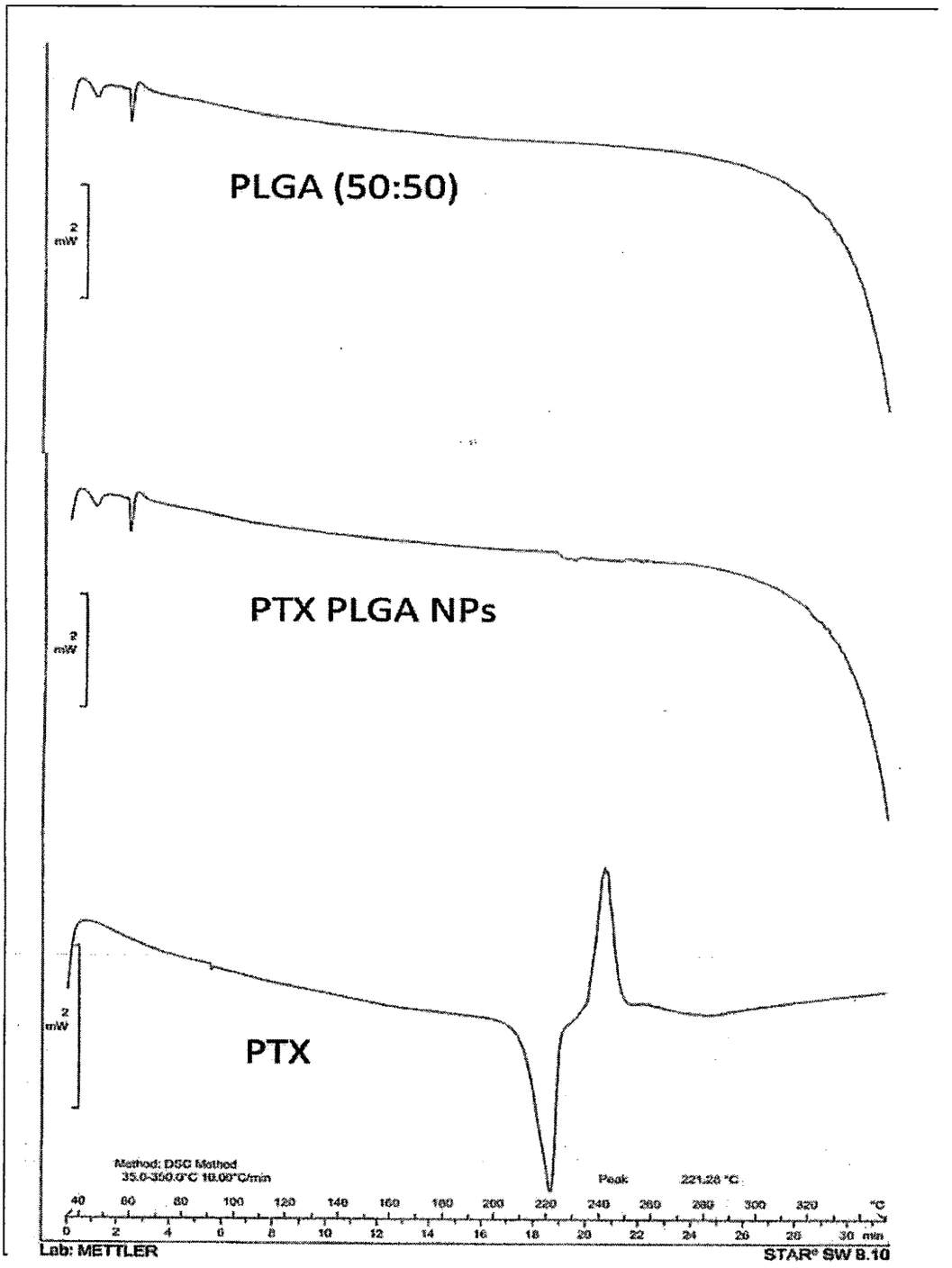

Figure 4. 9: DSC thermograms

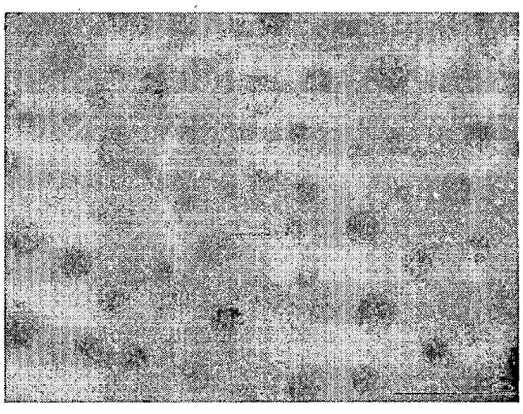

a)

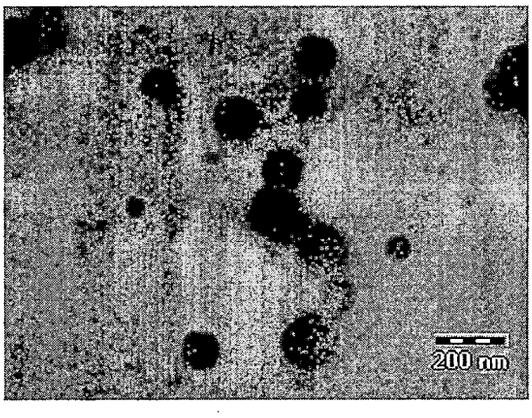

b)

Figure 4. 10: TEM images of PLGA NPs (a) unconjugated (b) Tf- conjugated

4.4.2 PTX LOADED PBCA NPS

4.4.2.1 Preparation and optimization of PTX loaded PBCA NPs

Anionic polymerization of cyanoacrylate monomers in aqueous acidic media (Figure4.11) containing a stabilizer leads to the formation of nanoparticles with high porosity and smooth surface (Couvreur et al., 1979; Kreuter 1983). The various experimental parameters that influenced the particle size and entrapment efficiency are 1) monomer concentration 2) concentration and type of steric stabilizer 3) pH of the polymerization medium 4) drug concentration 5) polymerization temperature. Size is one of the most important features of nanoparticles that governs the body distribution of the NPs. Other parameters, such as molecular weight and density, influence drug release from nanoparticles degradation properties, whereas charge, surface, hydrophilicity, and

hydrophobicity influence the interaction with the biological environment. Mechanism of anionic polymerization of the monomer in aqueous media is illustrated in Figure 4.11.

Mechanism of Emulsion Polymerization:

Polymerization of monomers in the presence of surfactants above the CMC of surfactant generally leads to the formation of particles with smaller size (Bhawal et al., 2002). Emulsion polymerization proceeds with high rate of polymerization with the formation of high molecular weight polymer with a small particles size. CMC of Poloxamer 188 (polyoxyethylene polyoxypropylene block copolymer) is 4.8×10^{-4}M. Polymerization of PBCA NPs was carried in the presence of Poloxamer 188 solution above CMC by anionic polymerization in acidic medium by slow addition of monomer into the aqueous phase. Here the polymerization is initiated first in micelles and then proceeds in primary particles. Micelles formed by the surfactant in aqueous phase takes up monomer to form swollen structures (Dunn et al., 1997). The entry of hydroxyl ions into the monomer swollen micelles initiates polymerization to form primary particles and then a small amount of surfactant is transferred from micelles to its surface, where it acts as a stabilizing agent. Consequently, surfactant in the free state disappears quickly and so do the micelles (Ballard et al., 1984). The function of surfactant at this stage has become as that of a protective colloid. The polymerization continues until all the monomer in the droplets is utilized. The entry of free radical (Hydroxyl ion) into a particle initiates polymerization that continues until it is terminated by the entry of another radical into the particle. Thus, it is possible for a molecule to grow to a very high molecular mass before the termination of radicles. This process occurs simultaneously in a large number of particles, and as the particles are isolated in the medium by the intervening aqueous phase, a growing polymer molecule in one particle cannot terminate its counterpart in another particle. Hence, the overall rate of polymerization is high (Bovey et al., 1955). The high degree of compartmentalization of the polymerization locus by the surfactant contributes to high monomer conversion and a smaller particle size (Behan et al., 2001). The size of the NPs prepared by emulsion polymerization is small because of high degree of compartmentalization of polymerization locus in the presence of surfactant.

Mechanism of Dispersion polymerization:

The mechanistic events involved in dispersion polymerization are as discussed subsequently. The controlled concentration of the hydroxyl ions present in the polymerization medium initiates the monomer units to form oligomers. These oligomers further propagate, increase in chain length and experience reduced solubility in the aqueous phase after attaining a critical molecular mass (CMM) and precipitate out to form primary particles. This is termed as homogenous nucleation. The monomer diffuses from dispersed droplets into the primary particles leading to the formation of swollen structures. The newly formed primary particles further absorb monomers from larger monomer droplets and polymerize to grow in size (Behan et al., 2001). Hence, the process is also called coagulative nucleation. At this stage, the stabilizer (dextran 70) covers the particle surface and prevents further aggregation by steric repulsion resulting in stabilized nanoparticles (Douglas et al., 1985 and Barret et al., 1975).

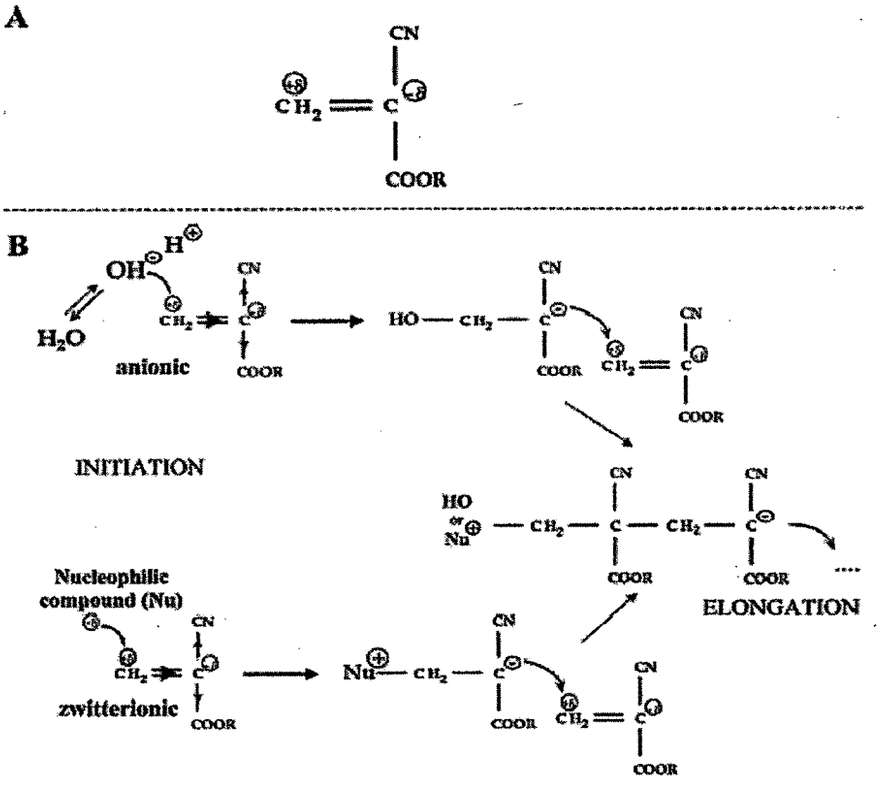

Figure 4. 11: A) Alkyl cyanoacrylate molecule B) Anionic polymerization process of alkyl cyanoacryaltes.

Paclitaxel loaded PBCA NPs were prepared by dissolving paclitaxel in ethanol and added to polymerization medium. The polymerization was affected in acidic medium (pH 2.5) in presence of surfactant (poloxamer 188 or dextran 70) which stabilizes the system. However, the effect of experimental variables such as monomer concentration, surfactant concentration, pH of the medium, concentration of PTX and temperature of polymerization on the properties of the NPs like drug entrapment efficiency, particle size and zeta potential were studied and optimized.

4.4.2.2 Effect of different formulation and process variables on PS, EE and Zeta potential

Effect of monomer concentration:

Effect of monomer concentration on the drug entrapment efficiency, particle size and zeta potential are depicted in Figure 4.12 and Table 4.19. Increase in the monomer concentration in the range between 0.5 % and 2.5%v/v, increased particle size and entrapment efficiency of the NPs in both the preparation techniques. At low monomer concentration, the amount of monomer molecules available for polymerization being very limited restricts the size of the nanoparticles. In addition, the small nanoparticles formed get effectively covered with available surfactant by adsorption which eventually prevents agglomeration. However, fast rate of nanoparticle formation and relatively low volume to surface ratio of small nanoparticles results in lower entrapment at initial low levels of monomer. At high monomer concentration, the primary particles formed undergo saturation with more monomer and further polymerization at this condition leads to overall increase in particle size (Reddy and Murthy, 2003). Such particles would contain polymers of higher molecular weight and could also incorporate more amount of drug. Higher monomer concentration could favor dendritic growth of particles and as a result show more number of functional group on the surface of NP which is evidenced by increase in zeta potential from -8.50 mV to -14.02 mV (Behan et al., 2001; Ballard et al., 1984)

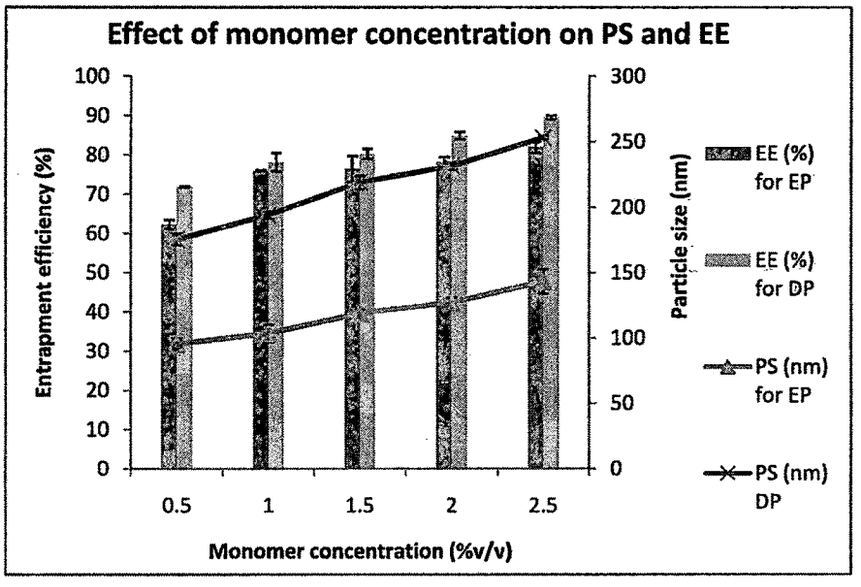

Figure 4. 12: Effect of monomer concentration on PS and EE of PBCA NPs prepared by EP and DP technique

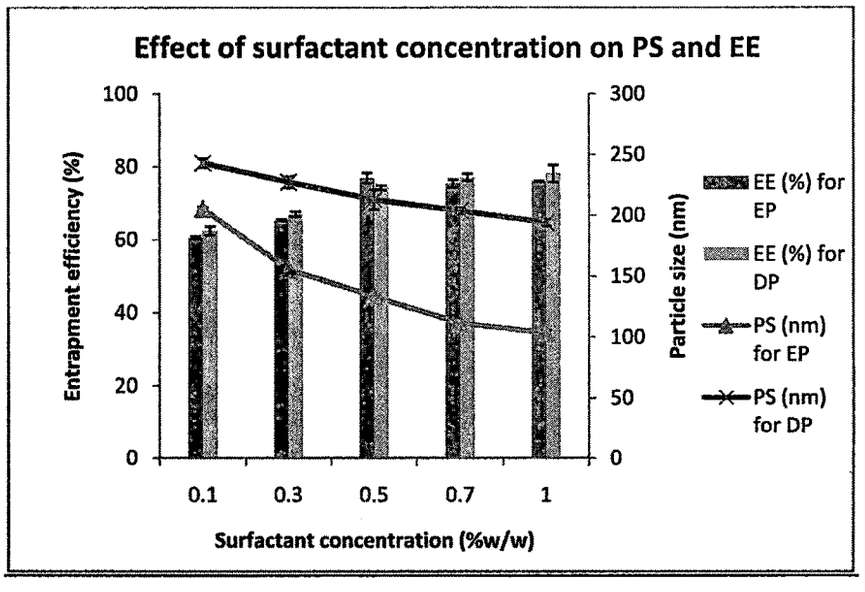

Figure 4. 13: Effect of surfactant concentration on PS and EE of PBCA NPs prepared by EP and DP technique

Table 4. 19: Effect of monomer concentration on PS, EE and zeta potential

Emulsion polymerization	**Monomer concentration (%v/v) at 1.0% surfactant at 25 °C (n=3)**				
	0.5	**1**	**1.5**	**2**	**2.5**
Entrapment efficiency (%)	62.29 ± 1.15	75.93 ± 0.15	76.43 ± 3.27	78.17 ± 1.28	81.97 ± 1.47
Particle size (nm)	95.50 ± 4.10	103.63 ±6.45	118.99 ±3.02	127.17 ±3.84	143.20 ±9.23
Zeta Potential (mV)	-8.50 ± 0.96	-8.92 ± 3.40	-11.43 ± 2.1	-13.24 ±0.75	-14.02 ±2.65
Dispersion polymerization	**Monomer concentration (%v/v) at 1.0% surfactant at 25 °C (n=3)**				
	0.5	**1**	**1.5**	**2**	**2.5**
Entrapment efficiency (%)	71.89 ± 0.12	78.13 ± 2.35	80.25 ± 1.24	84.9 ± 0.97	89.51 ± 0.46
Particle size (nm)	175.3 ± 4.3	194 ± 2.67	219 ± 5.31	231.4 ± 2.6	253.2 ± 1.4
Zeta Potential (mV)	-12.32 ± 2.1	-13.1 ± 0.86	15.35 ± 0.98	-18.2 ± 1.75	-19.3 ± 0.79

Effect of surfactant concentration and type

In case of EP non-ionic surfactants (poloxamer 188 and polxamine 904) provides steric repulsion between the particles causing a reduction in surface tension of the particles resulting in lower particle size (Behan et al., 2001; Huang et al., 2007). In EP and DP techniques as the surfactant concentration increased from 0.1% w/v to 1% w/v, the particle size of PBCA NPs decreased (Figure 4.13 and 4.14; Table 4.20 & 4.21). The initial high number of particle nuclei and their small particle size result in a very large total particle surface area. At low stabilizer/surfactant concentration, the amount of stabilizer/surfactant is insufficient to effectively cover the available surface, resulting in an unstable colloidal system. The smaller particles therefore agglomerate until the total particles surface area has decreased to a point such that the amount of poloxamer available is sufficient to produce a stable suspension.

PBCA-NPs fabricated with low amount of surfactant show porous and irregular surface (Kreuter 1983; Mitra and Lin 2003) which results in extensive drug loss due to large surface area available for drug to diffuse out from polymer matrix resulting in decreased entrapment efficiency. At increased stabilizer/surfactant concentration, it is possible to stabilize a larger total particle surface area, resulting in the formation of stable particles of a lower size. NPs formed were smooth and nearly spherical in shape with comparatively higher encapsulation efficiency because the total particles surface area is larger; a larger surface is available for binding PTX molecules. The consequence is that the total amount of drug bound to the particles increased as well as the drug loading. However, further increase in surfactant concentration beyond 0.5 %w/v showed no further increase in entrapment efficiency in case of EP technique but not in DP technique. It was interesting to note decrease in zeta potential from -16.3 mV to -8.92 mV with increase in surfactant concentration that may be attributed to shielding of polymer functional group by forming surfactant cloud on the surface of the nanoparticles that shifts the shear plane outwards, resulting in a reduction of the zeta potential (Ballard et al., 1984).

Table 4. 20: Effect of surfactant/stabilizer concentration on PS, EE and zeta potential

Emulsion polymerization	**Surfactant concentration (%v/v) at 1.0% monomer at 25 °C**				
	0.1	**0.3**	**0.5**	**0.7**	**1**
Entrapment efficiency (%)	60.50 ± 0.36	65.30 ± 0.62	76.87 ± 1.39	75.4 ± 1.10	75.93 ± 0.15
Particle size (nm)	205.27 ±8.72	155.57 ±5.09	133.23 ±4.07	111.43 ±3.49	103.63 ±6.45
Zeta Potential (mV)	-16.3 ± 1.64	-12.8 ± 0.74	-11.7 ± 1.05	-9.98 ± 2.65	-8.92 ± 3.40
Dispersion polymerization	**Stabilizer concentration (%v/v) at 1.0% monomer at 25 °C**				
	0.1	**0.3**	**0.5**	**0.7**	**1**
Entrapment efficiency (%)	62.43 ± 1.24	66.98 ± 0.75	74.23 ± 0.59	77.08 ± 0.93	78.13 ± 2.35
Particle size (nm)	243 ± 3.67	227.3 ± 4.75	212.87 ± 8.32	203.8 ± 2.30	194 ± 2.67
Zeta Potential (mV)	-19.34 ± 2.87	-16.1 ± 0.87	-15.81 ± 0.38	-14.21 ± 3.19	-13.1 ± 0.86

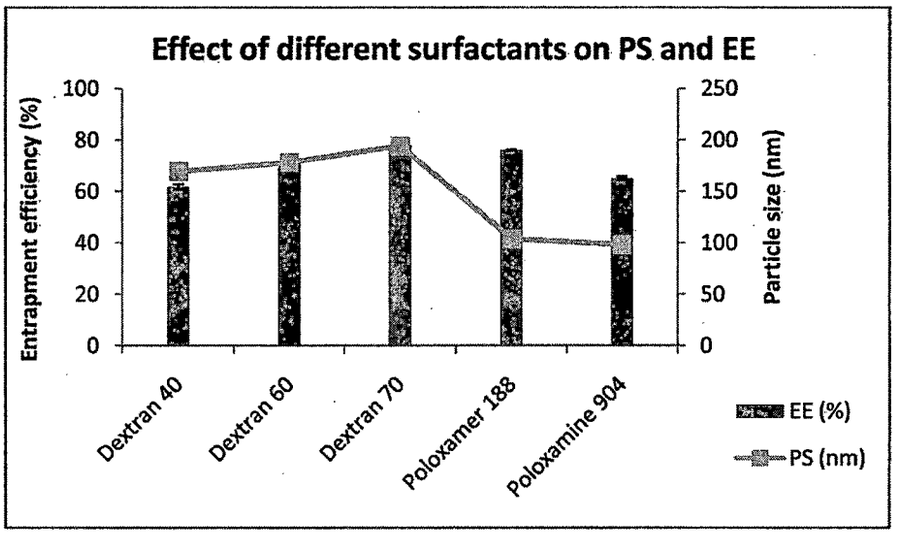

Figure 4. 14: Effect of surfactant type on PS and EE of PBCA NPs prepared by EP and DP technique

It was observed that the particle size reduced when Poloxamer 188 was used instead of Dextran 70 as a steric stabilizer. To explain this behavior it was necessary investigate the zeta potenzial of nanoparticles stabilized with dextran and poloxamer 188. It was found out that the zeta potential was -13.1 ± 0.86 for dextran nanoparticles and -8.92 ± 3.40 for poloxamer 188 nanoparticles. Douglas et al. (1985) reported the presence of residual amounts of dextran in cyanoacrylate nanoparticles in the bulk as well as at the surface. A similar observation was reported by Edman et al. (1980) in the development of polyacryl dextran biodegradable microparticles. High zeta potential values observed for the nanoparticles prepared using dextran were attributed to the contribution of charge by dextran 70 000 (dextran-O-), adsorbed onto the nanoparticle surface. This is not the case for nanoparticles prepared in the presence of the nonionic surfactant poloxamer 188. The nanoparticles stabilized by poloxamer 188 were surfactant stabilized during the polymerization, and hence the possibility of a masking effect on particle charge due to surfactant adsorption cannot be ruled out. Such a decrease in zeta potential after coating with block copolymers also was observed by Hawley et al. (1997) with poly(DL-lactide-co-glycolide) nanospheres.

Effect of temperature

Effects of temperature on the entrapment efficiency, particle size and zeta potential are tabulated in Table 4.22. Increase in polymerization temperature from 10°C to 25°C, increased percent drug entrapment with no significant effect on particle size and zeta potential. Higher temperature generally increases rate of polymerization and obviously increases drug entrapment effiency in polymer matrix. But, further increase in the polymerization temperature (beyond 25°C up to 60°C) reduced % drug entrapment efficiency probably due to increased flux of entrapped drug in softened polymer matrix. It also caused particle agglomeration due to increased kinetic energy of the system leading to increased inter–collision of particles (Reddy and Murthy 2004). In addition, efficacy of surfactant to stabilize the particles slowly reduces with increase in temperature thereby causing improper coating of surfactant on NP surface. Improper shielding of nanoparticles caused marginal increase in Zeta potential (from - 8.92 mV to - 10.5 mV) of these NPs (Behan et al., 2001). In case of EP the particle size is greater attributed to greater dehydration of propylene oxide (PO) and ethylene oxide (EO) blocks within the poloxamer 188 molecule facilitating aggregation of NPs. This clearly shows that there is no advantage gained at high polymerization temperature over ambient temperature with respect to both entrapment efficiency and particle size of NPs (Reddy and Murthy 2004).

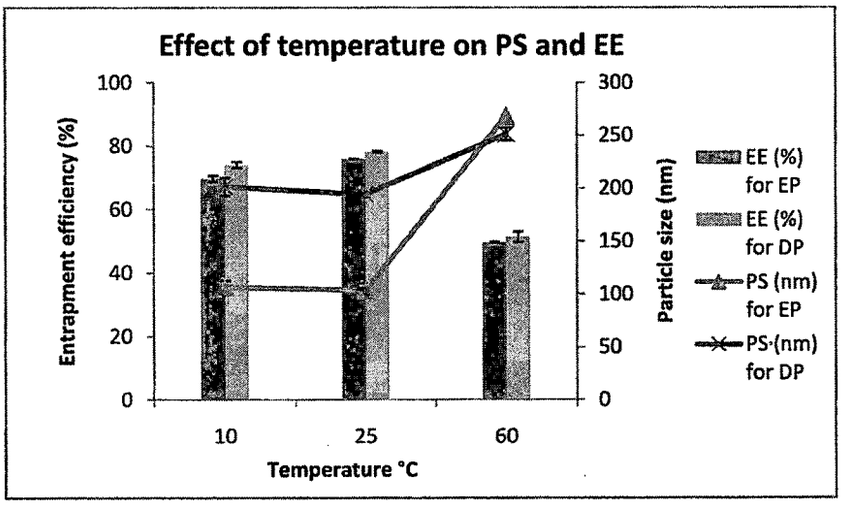

Figure 4. 15: Effect of temperature on PS and EE of PBCA NPs prepared by EP and DP technique

Effect of stirring speed

Stirring speed was found to have influence on particle size (Table 4.23). Because the solubility of the cyanoacrylate is exceeded at concentrations above 0.05%, monomer droplets are formed and the system has to be stirred constantly. The particle size increases slightly with increasing stirring speed (Douglas et al., 1984). This increase is caused by the higher kinetic energy of the system at higher agitation forces. The increased kinetic energy level of the system enables some oligomers, small semisolid particles, and even larger particles to overcome the interfacial energy barrier surrounding the particles, leading the coalescence with other particles (Douglas 1985, Tsukiyama et al., 1974). For the present study the optimized speed was 500rpm. At low speed there was not enough agitation in the medium resulting in polymerization occurring onto the magnetic stirrer with a resulting increase in particle size and film formation on the surface.

Effect of pH

A pH of 2.5 was found to be optimum for obtaining sufficient drug loading (Table 4.25 and Figure 4.17). Polymerization occurs via an anionic mechanism involving initiation by nucleophilic attack on the β-carbon of butyl-2-cyanoacrylate. The resulting carbanion produced reacts with further monomers to form oligomeric chains which nucleate leading to the formation of nanoparticles. The major initiating nucleophile is OH-, the concentration of which varies with pH. At high pH and hence high hydroxyl ion concentration, the polymerization rate is too rapid to allow discrete particle formation and leads to direct polymerization of monomer droplets producing an amorphous polymer mass. As pH decreases, the decrease in reaction rate allows nanoparticles formation to occur. However, if the pH is too low the polymerization period is greatly extended and nanoparticles in this system become swollen with monomer. Coagulation of these semi-fluid particles are not reversible and so produces a polydispersed system of larger particles and larger specific surface area on which molecules of drug can bound. Hence a minimum size and higher loading are observed in the pH profile when polymerization is slow enough to give discrete particles but not so slow as to allow excessive particle coagulation (Douglas et al. 1985).

Table 4. 21: Effect of different surfactants/stabilizers on PS and EE

	Surfactant type (1%v/v) at 1.0% monomer at 25 °C				
	Dextran 40	**Dextran 60**	**Dextran 70**	**Poloxamer 188**	**Poloxamine 904**
Entrapment efficiency (%)	61.75 ± 0.98	71.28 ± 1.36	78.13 ± 2.35	75.93 ± 0.15	64.98 ± 0.62
Particle size (nm)	169.3 ± 4.29	178 ± 6.12	194 ± 2.67	103.63 ±6.45	98.12 ± 2.32

Table 4. 22: Effect of temperature on PS and EE

1% monomer, 1% surfactant	**Temperature (°C ± 2 °C) for Emulsion polymerization**			**Temperature (°C ± 2 °C) for Dispersion polymerization**		
	10	**25**	**60**	**10**	**25**	**60**
Entrapment efficiency (%)	69.63 ± 0.99	75.93 ± 0.15	49.60 ± 0.10	73.98 ± 0.96	78.13 ± 2.35	51.32 ± 1.63
Particle size (nm)	106.37 ±6.10	103.63 ±6.45	267.90 ± 0.26	201.32 ± 8.32	194.0 ± 2.67	251.2 ± 5.78
Zeta potential (mV)	-8.54 ± 1.45	-8.92 ± 3.40	-10.5 ± 0.95	-12.26 ± 1.25	-13.0 ± 0.86	-16.23 ± 0.94

Table 4. 233: Effect of pH of polymerization medium on PS (nm) and EE (%)

	pH of polymerization medium, 1% surfactant, 1% monomer		
	1.5	**2.5**	**3.5**
Entrapment efficiency (%)	58.45 ± 1.87	75.93 ± 0.15	46.78 ± 2.08
Particle size (nm)	178.3 ± 3.2	103.63 ± 6.45	212.8 ± 2.32

Table 4. 244: Effect of stirring speed on PS

Particle size (nm)	Stirring speed (rpm)		
	250	**500**	**1000**
EP	154.4 ± 1.2	103.63 ± 6.45	187.2 ± 3.2
DP	245.7 ± 2.5	194.0 ± 2.67	293.0 ± 5.3

Table 4. 255: Effect of paclitaxel concentration on PS and EE

Emulsion polymerization	**Paclitaxel concentration (mg), 1% surfactant, 1% monomer (n=3)**			
	2.5	**5**	**7.5**	**10**
Entrapment efficiency (%)	50.12 ± 0.96	75.93 ± 0.15	74.23 ± 2.31	75.53 ± 2.3
Particle size (nm)	100.8 ± 1.2	103.63 ± 6.45	125.5 ± 4.2	136 ± 3.4
Dispersion polymerization	**Paclitaxel concentration (mg), 1% surfactant, 1% monomer (n=3)**			
	2.5	**5**	**7.5**	**10**
Entrapment efficiency (%)	73.14 ± 1.13	78.13 ± 2.35	80.24 ± 4.2	80.98 ± 0.21
Particle size (nm)	187.32 ± 6.2	194.0 ± 2.67	203 ± 5.3	218.5 ± 3.4

Effect of Paclitaxel concentration

It was observed that increase in concentration of PTX added during polymerization would increase the entrapment efficiency upto a concentration of 5mg in case of EP and

7.5mg for DP technique (Table 4.24 and Figure 4.16). This may be because the NPs get saturated with PTX at above concentrations and further addition of PTX does not have a significant effect on entrapment efficiency. Also the particle size of the NPs increases with increase in PTX content.

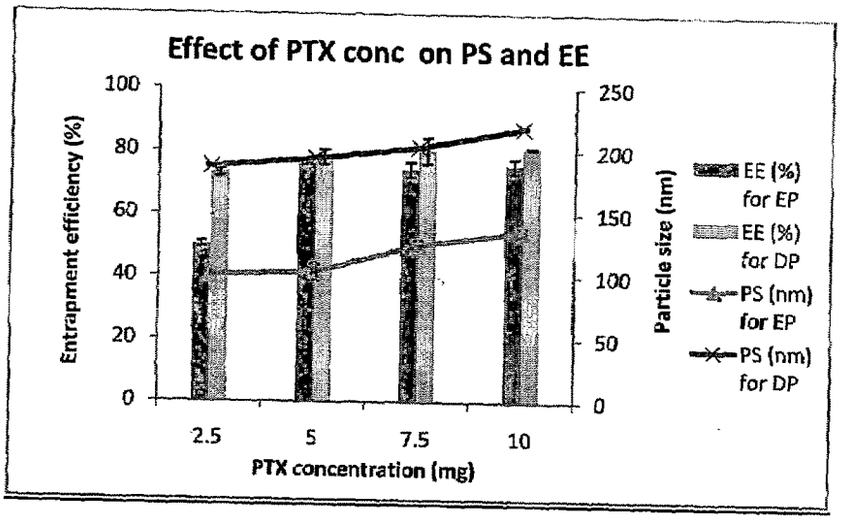

Figure 4. 16: Effect of PTX concentration on PS and EE of PBCA NPs prepared by EP and DP technique

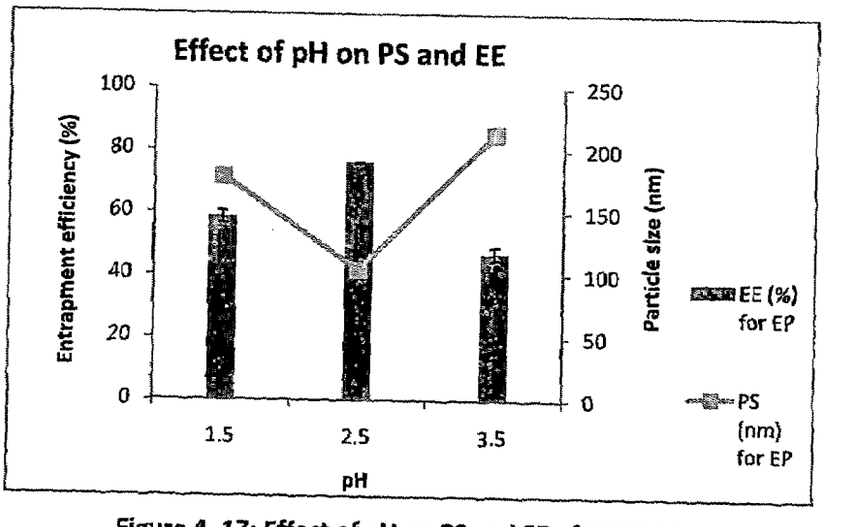

Figure 4. 17: Effect of pH on PS and EE of PBCA NPs

4.4.2.3 Turbidimetric measurements for particle formation

Emulsion polymerization

An important observation that %transmittance values were higher in case of emulsion polymerization signifies that smaller sized NPs are formed in comparison to dispersion technique. In EP the polymerization is initiated in surfactant micelles and also because of high degree of compartmentalization of polymerization locus in presence of surfactant the particle size obtained is small. The %transmittance values decreases with time indicative of particle formation (Figure 4.18). After three hours there is not much difference in %transmittance values indicating complete monomer conversion into to polymer.

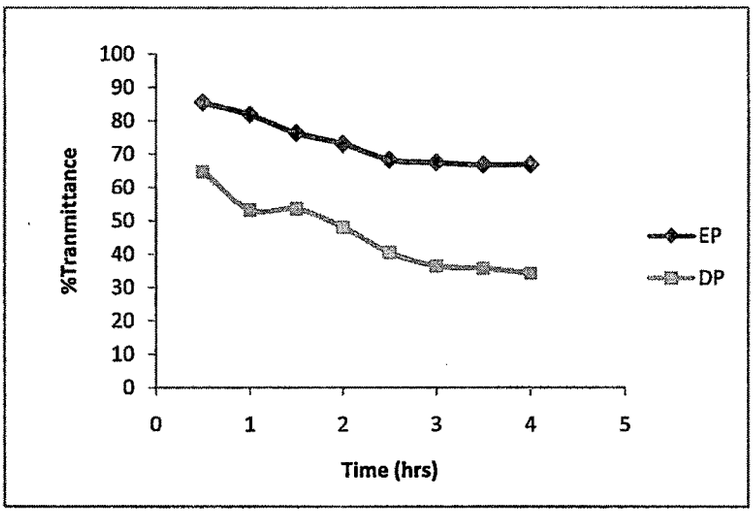

Figure 4. 18: Turbidimetric measurement for particle formation by EP and DP technique

Dispersion polymerization

At 25°C the %transmittance decreased slightly in the initial stages attributed to oligomer formation and formation of monomer droplets. Due to the diffusion of monomer into primary particles and disappearance of monomer droplets from the polymerization medium resulted in decrease %Transmittance values. The NPs formed have a greater particle size compared to EP technique as explained under the mechanism of dispersion polymerization.

4.4.2.4 Coumarin-6 loaded PBCA NPs

The PS and EE of coumarin-6 loaded PBCA NPs was found to be 114.5 ± 6.2nm and 98.32 ± 2.41% respectively and the zeta potential was found to be -10.34 ± 3.12mV.

4.4.2.5 Effect of different cryoprotectants added during freeze drying

Trehalose was found to be the most effective cryoprotectant for lyophilization of the PBCA NPs at a NP: Sugar ratio of 1:3 as depicted by the Sf/Si value. Glucose did not have any protective effect on particles size of NPs at any concentration tested in the present study. The lyophilized particle prepared using mannitol were found to be redispersed easily but there was a great increase in size as compared to those prepared with trehalose. Hence, trehalose is selected as an effective cryoprotectant in the present study. The results are tabulated in Table 4.26.

Table 4. 26: Effect of different cryoprotectants on PS and redispersion

Cryoprotectant (CP)	NPs: CP	Particle size (nm)		Sf/Si	Redispersibility
		Before (Si)	After (Sf)		
Glucose	1:1	118.4	-	-	Glassy mass, no redispersion
	1:2	118.4	536	4.52	Aggregates difficult to redisperse
	1:3	118.4	368	3.10	Redisperses with sonication
Mannitol	1:1	121	245	2.04	Difficult
	1:2	121	201	1.66	Easy
	1:3	121	198	1.63	Easy
Trehalose	1:1	115	156	1.35	Easy
	1:2	115	142	1.23	Easy
	1:3	115	122	1.06	Easy

4.4.2.6 In-vitro Drug Release Study

Drug release from biodegradable polymeric nanoparticles depends on the Fickian diffusion through the polymer matrix and on the degradation rate of the polymer. The

in-vitro drug release study of lyophilized drug-loaded NPs conducted in phosphate buffer (pH 7.4) containing 20% ethanol showed biphasic release profile for emulsion as well as dispersion polymerization (Figure 4.19).

Emulsion polymerization: The initial fast release phase rate (4.84 units/h) for about 12 hours is due to the immediate release of drug from the portion of the drug located on and near the surface of the NPs. Thereafter, the release rate decreased as the release rate (0.378 units/h) in this phase is controlled by diffusion rate of drugs across the polymer matrix.

Dispersion polymerization: The initial fast release phase rate (5.05 units/h) for about 12 hours is due to the immediate release of drug from the portion of the drug located on and near the surface of the NPs. Thereafter, the release rate decreased as the release rate (0.356 units/h) in this phase is controlled by diffusion rate of drugs across the polymer matrix.

In biodegradable systems like this, the mechanism of drug release in the first phase is dissolution of the adsorbed drug and drug diffusion across thin boundary layer of the matrix while in the slow release phase drug diffusion supported by very slow rate of bio-erosion of the polymer matrix predominates. Hence, in biodegradable matrix systems, the slow release phase depends on the molecular weight and hydrophobicity of the polymer. Several reports on such study showed that the longer hydrophobic alkyl side chains would shield effectively against the hydroxyl ions to attack the ester groups of PACA and therefore decrease the hydrolysis rate of PACA. In addition, presence of larger quantity of hydrophobic drugs like paclitaxel would contribute to increased hydrophobicity of the polymer matrix resulting in the increased barrier for water and hydroxyl ions responsible to cause degradation of PBCA polymer. Hence, the relative paclitaxel release rate decreases with increasing paclitaxel content in particles (Huang et al., 2007).

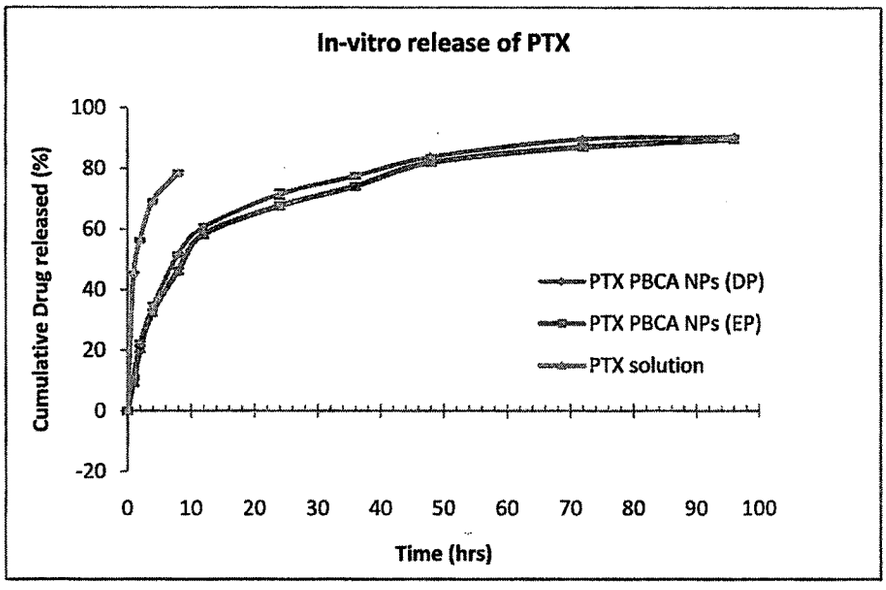

Figure 4.19: In-vitro release of PTX in pH 7.4 PBS containing 20% ethanol

4.4.2.6 FTIR

The Fourier transform infrared spectra of the PBCA NPs Figure 4.20 shows C-H (str) at 2957 cm^{-1} and C-H (def) at 1461 cm^{-1}. The characteristic C≡N (str) of the polymer was observed at 2200cm^{-1}. A prominent peak at 1750 cm^{-1} corresponds to C=O (str) and C-O (str) was observed at 1259 cm^{-1}. These peaks indicate the complete polymer formation with all functional groups related to its structure.

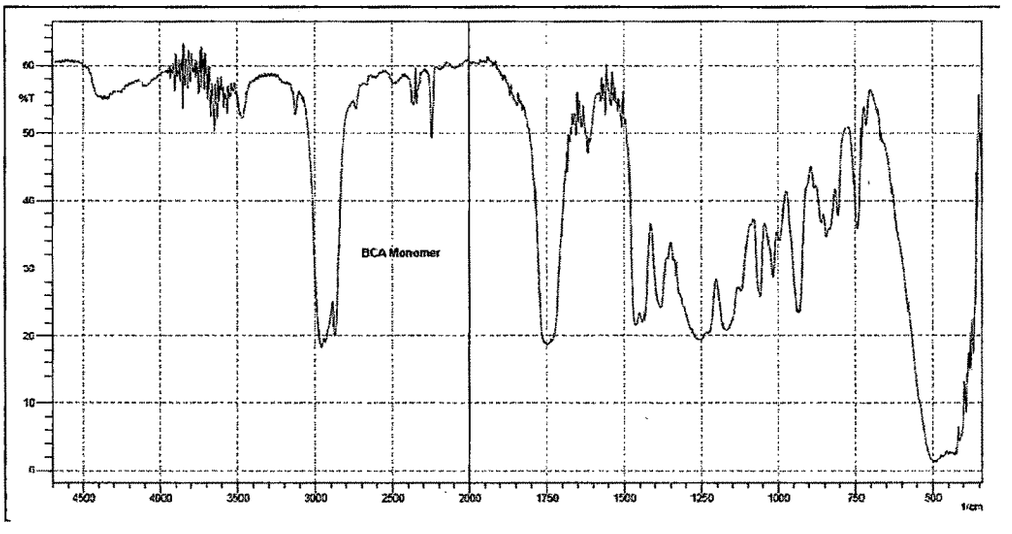

a)

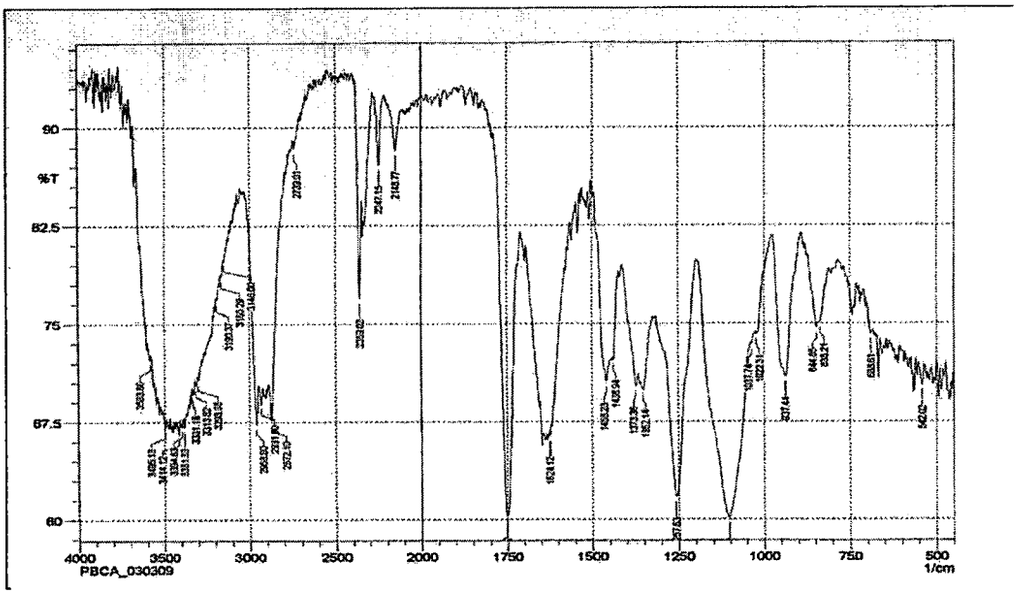

b)

Figure 4. 20: FTIR spectra of a) BCA monomer and b) PBCA NPs

4.4.2.7 Differential scanning calorimetry

DSC of PTX loaded PBCA NPs has peak broadening which is indicative of strong secondary interaction between drug and polymer (Sullivan and Birkinshaw 2004). The results thus indicate that Tx encapsulated in NPs is in the amorphous or disordered-crystalline phase or in the solid-state solubilized form in the polymer matrix of NPs

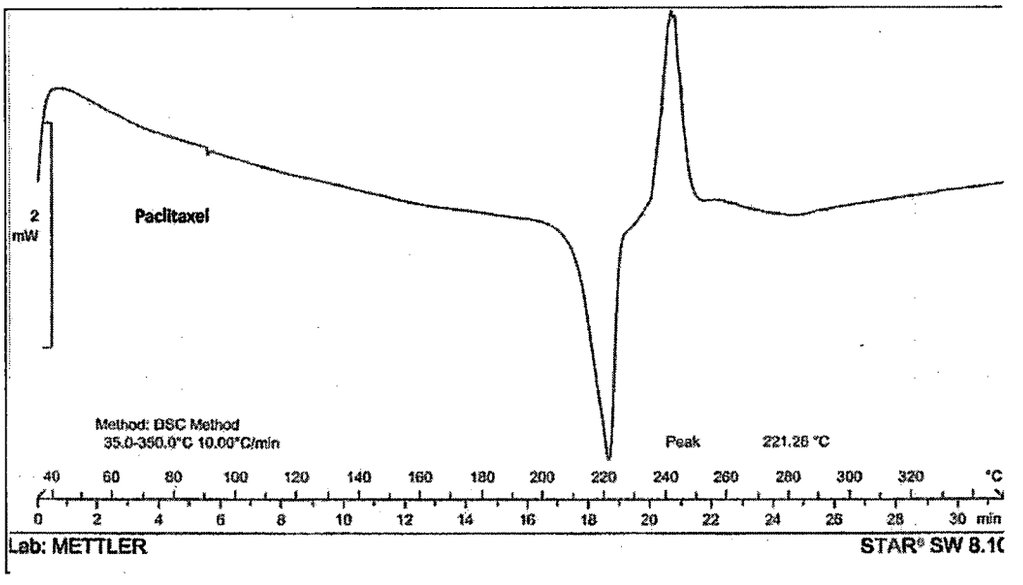

a)

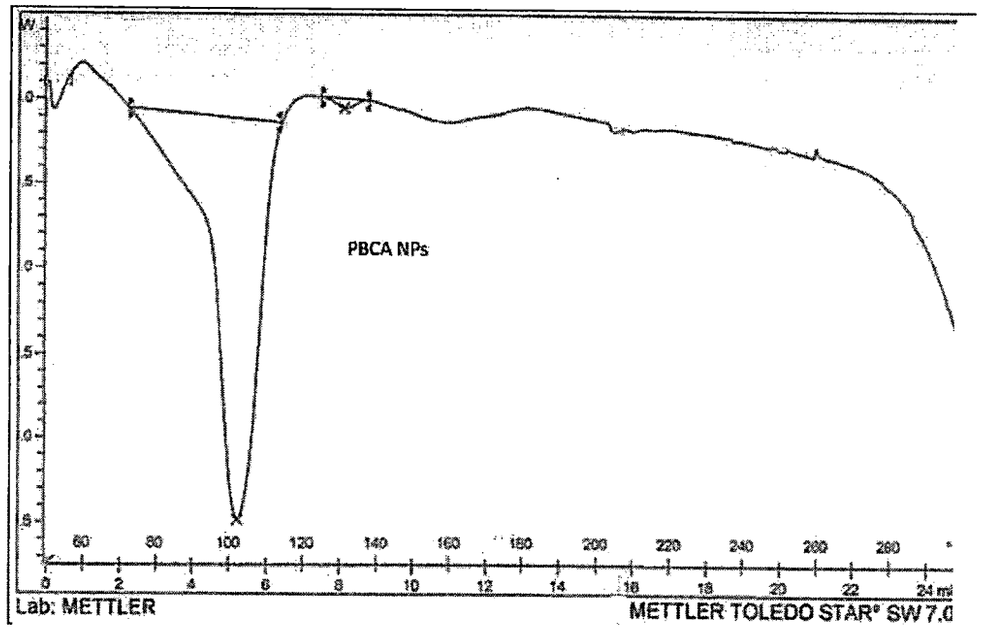

b)

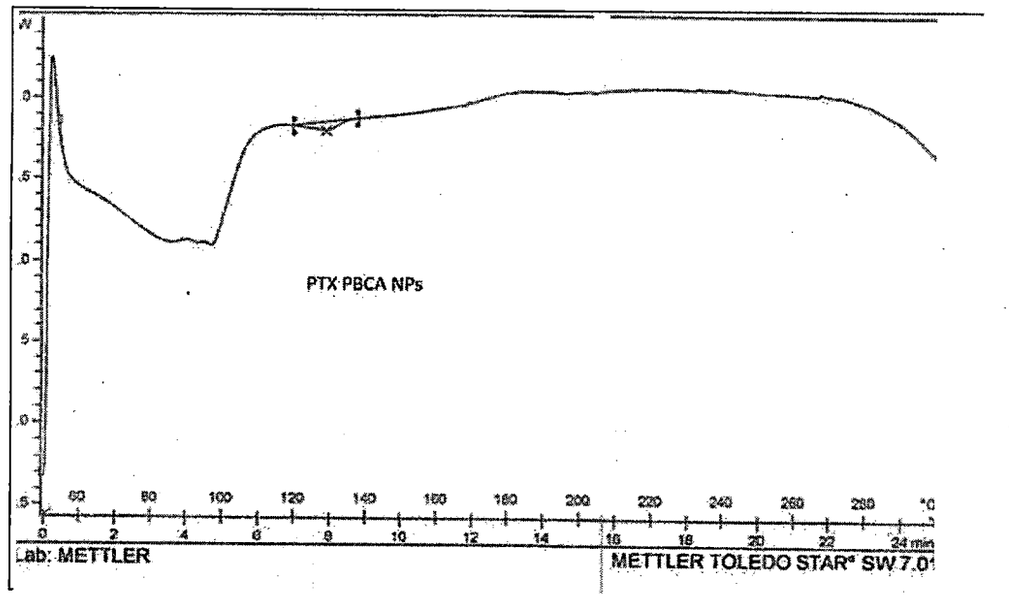

c)

Figure 4. 21: DSC thermograms of a) PTX b) PBCA NPs and c) PTX loaded PBCA NPs

4.4.2.8 Molecular weight determination

The molecular weight of PBCA nanoparticles was found to be 4216 Da by gel permeation chromatography.

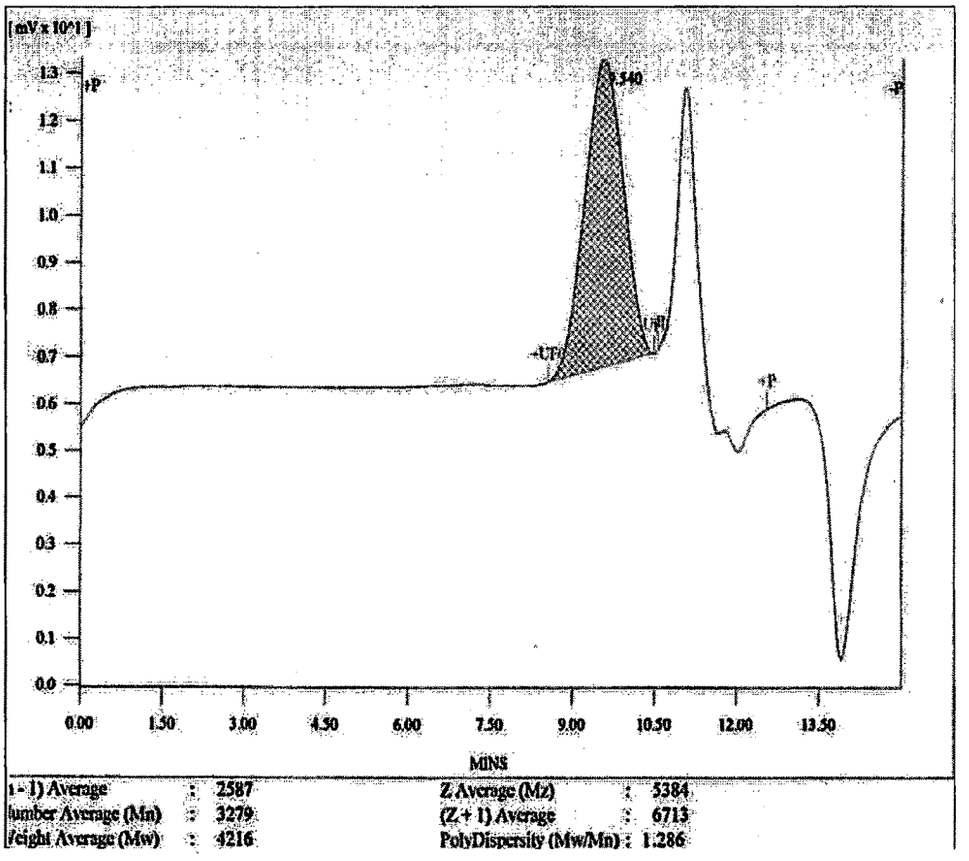

Figure 4. 22: GPC chromatogram

4.4.2.9 NMR spectroscopy

The double bond of vinyl group in the n-butyl cyanoacrylate (monomer) shows peak between 5.0 and 7.0. However there is no peak between 5.0 to 7.0ppm in the NMR spectra of poly(n-butyl cyanoacrylate) i.e. polymer, which indicates the absence of residual monomer and also confirms that complete polymerization of monomer has occurred.

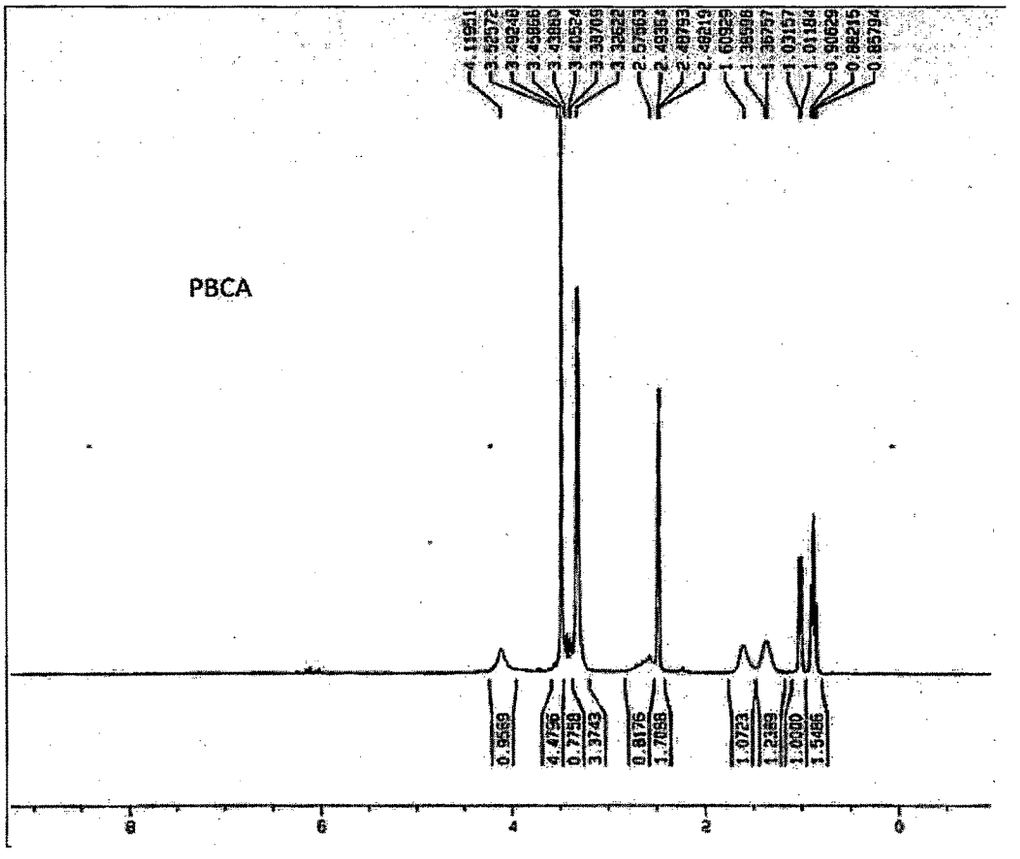

Figure 4.23: NMR spectra of PBCA

4.4.2.10 Transmission Electron Microscopy

The TEM images of PBCA NPs confirmed that the NPs are spherical in shape and in the nanometric range. Figure 4.24 illustrates TEM image of PTX loaded PBCA NPs.

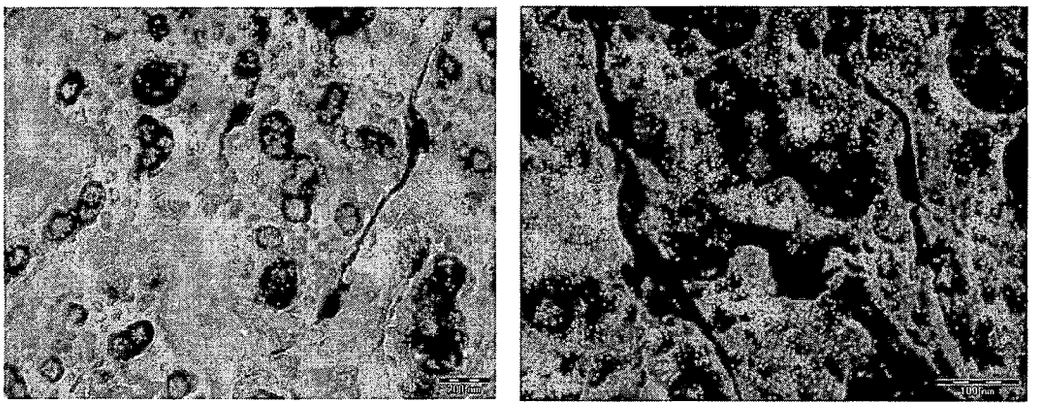

a) b)

Figure 4.24: TEM image of PBCA NPs a) NPs prepared by DP technique and b) NPs prepared by EP technique

4.4.3 PTX LOADED GLYCERYL TRISTEARATE (GTS) SLN

4.4.3.1 Partitioning of PTX between lipids and distilled water

Assessment of partition coefficient of drug in different lipids would provide an idea about the entrapment of drug in the SLN. The prerequisite to obtain adequate loading capacity of drug is high solubility of the drug in the lipid melt. In general, the solubility decreases after cooling down the lipid melt and might even be lower in the solid lipid. The presence of mono- and diglycerides in the lipid used as matrix material promotes drug solubilization (Muller et al., 2000). The chemical nature of the lipid is also important because lipids which form highly crystalline particles with a perfect lattice (e.g. monoacid triglycerides) lead to drug expulsion (Westesen et al., 1997). Lipids which are mixtures of mono-, di- and triglycerides and lipids containing fatty acids of different chain length form less perfect crystals with many imperfections offering space to accommodate the drugs. The partition coefficient was in the order of GTS > Compritol®888 > Precirol®ATO5. The difference in drug partitioning between the lipids can be explained as follows. PTX is a hydrophobic drug with a log P value of 3.0. Out of the three lipids studied GTS was found to retain most of the PTX in its lipid matrix in comparison to the aqueous phase (Partition coefficient = 2.81). This may be due to the fact that GTS is the most lipophilic and has a higher affinity for PTX. It was found that

Compritol®888 had a partition coefficient value of 2.35 where as Precirol®ATO5 had least partitioning into the lipid. The partitioning of PTX between different lipids and water has been described in Table 4.27.

Table 4. 27: Partitioning of PTX in different lipids

Lipid matrix	Partition coefficient
Compritol®888	2.35
Precirol®ATO5	1.83
Dynasan®118 (GTS)	2.81

4.4.3.2 Preparation of GTS SLN by solvent diffusion technique

In the solvent diffusion method in an aqueous system, the diffusion rate of the water miscible organic solvent (isopropyl alcohol) to aqueous phase was very rapid. The turbulence of the interface of the emulsion droplets occurred by the Marangoni effect (Fessi et al., 1989). At this time, the surfactant in aqueous phase, are absorbed around the emulsion droplets, resulting in spontaneous droplet formation in the submicron range. With the reduced solubility of lipid and drug at the interface of the resultant emulsion droplets, the lipid immediately precipitates, including the drug that is present in this lipid phase. With the solvent diffusion method in an aqueous system, the extent of SLN with smaller size and light density lipid was gained. Usually, the separation of nanoparticles from solvent system is using ultracentrifugation or ultrafiltration. Unfortunately, when the SLN suspension was ultracentrifuged (Sigma, 3K30, Germany) at 45000 rpm with 1 h, the SLN could not be separated completely, the supernatant has more SLN and the recovery was very low. This phenomena may be produced due to light density of lipid. Hence to collect the SLN the dispersion was treated with 0.1 ml of 10mg/ml protamine sulphate which causes aggregation of the NPs. SLN can be collected by centrifugation at 8000rpm and the obtained pellet redispersed in distilled water and lyophilized. Slower cooling protocols were associated with gelling of the dispersion with a resultant increase in particle size. In contrast, PTX loaded GTS SLN prepared by rapid cooling showed submicron sizes suitable for the parenteral use. The results are in accordance with Lee et al., 2007.

Effect of drug: lipid ratio and concentration of lecithin

It was observed that as the drug: lipid ratio was increased the entrapment efficiency increased with a maximum entrapment at 1: 20 with concurrent increase in particle size. Hence the optimum drug: lipid ratio that was selected was 1: 15. Also when the SLN were fabricated without the drug the particle size was less which increased when drug was loaded into the SLN. This may be attributed to increased amounts of solid phase. The results are in accordance with Reddy and Murthy, 2005. An interesting observation was that with increase in concentration of lecithin in the total lipids there was a decrease in particle size. This may be attributed to decrease in stress on the surface of droplets by lecithin and thereby controlling the droplet curvature due to its co-surfactant property. An increase in the entrapment efficiency of PTX was observed with increase in lecithin content in the lipid phase. It is due to the solubility of PTX in the lipid fraction. Lecithins are phospholipids hence they possess solubilization properties for lipophilic compounds (Reddy and Murthy., 2005).

Effect of surfactant concentration

The main function of the surfactant is stabilization of the nanoparticles in the colloidal state and prevents particle size growth during storage. In addition to its role in stabilization, surfactants have also been shown to play a role in the crystallization behavior of the lipids. Bunjes and co-workers demonstrated that the crystallization temperature of nanoparticles made from triglycerides depends on the stabilizer, which can lead to homogenous or surface heterogenous nucleation (Bunjes et al., 1996). The crystallization tendency of the particles increases with the length of the (saturated) hydrophobic chain of the stabilizer. The crystallization promoting effect of certain surfactants is believed to be caused by an ordering process of the surfactant molecules in the stabilizer layer. The non-ionic surfactants affect the polymorphic transitions. Non-ionic surfactants provide steric repulsion between the particles causing a reduction in surface tension of the particles resulting in lower particle size (Huang et al., 2007). In the present study poloxamer 188 was used as stabilizer as it has an approved GRAS status and is known to inhibit P-gp (Batrakova et al., 2008). It was observed that increase in concentration of surfactant exhibited decrease in particle size. At lower concentrations, SLN showed tendency to aggregate probably due to insufficient

surfactant coverage at the surface. SLN prepared with higher surfactant concentration were smooth and nearly spherical in shape and the amount of surfactant was appropriate so as to effectively cover the surface of the SLN and causing a reduction in PS. The results are in accordance with Reddy and Murthy, 2005.

4.4.3.2.1 Optimization and multiple regression analysis

27 batches of PTX loaded GTS SLN were prepared by solvent diffusion technique by using 3^3 factorial design varying three independent variables described in Table 4.8. The prepared SLN were characterized for particle size and entrapment efficiency and recorded in Table 4.9. The results were subjected to multiple regression analysis using Microsoft Excel 2007 to obtain a full model equation (Eq. 10 & 11).

The main effects of X_1, X_2 and X_3 represent the average result of changing one variable at a time from its low to high value. The interactions (X_1X_2, X_1X_3, X_2X_3 and $X_1X_2X_3$) show how the response changes when two or more variables were simultaneously changed. The significance of each coefficient of the equation of full model was determined by student't' test and p-value, which are listed in Table 4.10. The larger the magnitude of the t value and the smaller the p value, the more significant is the corresponding coefficient (Adinarayana et al, 2002; Akhnazarova et al, 1982). This implies that the quadratic main effects of the independent variables in the present study are very significant for PS and EE. The second order main effects of X_3 (Poloxamer concentration) are very significant for EE. Interaction between X_2X_3 is significant for PS. The interaction between X_1X_2, X_1X_3, X_2X_3 and $X_1X_2X_3$ are found to be non-significant for EE and except X_2X_3 they are non significant for PS from their p-values.

F statistic was applied to the results of analysis of variance (ANOVA) of full model and reduced model to check whether the non-significant terms can be omitted or not from the full model. For both the case $F_{cal} < F_{tab}$ (0.524 < 2.741 at α=0.05, V1= 6and V2= 16 for PS and 0.988 < 2.741 at α=0.05, V1= 6 and V2= 16 for EE) which indicates that the neglected terms do not significantly affect the PS and EE and therefore the hypothesis is accepted. The goodness of fit of the model was checked by the determination coefficient (R^2). In this case, the values of the determination coefficients (R^2 = 0.9312 for full model

and 0.9176 for reduced model of PS and R^2 = 0.9443 for full model and 0. 9237 for reduced model of EE) indicated that over 90 % of the total variations are explained by the model. The values of adjusted determination coefficients (adj R^2 = 0.8882 for full model and 0.9027 for reduced model of PS and adj R^2 = 0.9095 for full model and 0.9098 for reduced model of EE) are also very high which indicates a high significance of the model. A higher values of correlation coefficients (R = 0.9649 for full model and 0.9579 for reduced model for PS and R = 0.9717 for full model and 0.9611 for reduced model of EE) signifies an excellent correlation between the independent variables (Box et al, 1978). All the above considerations indicate an excellent adequacy of the regression model for preparation of PTX GTS SLN by sovent diffusion technique (Adinarayana et al, 2002; Akhnazarova et al, 1982; Box et al, 1978; Cochran et al, 1992; Yee et al, 1993).

4.4.3.2.2 Validation of established relationships

At fixed levels of -1, 0 and 1 of independent variable X_1, three check points were selected each on three plotted contours for PS and EE. The computed particle size (nm) and entrapment efficiency (%) values from the contours at -1, 0 and 1 level are tabulated (Table 4.13). PTX-GTS SLNs at these three checkpoints were prepared experimentally using the same procedure keeping the other process variables as constants with the amounts of independent variables at the selected check points. The experiment was repeated three times and the experimentally obtained mean PS (nm) and EE (%) values are shown in Table 4.28. Both experimentally obtained and theoretically computed PDE values were compared using student 't' test and the difference was found to be non significant ($p>0.05$). This proves the role of a derived reduced polynomial equation and contour plots in the preparation of PTX PLGA NPs of predetermined PS and EE (%).

Table 4. 28: Experimental and predicted values of Particle size and entrapment efficiency

Independent variables			Predicted	Experimental	Predicted	Experimenta
X_1	X_2	X_3	PS (nm)	PS (nm) ± SD	EE (%)	EE (%) ± SD
1:10	15.88	0.75	225.9	224.0 ± 3.5*	77.33	76.02 ± 1.08*
1:15	22.94	1.38	214.2	216.4 ± 4.1*	79.45	80.65 ± 0.76*
1:20	26.47	1.45	216.9	219.3 ± 3.8*	85.55	83.21 ± 1.14*

(*p>0.05, non-significant difference between predicted and experimental values of responses) (n=3)

4.4.3.3 Characterization of PTX loaded GTS SLN and coumarin-6 loaded GTS SLN

The optimized batches of PTX loaded GTS SLN was characterized for PS (nm) and EE (%). The optimum drug: lipid ratio was found to be 1:15 with concentration of lecithin to be 30% and surfactant concentration of 1%w/v. The particle size was found to be 210.7 ± 1.92 with an entrapment efficiency of 82.46 ± 3.49 with a zeta potential of -28.7 ± 3.17. The optimized batch was further subjected to in-vitro drug release study. The PS, EE and zeta potential of coumarin-6 loaded GTS SLN were found to be 204.8 ± 5.38nm, 92.17 ± 1.46% and -27.24 ± 1.65 respectively.

4.4.3.4 Effect of different cryoprotectants added during freeze drying on stability of NPs

Trehalose was found to be the most effective cryoprotectant for lyophilization of the GTS SLN at SLN to sugar ratio of 1:3 as depicted by the Sf/Si value. The NPs lyophilized with glucose formed a glassy mass at low glucose concentrations and even with higher concentrations of glucose it was very difficult to redisperse the cake by manual shaking. Glucose did not have any protective effect on particles size of SLN at any concentration tested in the present study. The lyophilized particle prepared using mannitol were found to be redispersed easily but there was a great increase in size as compared to those prepared with trehalose. Hence, trehalose is selected as an effective cryoprotectant in the present study.

Table 4. 29: PS of NPs before and after freeze drying

Cryoprotectant (CP)	NPs: CP	Particle size (nm)		Sf/Si	Redispersibility
		Before (Si)	After (Sf)		
Glucose	1:1	212.5	-	-	Glassy mass, no redispersion
	1:2	212.5	698.4	3.28	Aggregates difficult to redisperse
	1:3	212.5	538.0	2.53	Redisperses with sonication
Mannitol	1:1	215	528.4	2.45	Difficult
	1:2	215	432.1	2.01	Easy
	1:3	215	316.9	1.47	Easy
Trehalose	1:1	217.1	429.0	1.97	Easy
	1:2	217.1	296.5	1.36	Easy
	1:3	217.1	229.2	1.05	Easy

4.4.3.5 In-vitro drug release study

The release of active substances from the matrix is influenced by the crystal structure of the lipid (Lukowski G et al., 2000). Due to the solid property of the core at body temperature the drug release from the SLN was expected to be slow. In vitro release of PTX from the SLN formulation was studied in pH 7.4 Phosphate buffer containing 20% ethanol (ethanol was used to increase the solubility of PTX in release medium) (Figure 4.25). PTX loaded GTS SLN exhibited a biphasic release profile consisting of an initial burst effect followed by a sustained release of PTX from the lipid matrix. The initial burst release is probably caused by the drug adsorbed on the nanoparticle surface or precipitated from the superficial lipid matrix (Reddy and Murthy, 2005). The sustained release following the initial burst release is probably due to the diffusion of drug from the lipid matrix. GTS investigated in this study is long-chain fatty acid esters and is highly lipophilic (Hamdani et al., 2003) and gives a sustained release profile. The release profile of PTX from GTS SLN best fitted in the Higuchi model with R^2 value of 0.9736 and slope 8.914.

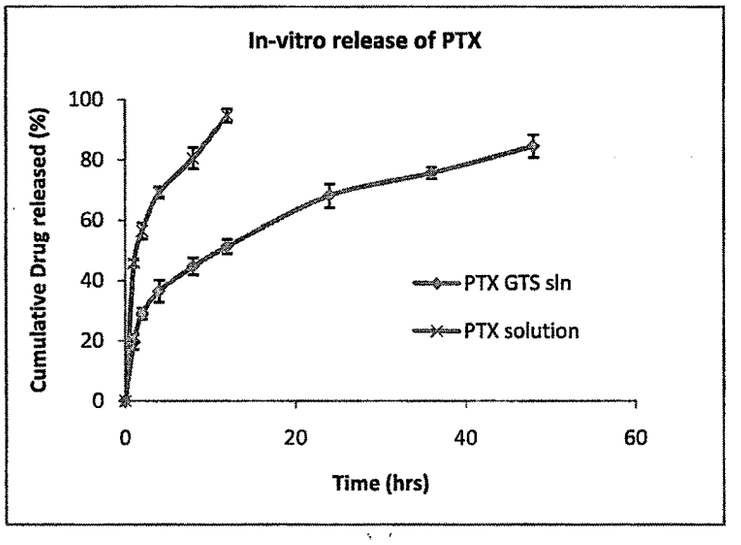

Figure 4. 25: In-vitro release of PTX in pH 7.4 PBS containing 20% ethanol

4.4.3.6 Differential Scanning Calorimetry

The crystalline structure of the nanoparticles can be assessed by differential scanning calorimetry (DSC). DSC thermograms demonstrated that only pure Tx had an endothermic peak of melting at 215-217°C whereas control or drug-loaded NPs had no such peak in the range 150-250 °C (Figure 4.26). The results thus indicate that Tx encapsulated in NPs is in the amorphous or disordered-crystalline phase of a molecular dispersion or in the solid-state solubilized form in the polymer matrix of NPs after fabrication (Mu and Feng, 2002, Esmaeili et al., 2008).

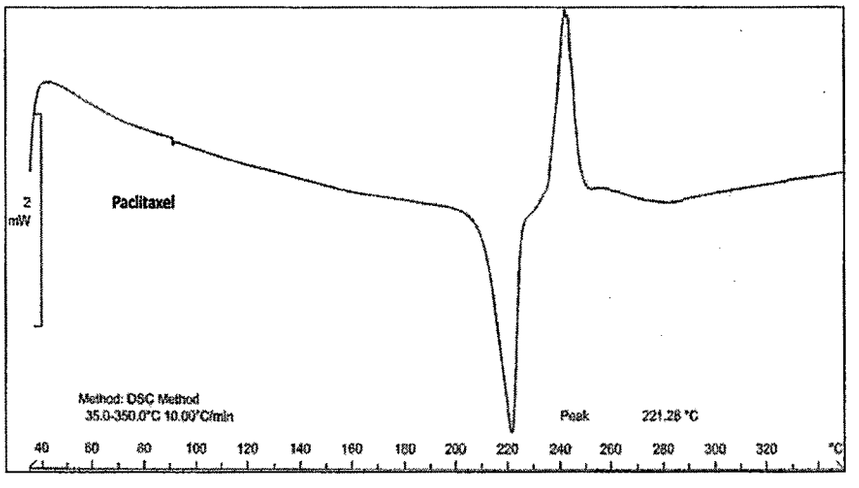

a)

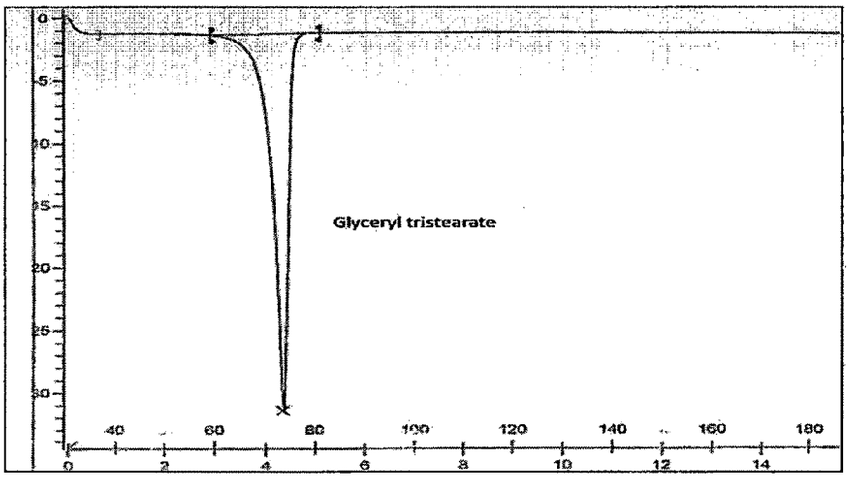

b)

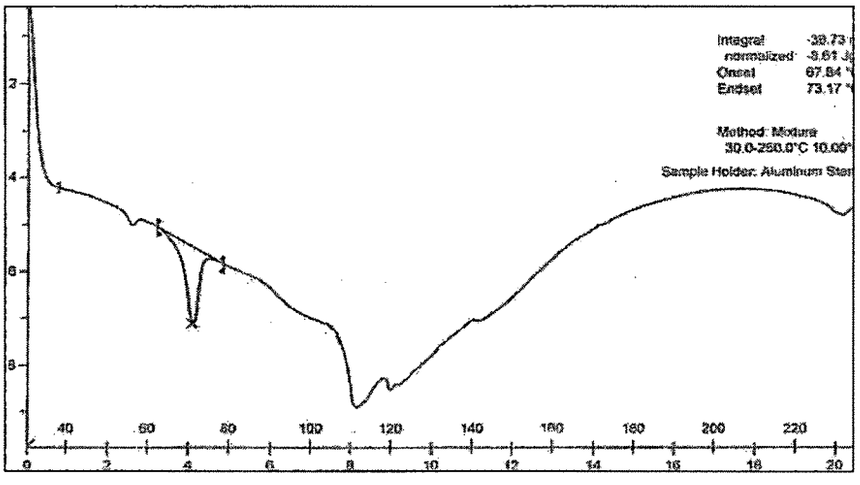

c)

Figure 4. 26: DSC thermograms a) PTX b) GTS and c) PTX GTS SLN

4.4.3.7 X-ray diffraction patterns

Crystal diffraction has wide applications in the study of crystal forms (such as polymorphs, solvates, and salts). In the present study, comparison of the XRD patterns (Figure 4.27) was done by considering the relative intensities of the diffracted peaks at a particular θ. The XRD pattern of PTX shows a principal peak at angle 12.32° 2θ. GTS had a principal peak at angle 19.27° 2θ. In the PTX loaded GTS SLN formulations, the principal peak of PTX was absent. Further, the principal peak of the lipid did not shift. However, there was a reduction in the intensity of the principal peak in the SLN formulation. This may be attributed to the incorporation of PTX in between the crystal lattice of the lipid leading to change in the crytallinity of the lipid. These values

complement the DSC data and clearly indicate the possible change in crystallinity of the lipid after PTX fabrication into GTS SLN.

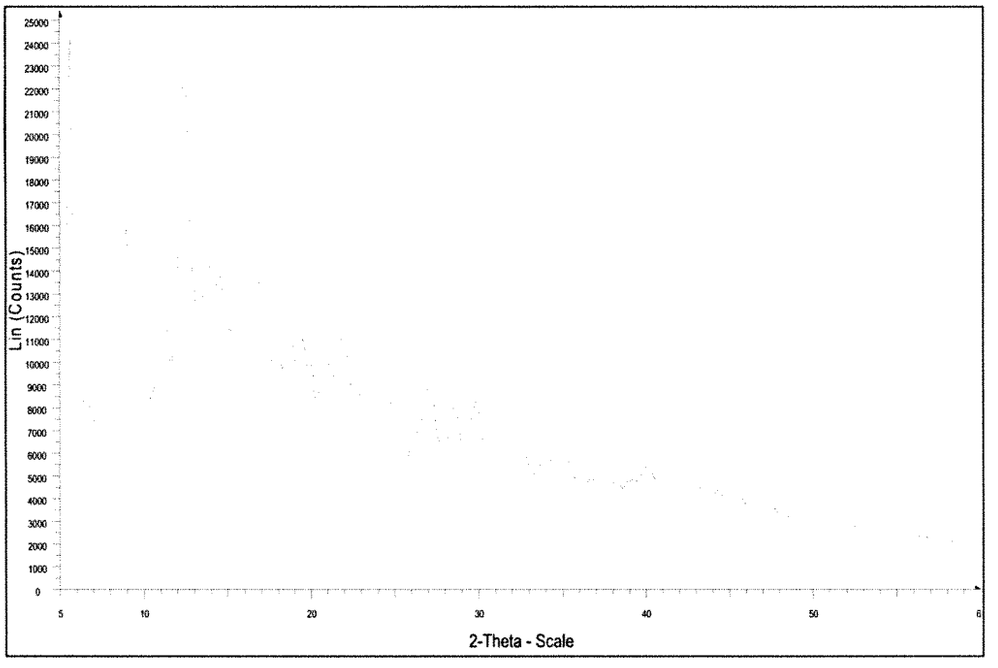

a)

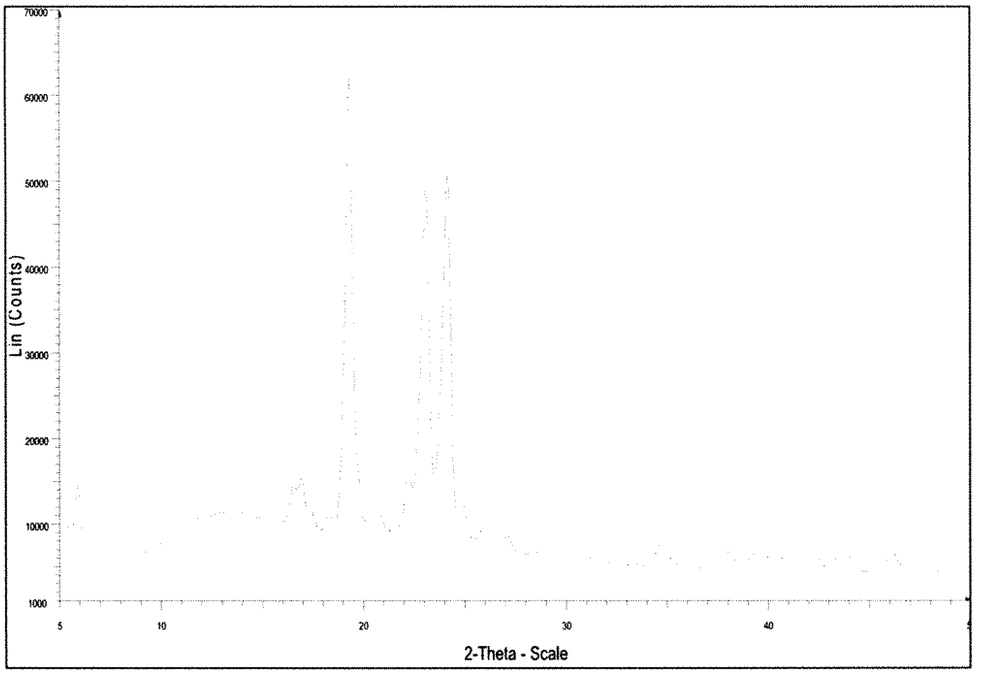

b)

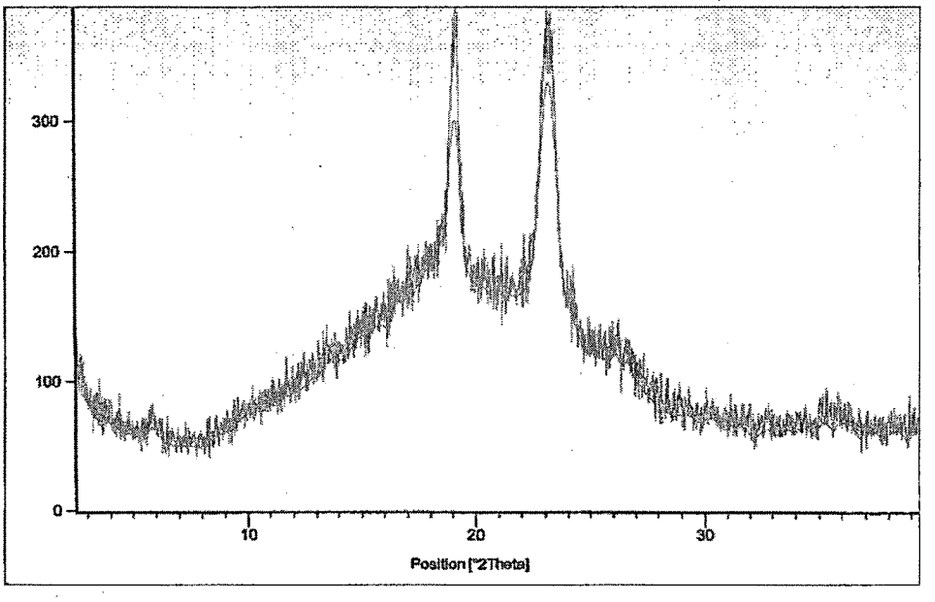

c)

Figure 4. 27: X-ray diffraction pattern of a) PTX, b) GTS and c) PTX GTS SLN

4.4.3.8 Transmission electron microscopy

The TEM images of PTX loaded GTS SLN reveal that the SLN are almost spherical in shape and confirms the size in the nanometric range.

Figure 4. 28: TEM image of PTX GTS SLN

4.4.3.9 Determination of in vitro steric stability by electrolyte flocculation test

The effect of poloxamer 188 on the ability of the nanoparticles to oppose electrolyte induced flocculation was investigated by this test. Coating the particulate systems with non-ionic surfactants provide steric stability by rendering a hydrophilic surface, which in turn reduces the binding of serum opsonins and also cells of the reticuloendothelial system (Huang et al., 1993). Addition of electrolyte compresses the electrical double layer around the particle. This results in flocculation of the particles with a corresponding increase in optical turbidity of the particle dispersion which can be measured by the absorbance of the dispersion at 600nm. In the present investigation, the nanoparticle formulations stabilized with 1%w/v poloxamer 188 showed no sign of flocculation as the concentration of electrolyte (sodium sulphate) was increased up to 1.2M. SLN dispersions showed signs of flocculation when the concentration of sodium sulphate was increased above 1.2M. Beyond this concentration, flocculation was observed. The results are given in Figure 4.29. In the present study poloxamer 188 imparts excellent steric stability to the PTX loaded GTS SLN probably due to effective coverage of particle surface, thereby preventing the interaction of flocculating agent with the lipid matrix. Poloxamers are reported to be excellent steric stabilizing agents and their use in enhancing the circulation half life of polymeric NPs has also been reported (Moghimi et al., 2001).

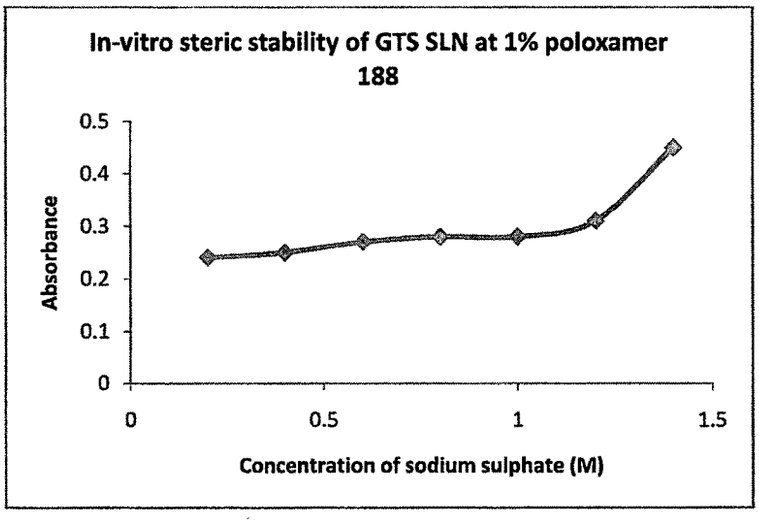

Figure 4. 29: Steric stability test of PTX loaded GTS SLN prepared with 1% poloxamer 188 concentration

4.4.4 STABILITY STUDIES

The different batches of the NPs were subjected to visual examination and each batch of NPs was analyzed for particle size, zeta potential and drug content. At the end of six months the in-vitro drug release was also performed. Aggregation and drug leaching is a common problem in case of nanoparticulate dispersions as observed from the results. Hence, the dispersions are lyophilized in presence of cryoprotectants to maintain the stability of the dispersions on freeze drying.

Table 4. 30: Stability data of PTX-PLGA NPs (n=3)

Time	Description	Particle size (nm) ± SD	Zeta potential (mV) ± SD	Drug content (%) ± SD
Initial	White porous cake	172.4 ± 6.2	-8.4 ± 2.14	100
5°C ± 3°C				
15 days	White porous cake, redispersed easily	173.5 ± 2.4	-8.98 ± 1.25	99.8 ± 0.78
1 month	White porous cake, redispersed easily	171.8 ± 4.6	-9.32 ± 0.87	98.5 ± 1.26
2 months	White porous cake, redispersed easily	174.2 ± 1.3	-8.76 ± 1.08	99.6 ± 1.03
3 months	White porous cake, redispersed easily	173.6 ± 2.5	-9.21 ± 2.35	99.3 ± 0.94
6 months	White porous cake, redispersed easily	176.5 ± 6.4	-9.33 ± 1.80	97.3 ± 1.23
25 ± 2°C/60 ± 5% RH				
15 days	White porous cake, redispersed easily	174.0 ± 1.8	-9.45 ± 2.01	98.7 ± 1.92
1 month	White porous cake, redispersed easily	175.4 ± 4.2	-9.18 ± 1.78	97.4 ± 1.35
2 months	White porous cake, redispersed easily	181.4 ± 3.1	-7.65 ± 1.65	96.6 ± 0.56
3 months	White porous cake, redispersed easily	183.6 ± 3.8	-8.75 ± 1.21	96.2 ± 1.14

Table 4. 31: Stability data for Transferrin conjugated PTX-PLGA NPs (n=3)

Time	Description	Particle size (nm) ± SD	Zeta potential (mV) ± SD	Drug content (%) ± SD
Initial	White porous cake, redispersed easily	185.4 ± 2.4	-11.72 ± 4.28	100
5°C ± 3°C				
15 days	White porous cake, redispersed easily	186.3 ± 1.5	-11.32 ± 2.34	98.3 ± 1.24
1 month	White porous cake, redispersed easily	188.0 ± 3.6	-12.15 ± 1.62	98.5 ± 0.53
2 months	White porous cake, redispersed easily	189.4 ± 1.2	-12.73 ± 2.58	96.3 ± 2.45
3 months	White porous cake, redispersed easily	191.2 ± 1.0	-13.18 ± 1.23	97.1 ± 0.49
6 months	White porous cake, redispersed easily	195.0 ± 4.3	-13.54 ± 2.16	96.9 ± 1.56
25 ± 2°C/60 ± 5% RH				
15 days	White porous cake, redispersed easily	192.0 ± 3.8	-11.56 ± 1.43	98.8 ± 0.65
1 month	White porous cake, redispersed easily	193.2 ± 2.0	-10.25 ± 0.21	97.2 ± 2.37
2 months	White porous cake, redispersed easily	195.0 ± 4.3	-9.37 ± 1.98	97.5 ± 1.76
3 months	Creamy porous cake, redispersed on sonication	196.1 ± 2.2	-11.02 ± 2.17	95.8 ± 0.89

Table 4. 32: Stability data for PTX-PBCA NPs (n=3)

Time	Description	Particle size (nm) ± SD	Zeta potential (mV) ± SD	Drug content (%) ± SD
Initial	White porous cake, redispersed easily	105 ± 2.45	-9.02 ± 1.37	100
5°C ± 3°C				
15 days	White porous cake, redispersed easily	105.6 ± 1.3	-8.97 ± 2.51	99.2 ± 2.12
1 month	White porous cake, redispersed easily	106.0 ± 2.1	-9.89 ± 1.64	98.7 ± 1.76
2 months	White porous cake, redispersed easily	107.5 ± 4.5	-9.24 ± 1.08	97.5 ± 2.31
3 months	White porous cake, redispersed easily	106.8 ± 2.7	-9.68 ± 3.42	98.1 ± 0.68
6 months	White porous cake, redispersed easily	110.3 ± 5.3	-9.43 ± 2.65	97.6 ± 1.23
25 ± 2°C/60 ± 5% RH				
15 days	White porous cake, redispersed easily	108.5 ± 2.1	-9.87 ± 1.22	98.3 ± 1.48
1 month	White porous cake, redispersed easily	109.0 ± 5.4	-9.69 ± 2.05	97.6 ± 1.03
2 months	White porous cake redispersed on sonication	106.4 ± 4.8	-10.23 ± 1.46	97.2 ± 2.17
3 months	Small aggregates, redispersed on sonication	117.0 ± 2.6	-9.12 ± 0.74	95.9 ± 1.25

Table 4. 33: Stability data for PTX-GTS SLN (n=3)

Time	Observations	Particle size (nm) ± SD	Zeta potential (mV) ± SD	Drug content (%) ± SD
Initial	White porous cake, redispersed easily	212.0 ± 1.5	-28.70 ± 1.38	100
5°C ± 3°C				
15 days	White porous cake, redispersed easily	214.3 ± 3.4	-27.35 ± 2.15	98.7 ± 1.06
1 month	White porous cake, redispersed easily	212.8 ± 4.8	-29.14 ± 0.96	98.5 ± 2.59
2 months	White porous cake, redispersed easily	215.0 ± 1.5	-27.75 ± 1.27	97.3 ± 1.23
3 months	White porous cake, redispersed easily	216.2 ± 2.2	-28.01 ± 2.46	96.6 ± 0.84
6 months	White porous cake, redispersed easily	221.5 ± 7.4	-29.14 ± 2.98	96.1 ± 1.72
25 ± 2°C/60 ± 5% RH				
15 days	White porous cake, redispersed easily	213.7 ± 4.0	-27.48 ± 0.59	99.4 ± 1.80
1 month	White porous cake, redispersed easily	214.2 ± 2.6	-28.13 ± 2.24	97.6 ± 2.05
2 months	White porous cake, redispersed easily	218.0 ± 1.6	-26.17 ± 2.67	96.2 ± 1.38
3 months	White porous cake, redispersed easily	224.5 ± 3.2	-29.32 ± 1.54	95.5 ± 0.59

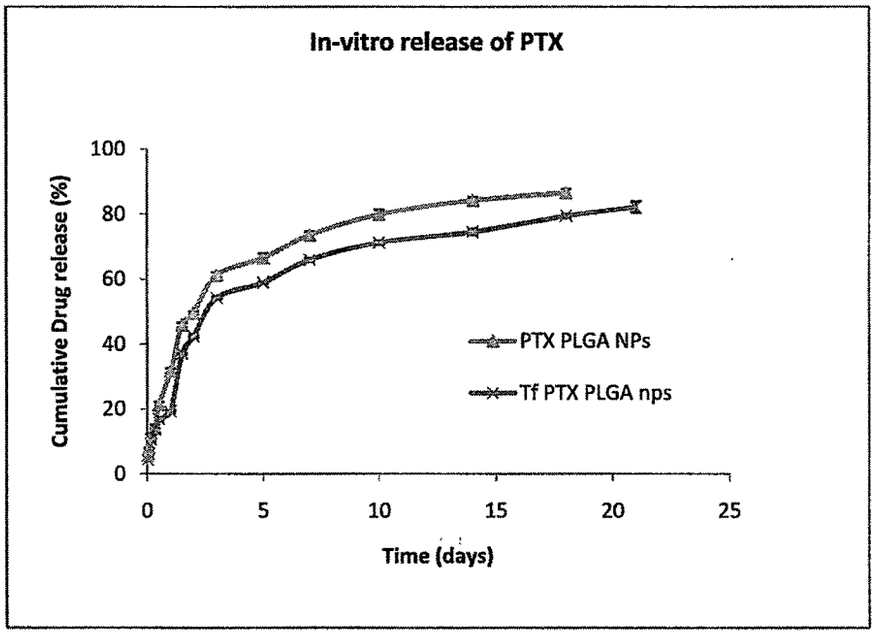

Figure 4.30: In-vitro release of PTX from NPs after storage for 6 months at 5°C ± 3°C

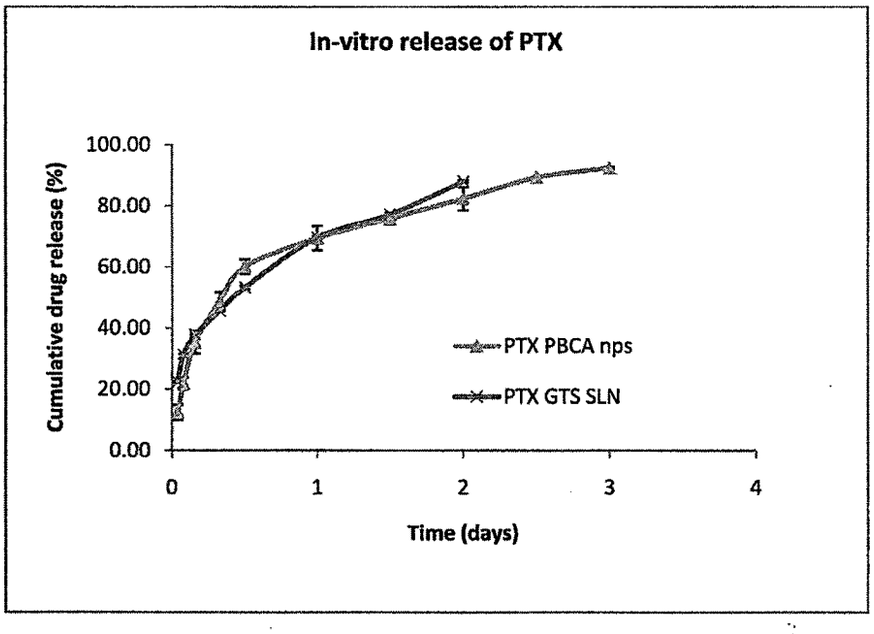

Figure 4.31: In-vitro release of PTX from NPs after storage for 6 months at 5°C ± 3°C

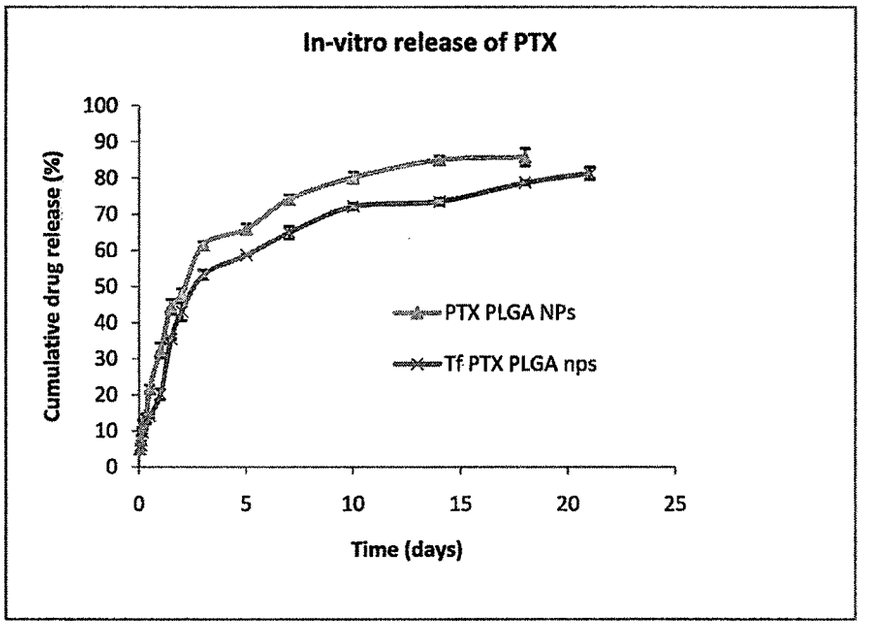

Figure 4. 32: In-vitro release of PTX from NPs after storage for 3 months at 25 ± 2°C/60 ± 5% RH

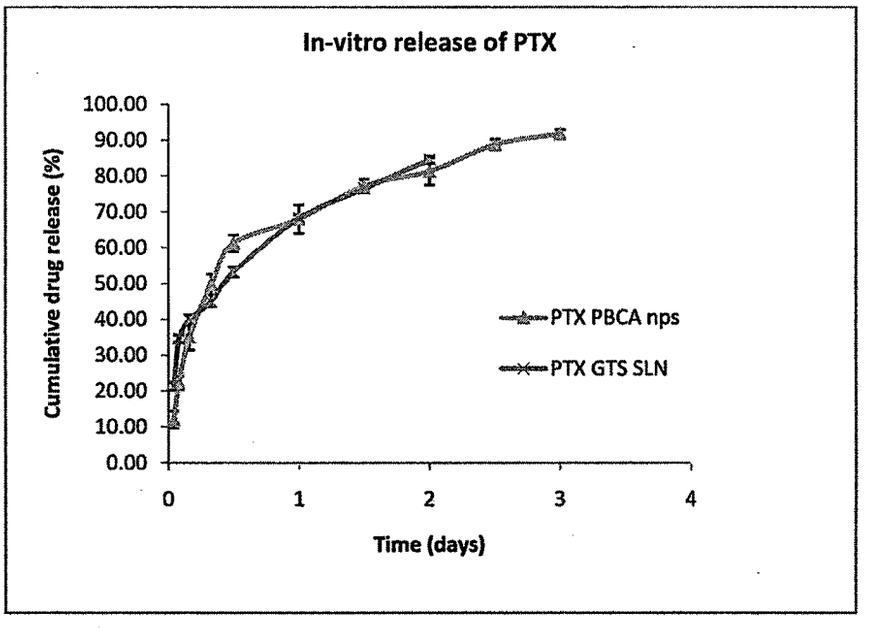

Figure 4. 33: In-vitro release of PTX from NPs after storage for 3 months at 25 ± 2°C/60 ± 5% RH

The stability studies were carried out according to ICH guidelines for drug substances intended for storage in a refrigerator. The long term stability study of lyophilized NPs was carried out at 5°C ± 3°C for six months. The nanoparticles short term stability was conducted for three months at 25 ± 2°C/60 ± 5% RH. Sampling was done at 15 days, 1, 2, 3 and 6 months. The stability profiles are shown in Tables 4.30-4.33.

It can be observed that when stored at 5°C ± 3°C , NPs are stable upto a period of six months with no significant change ($p>0.05$) in either particle size, zeta potential or the drug content. The short term studies also indicate that nanoparticle formulation when stored at 25 ± 2°C/60 ± 5% RH are also stable with no significant change in drug content. All the samples stored at 5°C ± 3°C and 25 ± 2°C/60 ± 5% RH were redispersed easily within 2 minutes.

In case of PLGA NPs(unconjugated and conjugated) the NPs stored at 5°C ± 3°C and 25 ± 2°C/60 ± 5% RH were found to be stable for six months based on the non-significant ($p>0.05$) differences in initial and final particle size, zeta potential and drug content. When conjugated NPs were stored at 25 ± 2°C/60 ± 5% RH the formulation was cream in color after three month but the porous cake was redispersed easily. No significant change in the drug release was observed for the NPs stored at 5°C ± 3°C and 25 ± 2°C/60 ± 5% RH (Figure 4.30-4.33)

Hence, it can be concluded that the NPs should be stored at 5°C ± 3°C for maximum stability and a long term stability study is necessary for determining the optimum storage conditions for the lyophilized NPs.

4.5 Conclusions

We can conclude that PTX can be effectively loaded into PLGA and PBCA polymeric carriers and a PS suitable for parenteral administration can be obtained. Coating and conjugation of PLGA NPs can be done effectively without significantly increasing the PS of the NPs. NPs that give a controlled release of PTX are obtained. Also PTX can be

effectively loaded into solid lipids like glyceryl tristearate which also demonstrates a sustained release effect.

References

Adams JD, Flora K, Goldspiel BR, Wilson JW, Finley R. Taxol: a history of pharmaceutical development and current pharmaceutical concerns J. Nat. Cancer Inst. Monogr. 15 (1993) 141.

Adinarayana K, Ellaiah P. Response surface optimization of the critical medium components for the production of alkaline protease by a newly isolated Bacillus sp. J.Pharm Pharmaceut Sci. 5(3) (2002) 281-287.

Akhnazarova S, Kafarov V. Experiment optimization in chemistry and chemical engineering; Mir Publications, Moscow. (1982)

Alakhov VY, Moskaleva EY, Batrakova EV, Kabanov AV. Hypersensitization of multidrug resistant human ovarian carcinoma cells by pluronic P85 block copolymer. Bioconjug. Chem. 7 (1996) 209–216.

Ambruosi A, Gelperina S, Khalansky A, Tanski S, Theisen A, Kreuter J. Antitumor effect of doxorubicin loaded in poly(butyl cyanoacrylate) nanoparticles in rat glioma model: influence of formulation parameters. J. Microencapsulation 23 (2006) 582–592.

Ambudkar S, Lelong I, Zhang J, Cardarelli C, Gottesman M, Pastan I. Partial purification and reconstitution of the human multidrug resistance pump: characterization of the drug-stimultable ATP hydrolysis. Proc. Natl. Acad. Sci. USA 89 (1992) 8472-8476.

Ballard M, Napper D, Gilbert R. Kinetics of emulsion polymerization of methyl methacylate. J of Polymer Sci: Polymer Chemistry edition. 22 (1984) 3225-3253.

Barret KEJ, Thomas HR. Dispersion Polymerization on Organic Media. Barret KEJ, Ed. Wiley, London (1975) p. 115.

Batrakova EV, Lee S, Li S, Venne A, Alakhov V, Kabanov A. Fundamental relationships between the composition of pluronic block copolymers and their hypersensitization effect in MDR cancer cells, Pharm. Res. 16 (1999)

Batrakova EV, Kabanov AV. Pluronic block copolymers: Evolution of drug delivery concept from inert nanocarriers to biological response modifiers. J. Control Rel 130 (2) (2008) 98-106

Behan N, Birkinshaw C, Clarke N. Poly n- butyl cyanoacrylate nanoparticles: a mechanistic study of polymerization and particle formation. Biomaterials 22 (2001) 1335-1344.

Bennis S, Chapey C, Couvreur P, Robert J. Enhanced cytotoxicity of doxorubicin encapsulated in polyisohexylcyanoacrylayte nanospheres against multidrug-resitant tumour cells in culture, Eur. J. Cancer. 30 (1) (1994) 89–93.

Bhavsar MD, Tiwari SB, Amiji MM. Formulation optimization for the nanoparticles-in-microsphere hybrid oral delivery system using factorial design. J of Control Release 110 (2006) 422–430.

Bhawal S, Pokhriyal NK, Devi S. Transluscent nanolatexes through emulsion polymerization of ethyl acrylate. European Polymer J 38 (2002) 735-744.

Boury F, Ivanova T, Panaitov I, Proust JE, Bois A, Richou J. Dynamic properties of poly(DL-lactide) and polyvinly alcohol monolayers at the air/water and dichloromethane/water interfaces. J Colloid Interf. Sci. 169 (1995) 380-392.

Bovey FA, Kolthoff IM, Medalia AI, Mechan E J. In. Bovey FA, Kolthoff IM, Medalia AI, Mechan E J.(eds.) Emulsion polymerization, Interscience publishers, New York, 1955;pp1-22.

Box G, Wilson KB. On the experimental attainment of optimum conditions. J. R. Stat. Soc., Ser. B. Methodol 13 (1951) 1– 45.

Box GEP, Hunter WG, Hunter JS. Statistics for experiments; John Wiley and Sons, New York, (1978) 291-334.

Budhian A, Siegel SJ, Winey KL. Haolperidol loaded PLGA nanoparticles: systematic study of particle size and drug content. Int. J. of Pharm 336 (2007) 367-375.

Bunjes H, Westesen K, Koch MHJ, Crystallization tendency and polymorphic transitions in triglyceride nanoparticles. Int. J. Pharm. 129 (1996) 159–173.

Cavalli R, Caputo O, Gasco MR. Preparation and characterization of solid lipid nanospheres containing paclitaxel. Eur. J. Pharm. Sci. 10 (2000) 305–309.

Ceruti M, Crosasso P, Brusa P, Arpicco S, Cattel L. Preparation, characterization, cytotoxicity and pharmacokinetics of liposomes containing water soluble prodrugs of paclitaxel. J. Control Release 63 (2000) 141–153.

Chang AY, Kim K, Glick J, Anderson T, Karp D, Johnson D. Phase II study of taxol, merbarone, and piroxantrone in stage IV non-small-cell lung cancer: The Eastern Cooperative Oncology Group Results, J. Natl. Cancer Inst. 85 (1993) 388–394.

Chen DB, Yang TZ, Lu WL, Zhang Q. In vitro and invivo study of two types of long-circulating solid lipid nanoparticles containing Paclitaxel. Chem. Pharm. Bull 49 (11) (2001) 1444-1447.

Chorny M, Fishbein I, Danenberg HD, Golomb G. Lipophilic drug loaded nanospheres prepared by nanoprecipitation: effect of formulation variables on size, drug recovery and release kinetics. J. of Control Rel 83 (2002) 389–400.

Cochran WG, Cox G. Experimental designs. 2nd edn; John Wiley and Sons, New York, (1992) 335-375.

Colin de Verdie`re A, Dubernet C, Ne´mati F, Soma E, Appel M, Ferte´ J, Bernard S, Puisieux F, Couvreur P. Reversion of multidrug resistance with polyalkylcyanoacrylate nanoparticles: towards a mechanism of action. Br. J. Cancer 76 (1997) 198–205.

Couvreur P, Blanco-Prieto MJ, Puisieux F, Roques B, Fattal E. Multiple emulsion technology for the design of microspheres containing peptides and oligopeptides. Adv. Drug Delivery Rev. 2 (1997) 85–96.

Couvreur P, Kante B, Roland M, Guiot P, Bauduin P, Speiser P. Polycyanoacrylate nanocapsules as potential lysomotrophic carriers: preparation, morphological and sorptive properties. J Pharm Pharmcol. 3 (1979) 1331-1332.

Davis JT, Rideal EK. Interfacial phenomena. J. Electrochem. Soc. 109 (7) (1962)175C-175C.

Derakhshandeh K, Erfan M, Dadashzadeh S. Encapsulation of 9-nitrocamptothecin, a novel anticancer drug, in biodegradable nanoparticles: Factorial design, characterization and release kinetics. European J. of Pharm. and Biopharm 66 (2007) 34–41.

Desai MP, Labhasetwar V, Walter E, Levy RJ. The mechanism of uptake of biodegradable microparticles in Caco-2 cells is size dependent. Pharm. Res. 14 (1997)1568–73.

Dosio F, Arpicco S, Brusa P, Stella B, Cattel L. Poly (ethylene glycol)-human serum albumin-paclitaxel conjugates: preparation, characterization and pharmacokinetics, J. Control. Release 76 (2001) 107–117.

Douglas S, Illum L, Davis SS. Particle Size and Size Distribution of Poly(butyl 2- cyano acrylate) Nanoparticles. II: influence of the stabilizer. J of Colloid and Interface Science, 103 (1985) 154-163.

Douglas SJ, Illum L, Davis SS, Kreuter J. Particle size and size distribution of poly(butyl-2-cyanoacrylate) nanoparticles. I. Influence of physicochemical factors. J. Colloid Interface Sci. 101 (1984) 149.

Duncan R, Gac-Breton S, Keane R, Musila R, Sat YN, Satchi R, Searle F. Polymer-drug conjugates, PDEPT and PELT: basic principles for design and transfer from the laborator y to clinic, J. Control. Release 74 (2001) 135–146.

Dunn AS. In Lovell PA, EL-Asser MS (eds.) Emulsion polymerization and emulsion polymers. John Wiley Inc., New York, 1997, pp 126-135.

Dunn SE, Coombes AG, Garnett MC, Davis SS, Davies MC, Illum L. In vitro cell interaction and in vivo biodistribution of poly(lactideco-glycolide) nanospheres surface modified by poloxamer and poloxamine copolymers. J of Control Release 44 (1997) 65–76.

Duro R, G´omez-Amoza JL, Martinez-Pacheco R, Souto C, Concheiro A. Adsorption of polysorbate 80 on pyrantel pamoate: effects on suspension stability. Int. J. Pharm. 165 (1998) 211–216.

Edman P, Ekman B, Sjoholm I. Immobilization of proteins in microspheres of biodegradable polyacryl dextran. J. Pharm. Sci. 69 (1980) 838–842.

Eisenhauer EA, Bokkel H, Swenerton KD, Gianni L, Myles J, Burg ME. European–Canadian randomized trial of paclitaxel in relapsed ovarian cancer: high-dose versus low-dose and long versus short infusion, J. Clin. Oncol. 12 (1994) 2654–2666.

El-Gibaly, Abdel-Ghaffar S. Effect of hexacosanol on the characteristics of novel sustained-release allopurinol solid lipospheres (SLS): factorial design application and product evaluation, Int. J. Pharm. 294 (2005) 33– 51.

Endicott J, Ling V. The biochemistry of P glycoprotein mediated multidrug resistance. Annu. Rev. Biochem 58 (1989) 137-171.

Esmaeili et al., PLGA nanoparticles of different surface properties: Preparation and evaluation of their body distribution, Int. J. Pharm 349 (2008) 249–255.

Feng S, Huang G. Effects of emulsifiers on the controlled release of paclitaxel (Taxol) from nanospheres of biodegradable polymers. J. Control. Release 71 (2001) 53–69.

Fessi H, Puisieux F, Devissaguet JP, Ammoury N, Benita S. Nanocapsule formation by interfacial deposition following solvent displacement. Int. J. Pharm. 55 (1989) R1–R4.

Fonseca C, Simoes S, Fonseca C, Simoes. Paclitaxel-loaded PLGA nanoparticles: preparation, physicochemical characterization and in vitro anti-tumoral activity. J Control Release 83 (2002) 273–86.

Franks, F. Freeze-drying of bioproducts: putting principles into practice. Eur. J. Pharm. Biopharm. 45(1998) 221–229.

Freitas C, Muller RH. Correlation between long-term stability of solid lipid nanoparticles (SLN) and crystallinity of the lipid phase. Eur. J. Pharm. Biopharm. 47 (1999) 125–132.
Friedland D, Gorman G, Treat J. Hypersenstivity reactions from taxol and etoposide. J. Natl. Cancer Inst. 85 (1993) 2036.

Gohel M, Amin A. Formulation optimization of controlled release diclofenac sodium microspheres using factorial design. J. Control. Release 51 (1998) 115– 122.

Govender T, Riley T, Ehtezazi T, Garnett MC, Stolnik S, Illum L, Davis SS. Defining the drug incorporation properties of PLA–PEG nanoparticles. Int. J. Pharm. 199 (2000) 95–110.

Hagemann JW. Thermal behavior and polymorphism of acylglycerides, in: Garti G, Sato K (Eds.), Crystallization and Polymorphism of Fats and Fatty Acids, Marcel Dekker, New York, Basel, 1988, pp. 9 – 96.

Hawley AE, Illum L, Davis SS. Lymph node localization of biodegradable nanospheres surface modified with poloxamer and poloxamine block co polymers. FEBS Lett. 400 (1997) 319–323.

Heiati H, Tawashi R, Phillips NC. Solid lipid nanoparticles as drug carriers. Plasma stability and biodistribution of solid lipid nanoparticles containing the lipophilic prodrug 3-azido-3deoxythymidine palmitate in mice. Int. J. Pharm. 174 (1998) 71–80.

Hernqvist L. Crystal structures of fats and fatty acids, in: Garti N, Sato K (Eds.), Crystallization and Polymorphism of Fats and Fatty Acids, Marcel Dekker, New York, Basel, 1988, pp. 97–138.

Hu YP, Jarillon S, Dubernet C, Couvreur P, Robert J. On the mechanism of action of doxorubicin encapsulation in nanospheres for the reversal of multidrug resistance. Cancer Chemother. Pharmacol. 37 (1996) 556– 560.

Huang CY, Chen CM, Lee YD. Synthesis of high loading and encapsulation efficient paclitaxel-loaded poly(n-butyl cyanoacrylate) nanoparticles via miniemulsion. Int. J. of Pharm. 338 (2007) 267–275.

Huang SK, Martin FJ, Jay G. Extravasation and transcytosis of liposomes in Kaposi's sarcoma – like dermal lesions of transgenic mice bearing HIV Tat gene. Am J Pathol. 143 (1993) 10-14.

Hyvonen S, Peltonen L, Karjalainen M, Hirvonen J. Effect of nanoprecipitation on the physicochemical properties of low molecular weight poly(l-lactic acid) nanoparticles loaded with salbutamol sulphate and beclomethasone dipropionate. Int. J of Pharm 295 (2005) 269–281.

Illum L, Davis SS, Muller RH, Mak E, West P. The organ distribution and circulation time of intravenously injected colloidal carriers sterically stabilized with a block copolymer: poloxamine 908. Life Sci. 40 (1987) 367–374.

Jenning V, Gysler A, Scha¨fer-Korting M, Gohla S. Vitamin A loaded solid lipid nanoparticles for topical use: occlusive properties and drug targeting to the upper skin. Eur. J. Pharm. Biopharm. 49 (2000) 211 – 218.

Joshi DP, Lan-Chun-Fung YL, Pritchard JW. Determination of poly (vinyl alcohol) via its complex with boric acid and iodine. Anal. Chim. *Acta* 104 (1979) 153–160.

Kante B, Couvreur P, Dubois-Krack G, De Meester C, Guiot P, Roland M, Mercier M, Speiser P. Toxicity of polyalkylcyanoacrylate nanoparticles I: Free nanoparticles. J Pharm Sci 71 (1982) 786-90.

Kaufman RJ, Richard TJ, Fuhrhop RW. Stable O/W emulsion incorporating a taxine (taxol) and method of making same. USA Patent 5,616,330, 1 April. (1997).

Konan YN, Gurny R, Konan YN, Gurny R. Preparation and characterization of sterile and freeze-dried sub-200nm nanoparticles. Int J Pharm 233 (2002) 239–352.

Koziara JM, Lockman PR, Allen DD, Mumper RJ. Paclitaxel nanoparticles for the potential treatment of brain cancers. J. Control. Release 99 (2004) 259–269.

Koziara JM, Whisman TR, Tseng MT, Mumper RJ. In-vivo efficacy of novel paclitaxel nanoparticles in paclitaxel resistant human colorectal tumors. J. Control. Release 112 (2006) 312-319.

Kreuter J, Alyautdin RN, Kharkevich DA, Ivanov AA. Passage of peptides through the blood–brain barrier with colloidal polymer particles (nanoparticles). Brain Res. 674 (1995) 171–174.

Kreuter J, Petrov VE, Kharkevich DA, Alyautdin RN. Influence of the type of surfactant on the analgesic effects induced by the peptide dalargin after its delivery across the blood–brain barrier using surfactant-coated nanoparticles. J. Control. Release. 49 (1997) 81–87.

Kreuter J, Shamenkov D, Petrov V, Ramge P, Cychutek K, Koch-Brandt C, Alyautdin R. Apoliporoteinmediated transport of nanopar ticle-bound drugs across the blood-brain barrier. J. Drug Target. 10 (2002) 317–325.

Kreuter J. Physicochemical characterization of polyacrylic nanoparticles. Int. J Pharm. 14 (1983) 43-58.
Lam YW, Chan CY, Kuhn JG. Pharmacokinetics and pharmacodynamics of the taxanes. J. Oncol. Pharm. Practice. 3 (1997) 76–93.

Layre AM, Gref R, Richard J, Requier D, Chacun H, Appel M, Domb AJ, Couvreur P. Nanoencapsulation of a crystalline drug. Int. J. Pharm. 298 (2005) 323–327.

Lee MK, Lim S J, Kim CK. Preparation, characterization and in-vitro cytotoxicity of paclitaxel loaded sterically stabilized solid lipid nanoparticles. Biomaterials 28 (2007) 2137-2146.

Lee S, Seo D, Kim HW, Jung S. Investigation of inclusion complexation of paclitaxel by cyclohenicosakis-(1-2)- (- -D-glucopyranosyl), by cyclic-(1-2)-D-glucans (cyclosophoraoses), and by cyclomaltohepta oses (- - cyclodextrins). Carbohydr. Res. 334 (2001) 119–126.

Lherm C, Müller RH, Puisieux F, Couvreur P. Alkylcyanoacrylate drug carriers: II. Cytotoxicity of cyanoacrylate nanoparticles with different alkyl chain length. Int J Pharm 84 (1992) 13–22.

Li JT, Caeldwell KD. Plasma protein interactions with Pluronic treated colloids. Colloids Surfaces B-Biointerfaces 7 (1996) 9–22.

Li W, Nadig D, Rasmussen H, Patel K, Shah T. Sample preparation optimization for assay of active pharmaceutical ingredients in a transdermal drug delivery system using experimental designs. J. Pharm. Biomed. Anal. 37 (2005) 493–498.

Magenheim B, Levy MY, Benita S. A new in vitro technique for evaluation of drug release profile from colloidal carriers-ultrafiltration technique at low pressure. Int. J. Pharm. 94 (1993) 115–123.

Mehnert W, Ma¨der K. Solid lipid nanoparticles: Production, characterization and applications. Advanced Drug Delivery Reviews 47 (2001) 165–196.

Mehnert W, zur Mu¨hlen A, Dingler A, Weyhers H, Muller RH. Solid lipid nanoparticles (SLN)—ein neuartiger Wirkstoff-Carrier fu¨ r Kosmetika und Pharmazeutika: II. Wirkstoff-Inkorporation, Freisetzung und Sterilisierbarkeit. Pharm. Ind. 59 (6) (1997) 511– 514.

Mitra A, Lin S. Effect of surfactant on fabrication and characterization of paclitaxel-loaded polybutylcyanoacrylate nanoparticulate delivery systems. J. Pharm Pharmacol 55 (2003) 895–902.

Miwa A, Ishibe M, Nakano T, Yamahira S, Itai S, Jinno H, Kawahara. Development of novel chitosan derivatives as micellar carriers of taxol. Pharm. Res. 15 (1998) 1844–1850.

Moghimi SM, Hunter AC, Murray JC. Long circulating and target specific nanoparticles: theory to practise. Pharmacol Rev. 53 (2001) 283-318.

Moghimi SM, Muir IS, Illum L, Davis SS, Kolb-bachofen V. Coating particles with block co-polymer (poloxamine-908) suppresses opsonization but permits the activity of dysopsonins in the serum. Biochim. Biophys. Acta 1179 (1993) 157–165.

Mu L, Feng SS. PLGA/TPGS nanoparticles for controlled release of paclitaxel: effects of the emulsifier and the drug loading ratio. Pharm Res 20(11) (2003) 1864–1872.

Mu L, Feng SS. Vitamin E TPGS used as emulsifier in the solvent evaporation/extraction technique for fabrication of polymeric nanospheres for controlled release of paclitaxel (Taxol). J. Control Release 80 (2002) 129-144.

Müller RH, Lherm C, Herbort J, Blunk T, Couvreur P. Alkylcyanoacrylate drug carriers: I. Physicochemical characterization of nanoparticles with different alkyl chain length. Int J Pharm 84 (1992) 1–11.

Müller RH, Lherm C, Herbort J, Couvreur P. In vitro model for the degradation of alkylcyanoacrylate nanoparticles. Biomaterials 11 (1990) 590–595.

Muller R H, Wallis K H. Surface modification of i.v. injectable biodegradable nanoparticles with poloxamer polymers and poloxamine 908. Int. J. Pharm 89 (1993) 25-31.

Muller RH, Lucks JS. Arzneistofftrager aus festen Lipidteilchen, Feste Lipidnanospharen (SLN). Eur. Patent No. 0605497. (1996)

Muller RH, Mader K, Gohla S. Solid lipid nanoparticles (SLN) for controlled drug delivery—a review of the state of the art. Eur. J. Pharm. Biopharm. 50 (2000) 161–177.

Muller RH, Mehnert W, Lucks JS, Schwarz C, zur Muhlen A, Weyhers H, Freitas C, Ruhl D. Solid lipid nanoparticles (SLN)—An alternative carrier system for controlled drug delivery. Eur. J. Pharm. Biopharm. 41(1) (1995) 62–69.

Musumeci T, Ventura CA, Giannone I, Ruozi B, Montenegro L, Pignatello R, Puglisi G. PLA/PLGA nanoparticles for sustained release of docetaxel. Int. J. of Pharma 325 (2006) 172–179.

Nabholtz JM, Gelmon K, Bontenbal M, Spielmann M, Catimel G, Conte P, Klaassen U, Namer M, Bonneterre J, Fumoleau P, Winograd B. Multicenter randomized comparative study of two doses of paclitaxel in patients with metastatic breast cancer. J. Clin. Oncol. 14 (1996) 1858–1867.

Nemati F, Dubernet C, Fessi H, Colin de Verdiere A, Puisieux F, Couvreur P. Reversion of multidrug resistance using nanoparticles in vitro: Influence of the nature of the polymer. Int. J. Pharm. 138 (1996) 237-246.

Owens J. Stealthy polymers target drug-resistant tumour cells. Drug Discovery Today 6 (2001) 551-552.

Panyam J, Sahoo SK, Prabha S, Bargar T, Labhasetwar V. Fluorescence and electron microscopy probes for cellular and tissue uptake of poly(D,L-lactide-co-glycolide) nanoparticles. Int. J. Pharm. 262 (2003) 1-11.

Petri B, Bootz A, Khalansky A, Hekmatara T, Müller RH, Uhl R, Kreuter J, Gelperina S. Chemotherapy of brain tumour using doxorubicin bound to surfactant-coated poly(butyl cyanoacrylate) nanoparticles: Revisiting the role of surfactants. J. of Control. Release. 117 (2007) 51–58.

Qian zm, Li H, Sun H, Ho K. Targeted Drug Delivery via the Transferrin Receptor- Mediated Endocytosis Pathway. Pharmacol Rev 54 (2002) 561–587.

Quintanar-Guerrero D, Allemann E, Fessi H, Doelker E. Preparation techniques and mechanisms of formation of biodegradable nanoparticles from performed polymers. Drug Dev. Ind. Pharm. 24 (12) (1998) 1113–1128.

Quintanar-Guerrero D, Ganem-Quintanar A, Alle´man E, Fessi H, Doelker E. Influence of the stabilizer coating layer on the purification and freeze-drying of poly(D,L-lactic acid) nanoparticles prepared by an emulsion diffusion technique. J. Microencaps. 15 (1) (1998) 107–109.

Radtke M, Muller RH. NLC—nanostructured lipid carriers: the new generation of lipid drug carriers, New Drugs 2 (2001) 48– 52.

Reddy LH, Murthy RSR. Etoposide loaded nanoparticles made from glyceride lipids: formulation, characterization, in-vitro release, and stability evaluation. AAPS PharmSciTech 2005; 6 (2) article 24.

Reddy LH, Murthy RSR. Polymerization of n-butyl cyanoacrylate in presence of surfactant: study of influence of polymerization factors on particle properties, drug loading and evaluation of its drug release kinetics. ARS Pharmaceutica 44 (2003) 351-369.

Reddy LH, Murthy RSR. Influence of polymerization technique and experimental variables on the particle properties and release kinetics of methotrexate from poly(butylcyanoacrylate) nanoparticles. Acta Pharm. 54 (2004) 103–118.

Rizkalla N, Range C, Lacasse FX, Hildgen P. Effect of various formulation parameters on the properties of polymeric nanoparticles prepared by multiple emulsion method. J. Microencap 23(1): (2006) 39–57.

Rodriguez SG, Allemann E, Fessi H, Doelkar E. Physicochemical parameters associated with nanoparticle formation in the saltingout, emulsification-diffussion and nanoprecipitation methods. Pharm. Res. 21 (2004) 1428-1439.

Saez A, Guzman M, Molpeceres J, Aberturas MR. Freeze drying of polycaprolactone and poly(D,L-lactic-glycolic) nanoparticles induce minor particle size changes affecting the oral pharmacokinetics of loaded drugs. Eur. J. Pharm. Biopharm. 50 (2000) 379–387.

Sahoo SK, Labhasetwar V. Enhanced Antiproliferative Activity of Transferrin-Conjugated Paclitaxel-Loaded Nanoparticles Is Mediated via Sustained Intracellular Drug Retention. Mol Pharm . 2 (2005) 373-383.

Sahoo SK, Panyam J, Prabha S, Labhasetwar V. Residual polyvinyl alcohol associated with poly (D,L-lactide-co-glycolide) nanoparticles affects their physical properties and cellular uptake. J. Control Release 82 (2002) 105-114.

Sahoo SK, Wenxue MA, Labhasetwar V. Efficacy of transferrin-conjugated paclitaxel-loaded Nanoparticles in a murine model of prostate cancer. Int. J. Cancer 112 (2004) 335–340.

Sameti M, Bohr G, Ravi Kumar MNV, Kneuer C, Bakowsky U, Nacken M, Schmidt H, Lehr CM. Stabilisation by freeze-drying of cationically modified silica nanoparticles for gene delivery. Int. J. Pharm. 266 (2003) 51–60.

Schinkel, A. P Glycoprotein, a gatekeeper in the blood brain barrier. Annu. Rev. Neurosci. 22 (1999) 11-28.

Sharma A, Sharma S, Khuller GK. Lectin-functionalized poly (lactide-co-glycolide) nanoparticles as oral/aerosolized antitubercular drug carriers for treatment of tuberculosis. Journal of Antimicrobial Chemotherapy 54 (2004) 761–766.

Song X, Zhao Y, Hou S, Xu F, Zhao R, He J, Cai Z, Li Y, Chen Q. Dual agents loaded PLGA nanoparticles: systematic study of particle size and drug entrapment efficiency. European J. of Pharm Biopharm 69 (2008) 445-453.

Song X, Zhao Y, Wu W, Bi Y, Cai Z, Chen Q, Li Y, Hou S. PLGA nanoparticles simultaneously loaded with vincristine sulfate and verapamil hydrochloride: Systematic study of particle size and drug entrapment efficiency. Int. J. Pharm 350 (2008) 320–329.

Spencer CM, Faulds D. Paclitaxel—a review of its pharmacodynamic and pharmacokinetic properties and therapeutic potential in the treatment of cancer. Drugs 48 (1994) 794–847.

Stella B, Arpicco S, Peracchia MT, Desmaële D, Hoebeke H, Renoir M, D'Angelo J, Cattel L, Couvreur P. Design of folic-acid-conjugated nanoparticles for drug delivery. Journal of Pharmaceutical Sciences. 89 (11) (2000) 1452-1464.

Storm G. et al. Surface modification of nanoparticles to oppose uptake by the mononuclear phagocyte system. Adv. Drug. Deliv. Rev. 16 (1995) 31–48.

Subramanian N, Murthy RSR. Use of electrolyte induced flocculation technique for an in vitro steric stability study of steric study of steric stabilized liposome formulations. PharmaziE 59 (2003) 74-76.

Sullivan CO, Birkinshaw C. In vitro degradation of insulin-loaded poly (n-butylcyanoacrylate) Nanoparticles. Biomaterials 25 (2004) 4375–4382.
Tamai I, Tsuji A. Drug delivery through the blood-brain barrier. Adv Drug Deliv Rev. 19 (1996) 401–424.

Tan JS, Butterfield DE, Voycheck CL, Caldwell KD, Li JT. Surface modification of nanoparticles by PEO/PPO in block copolymers to minimize interactions with blood components and prolong blood circulation in rats. Biomaterials - 14 (1993) 823–833.

Tarr BD, Yalkowsky SH. A new parenteral vehicle for the administration of some poorly soluble anti-cancer drugs. J. Parentral Sci. Technol. 41 (1987) 31.

Tsukiyama S, Takamura A. Activation energy for the deformation and breakup of droplet on mechanical agitation. Chem. Pharm. Bull. 22 (1974) 2538.

Vandervoort J, Ludwig A. Biocompatible stabilizers in the preparation of PLGA nanoparticles: a factorial design study. Int. J. Pharm 238 (2002) 77–92.

Venkateswarlu V, Manjunath K. Preparation, characterization and in vitro release kinetics of clozapine solid lipid nanoparticles. J. Control. Release 95 (2004) 627– 638.

Wall ME, Coggon P, McPhail AT. Plant antitumor agents. VI. Isolation and structure of taxol, a novel antileukemic and antitumor agent from Taxus brevifolia, J. Am. Chem. Soc. 93 (1971) 2325–2327.

Wang YM, Sato H, Adachi I, Horikoshi I. Preparation and characterization of poly(lactic-co-glycolic acid) microspheres for targeted delivery of novel anticancer agent, taxol. Chem. Pharm. Bull. 44 (1996) 1935–1940.

Wani MC, Taylor HL, Wall, Coggon P, McPhail AT. Plant antitumor agents. VI. Isolation and structure of taxol, a novel antileukemic and antitumor agent from Taxus brevifolia. J. Am. Chem. Soc. 93 (1971) 2325–2327.

Waugh WN, Trissel LA, Stella VJ. Stability, compatibility, and plasticizer extraction of taxol (NSC125973) injection diluted in infusion solutions and stored in various containers. Am. J. Hosp. Pharm. 48 (1991) 1520.

Weiss RB, Donehower RC, Wiernik PH, Ohnuma T, Gralla RJ, Trump DL, Baker JR, VanEcho DA, VonHoff DD, Leyland-Jones B. Hypersenstivity reactions with taxol. J. Clin. Oncol. 8 (1990) 1263.

Woods. Cyanoacrylates. In: J.C. Salamone (Eds.), Polymeric materials encyclopedia, Vol. 2. CRC Press Inc, New York, (1996) pp, 1632–1637.

www.ich.org

Xie J, Wang CH. Self-Assembled Biodegradable Nanoparticles Developed by Direct Dialysis for the Delivery of Paclitaxel. Pharm Res 22 (2005) 2079-2090.

Yang S, Lu FL, Cai Y, Zhu J, Liang BW, Yang CZ. Body distribution in mice of intravenously injected camptothecin solid lipid nanoparticles and targeting effect on brain. J. Control. Rel. 59 (1999) 299–307.

Yang S, Zhu J, Lu Y, Liang B, Yang C. Body distribution of camptothecin solid lipid nanoparticles after oral administration. Pharm.Res. 16 (1999) 751–757.

Yee L, Blanch HW. Defined media optimization for the growth of recombinant Escherichia coli x90. Biotechnol. Bioeng. 41 (1993) 221-227.

Yu L, Mishra DS, Rigsbee DR. Determination of the glass properties of D-mannitol using sorbitol as an impurity. J. Pharm. Sci. 87 (1998) 774–777.

Yuan H, Miao J, Du YZ, You J, Hu FQ, Zeng S. Cellular uptake of solid lipid nanoparticles and cytotoxicity of encapsulated paclitaxel in A549 cancer cells. Int. J. Pharm 348 (2008) 137–145.